

Topical Report

An Engineering and Geologic Evaluation of a Horizontal Gas Well Completion in the Almond Sandstone - Echo Springs Field, Greater Green River Basin

Prepared by:

CER Corporation

955 Grier Drive, Suite A
Las Vegas, NV 89119

Amoco Corporation, E&P Sector

1670 Broadway, P.O. Box 800
Denver, Colorado 80201

Institute for Energy Research

University of Wyoming
P.O. Box 4068
Laramie, Wyoming 82071-4068

Branagan & Associates

4341 Soria Way
Las Vegas, NV 89121

S.A. Holditch & Associates

900 Southwest Parkway East, Suite 200
College Station, Texas 77840

Prepared for:

Gas Research Institute

8600 W. Bryn Mawr Avenue
Chicago, IL 60631

Contract No. 5092-212-2589

March 1995

GRI DISCLAIMER

LEGAL NOTICE: This publication was prepared as an account of work sponsored by the Gas Research Institute (GRI), and other organizations. Neither GRI, members of GRI, nor any person acting on behalf of either:

- makes any warranty or representation, express or implied, with respect to the accuracy, completeness, or usefulness of the information contained in this report, or that the use of any information, apparatus, method, or process disclosed in this report may not infringe privately-owned rights; or
- assumes any liability with respect to the use of, or for damages resulting from the use of, any information, apparatus, method, or process disclosed in this report.

Reference to trade names or specific commercial products, commodities, or services in this report does not represent or constitute an endorsement, recommendation, or favoring by GRI of the specific commercial product, commodity, or service.

CER CORPORATION DISCLAIMER

In the preparation of this report, CER Corporation has provided GRI with the benefit of its best judgement. However, because of the many variables and uncertainties inherent in data acquisition and analysis, CER Corporation cannot and does not guarantee results in utilizing the recommendations herein expressed and shall not be liable for any loss, cost or damage resulting from reliance upon its judgement.

REPORT DOCUMENTATION PAGE	1. Report No. GRI-95/0066	2.	3. Recipient's Accession No.
4. Title and Subtitle An Engineering and Geologic Evaluation of A Horizontal Gas Well Completion in the Almond Sandstone, Echo Springs Field, Greater Green River Basin, Wyoming		5. Report Date March 1995	
7. Author(s) R.E. Hill, L.W.E. Reinert, R. Billingsley, T.L. Dunn, W.P. Iverson, B. Aguado, J. Humphreys, R.C. Surdam, P.T. Branagan, B.M. Robinson		8. Performing Organization Report No.	
9. Performing Organization Name and Address CER Corporation Amoco Corporation Institute for Energy Research 955 Grier Drive, Ste. A 1670 Broadway, P.O. Box 800 University of Wyoming Las Vegas, NV 89119 Denver, CO 80201 P.O. Box 4068 Branagan & Assoc. S.A. Holditch & Assoc., Inc. Laramie WY 87071-4068 4341 Soria Way 900 Southwest Parkway East, Suite 200 Las Vegas, NV 89121 College Station, TX 77840		10. Project/Task/Work Unit No. 11. Contract (C) or Grant (G) No. (C)5092-212-2589 (G)	
12. Sponsoring Organization Name and Address Gas Research Institute Project Manager: 8600 West Bryn Mawr Avenue John Hansen Chicago, IL 60631		13. Type of Report & Period Covered Topical March 1995	
15. Supplementary Notes			
16. Abstract (Limit: 200 words) Amoco has drilled and completed two horizontal wells in the Almond Formation in the Greater Green River Basin. One of the wells is not productive from the Almond, but the other well, the Champlin 254 Amoco B 2-H, is an Almond producer. The wells were drilled to evaluate horizontal completions as a means to improve the per well productivity in areas of below average production in the Echo Springs Field. Both wells were cored and logged to obtain geologic data necessary to better evaluate the wells and improve understanding of the Almond Formation reservoir. This report is a compendium of papers that describes the drilling and completion of the Champlin 254 Amoco B 2-H well, the natural fractures and maximum horizontal stress direction determined in the wells, the microscopic characteristics of fractures including in situ aperture, the petrophysical properties of the core, the reservoir modeling performed in the well, and the economic evaluation of horizontal completions in the Almond Formation compared with stimulated vertical wells.			
17. Document Analysis a. Descriptors Wyoming, Greater Green River Basin, Wamsutter Arch, Standard Draw, Echo Springs Field, Almond Formation, tight gas sandstones, horizontal well, reservoir simulation, natural fractures, horizontal stress, fracture aperture, economic evaluation b. Identifiers/Open-Ended Terms natural fracture spacing, aperture, and mineralization, core petrophysics, naturally fractured reservoir simulation, economic comparison of horizontal well with vertical wells, reservoir parameters of the Almond Formation c. COSATI Field/Group			
18. Availability Statement: Unlimited		19. Security Class (This Report) Unclassified	21. No. of Pages 106 + App.
		20. Security Class (This Page) Unclassified	22. Price

Contents

PREFACE 1

**DESIGN, IMPLEMENTATION, AND COMPLETION
OF A HORIZONTAL TIGHT GAS WELLBORE CASE STUDY:
GREEN RIVER BASIN, WYOMING** 3

*Lesley W.E. Reinert and Randy Billingsley
Amoco Corporation, E&P Sector*

INTRODUCTION 3

LOCATION 3

DRILLING AND GEOSCIENCE PROGRAM 5

 Pilot Hole 5

 Horizontal Hole 5

COMPLETION 7

PRODUCTION HISTORY 7

RE-DRILL HISTORY 7

COST 8

CONCLUSIONS 9

**NATURAL FRACTURES AND STRESS ORIENTATIONS
IN THE ALMOND FORMATION, WAMSUTTER AREA,
GREEN RIVER BASIN** 11

*Robin E. Hill
CER Corporation*

INTRODUCTION 11

REGIONAL SETTING 11

FRACTURE CHARACTERIZATION	13
Champlin 254 Amoco B 2-H Core Results	13
Champlin 254 Amoco B 2-H FMI Analysis	13
Champlin 254 Amoco B 2-H FMS Analysis	16
Orientation	16
Spacing	16
Champlin 320 C-1A-H Core Results	18
Champlin 320 C-1A-H FMI Analysis	19
Champlin 320 C-1A-H FMS Interpretation	19
INTERPRETATION OF IN SITU STRESS DIRECTION	19
ASR Results from Champlin 254 Amoco B 2-H Pilot Core	21
Horizontal Core ASR Results	22
Drilling-Induced Fractures	22
FMI Breakout Analysis	24
CONCLUSIONS	26
ACKNOWLEDGMENTS	26
REFERENCES	28
IMPROVEMENTS TO RESERVOIR EVALUATION AND CHARACTERIZATION, ALMOND FORMATION, GREEN RIVER BASIN, WYOMING	31
<i>Thomas L. Dunn, William P. Iverson, Bernabe Aguado, John Humphreys and Ronald C. Surdam The Institute for Energy Research, University of Wyoming</i>	
INTRODUCTION	31
PETROLOGY	32

CLAY MINERALOGY	34
Procedures	34
Results	37
FRACTURES	39
Spacings and Orientations	39
Fracture Apertures	39
Prior Work	39
Champlin 254 Amoco B 2-H Natural Fractures	40
Fracture Aperture Measurements	40
Procedures	40
Measured Values	41
Discussion	45
Fracture Cementation	45
Mineralogy	45
Paragenesis	46
Discussion	48
FORMATION EVALUATION AND CHARACTERIZATION	48
Need for Permeability Versus Confining Stress Data	49
Need for Petrophysical Constants	49
Need for Capillary Pressure Data	50
Laboratory Experiments	51
Laboratory Results: Permeability Versus Confining Stress	51
Laboratory Results: Petrophysical Data	57
Laboratory Results: Capillary Pressure Curves	59

Laboratory Results: Effective Permeability	65
CONCLUSIONS	66
ACKNOWLEDGMENTS.....	68
REFERENCES	69
RESERVOIR ENGINEERING STUDY OF THE CHAMPLIN 254 AMOCO B 2-H, WAMSUTTER FIELD, WYOMING	71
<i>Paul T. Branagan</i> <i>Branagan & Associates</i>	
RESERVOIR ENGINEERING SUMMARY	71
RESERVOIR DESCRIPTION	72
Natural Fractures	72
Reservoir Matrix Properties.....	73
RESERVOIR MODELING.....	74
Simulation Results (Original Wellbore)	74
Original Well Model Summary	79
Field Testing Recommendations.....	79
CHAMPLIN 254 AMOCO B 2-H REDRILL.....	80
Effects of Prior Production.....	80
Simulation Results (Redrill)	83
Redrill Well Model Summary.....	84
REFERENCES	86

**EVALUATION AND COMPARISON OF HYDRAULICALLY-FRACTURED
VERTICAL WELLS WITH THE CHAMPLIN 254 AMOCO B 2-H
HORIZONTAL WELL..... 87**

*Bradley M. Robinson
S.A. Holditch & Associates*

INTRODUCTION..... 87

ANALYSIS OF VERTICAL WELLS..... 88

**COMPARISON OF VERTICAL WELL PERFORMANCE TO HORIZONTAL
WELL PERFORMANCE..... 96**

REFERENCES 101

APPENDIX 1

Champlin 254 Amoco B 2-H Data Inventory..... 103

APPENDIX 2

Core Information 105

Figures

Figure 1	Greater Green River Basin Map Showing the Amoco Horizontal Well Locations	2
Figure 2	Upper Almond (Marine) Net Sandstone Isopach Map	4
Figure 3	Brittle Deformation in the Champlin 254 B 1 Core	4
Figure 4	Drilling Plat for Champlin 254 Amoco B 2-H Showing Target Area.....	6
Figure 5	Pilot and Horizontal Wellbore Diagram.....	6
Figure 6	Production History for the Champlin 254 Amoco B 2-H.....	8
Figure 7	Plan View Showing the Trajectory of the Redrilled Horizontal Lateral	9
Figure 8	Regional Geologic Map of the Greater Green River Basin	12
Figure 9	Natural Fracture Strikes from Core No. 1 (Pilot Hole), Champlin 254 Amoco B 2-H Well	14
Figure 10	Natural Fracture Strikes from Cores 2, 3 and 4, Champlin 254 Amoco B 2-H Well	14
Figure 11	Rose Diagram of FMI-Interpreted Fractures from Pilot Hole, Champlin 254 Amoco B 2-H Well	15
Figure 12	Rose Diagram of Core Fractures from Pilot Hole, Champlin 254 Amoco B 2-H.....	15
Figure 13	Rose Diagram of FMS-Interpreted Fracture Strikes in the Horizontal Well, Champlin 254 Amoco B 2-H	17
Figure 14	Rose Diagram of Natural Fractures in Horizontal Core, Champlin 254 Amoco B 2-H.....	17
Figure 15	Frequency Histogram of Fracture Spacing, Champlin 254 Amoco B 2-H.....	18
Figure 16	Fracture Strikes from Cores 1 and 2, Champlin 320 C-1A-H.....	20
Figure 17	Fracture Strikes from Cores 3 and 4, Champlin 320 C-1A-H.....	20

Figure 18	Rose Diagram of FMI Interpretation of Pilot Hole, Champlin 320 C-1A-H.....	21
Figure 19	Rose Diagram of Drilling-Induced Fracture Strikes, Champlin 320 C-1A-H.....	23
Figure 20	σ_H Interpreted from Borehole Breakouts, Champlin 254 Amoco B 2-H.....	25
Figure 21	σ_H Interpreted from Borehole Breakouts, Champlin 320 C-1A-H.....	25
Figure 22	Composite Figure of Fractures, Breakouts, and Stress Directions in the Champlin 254 Amoco B 2-H.....	27
Figure 23	Composite Figure of Fractures, Breakouts, and Stress Directions in the Champlin 320 C-1A-H.....	27
Figure 24	Location Map of the Champlin 254 Amoco B-2H Along the Northern Edge of the Echo Springs Field.....	32
Figure 25	Model Compositions of Almond Formation Sandstones from the Amoco Champlin 254 B 2-H.....	33
Figure 26	Photomicrograph of the Almond Formation (Partially Crossed Polars).....	33
Figure 27	X-Ray Diffractogram of the <2 μ m Size Fraction of Sample 10,791.5 ft.....	38
Figure 28	X-Ray Diffractogram of the <0.01mm Size Fraction of Sample 10,791.5 ft, Sandstone from the Horizontal Core.....	38
Figure 29	Scanning Electron Photomicrograph of Crenulated Flakes of Corrensite Which are Typically Attached to Lithic Fragments.....	39
Figure 30	Sequence of Procedures for Producing Polished Thin Sections Containing Natural Fracture Traces.....	41
Figure 31	In Situ Fracture Aperture Distributions in Microns for Three Samples from the Champlin 254 Amoco B 2-H.....	42
Figure 32	Plot of Apparent Plug Permeability for Different Fracture Apertures.....	43
Figure 33	Calculated Plug Permeabilities from the Measured In Situ Fracture Aperture Data.....	44

Figure 34	Backscattered Electron Photomicrographs of a Fracture in the 10,033.5-ft Sample.....	45
Figure 35	Photomicrographs of Natural Fracture Filling and Lining Cements	47
Figure 36	Paragenetic Sequence for the Champlin 254 Amoco B 2-H Fracture Fill.....	48
Figure 37	Backscattered Electron Images of Polished Thin Sections Showing Drilling Mud in the Fractures	49
Figure 38	Open-Hole Logs for the Champlin 254 Amoco B-1 (Vertical Well).....	50
Figure 39	Porosity vs. Log Permeability for Samples at Two Confining Pressures from the Pilot Core of the Champlin 254 Amoco B 2-H Well	56
Figure 40	Permeability vs. Confining Stress for Four Samples from the Champlin 254 Amoco B 2-H Well	56
Figure 41	Pickett Plot for Samples from the Champlin 254 Amoco B 2-H Showing that $m = 2$ Provides a Good Match for Varying Water Saturation.....	59
Figure 42	Saturation Exponent Measured on Champlin 254 Amoco B 2-H Pilot Core Samples	64
Figure 43	Capillary Pressure Curves for Two Almond Formation Sandstones, Champlin 254 Amoco B 2-H Well	64
Figure 44	Threshold Displacement Pressures, as Derived Using a Method Described by Showalter (1979)	65
Figure 45	Common Air Permeability Vs. In Situ Effective Gas Permeability for Almond Sands.....	66
Figure 46	Production Histories for the Champlin 254 Amoco B-1 (solid line) and the Champlin 254 Amoco B 2-H (dots).....	68
Figure 47	Frontier Outcrop Showing Typical Natural Fractures in the Greater Green River Basin	73
Figure 48	Schematic of the 3-D Naturally Fractured Reservoir Model Used to Simulate the Champlin 254 Amoco B 2-H Field Data.....	75
Figure 49	Daily Production Rates and Surface Pressures from the Original Champlin 254 Amoco B 2-H Borehole	76

Figure 50	History Match Data from a Homogeneous Reservoir Model Overlaying the Field Measured Data from the Champlin 254 Amoco B 2-H.....	77
Figure 51	History Match Data from the Naturally Fractured Reservoir Model Overlaying the Field Measured Data	79
Figure 52	Simulated Pressure Buildup Data with the Full Horizontal and Vertical Wellbore Volumes.....	81
Figure 53	Simulated Pressure Buildup Data with the Horizontal Wellbore Volume Only	81
Figure 54	3-D Pressure Contour Map Surrounding the Champlin 254 Amoco B 2-H at the End of Initial Production Period, March 1994	82
Figure 55	3-D Pressure Contour Map Surrounding the Champlin 254 Amoco B 2-H Just Prior to Production from the Redrill, June 1994	82
Figure 56	Daily Production Rates and Surface Pressures from the Redrill, Champlin 254 Amoco B 2-H.....	83
Figure 57	Bottomhole and Surface Pressure Data During a Pressure Buildup Test on the Redrill, Champlin 254 Amoco B 2-H	85
Figure 58	Derivative Plot for the Redrill Bottomhole Pressure Buildup Test, Showing Radial, Bilinear and Linear Flow Derivatives	85
Figure 59	Final Simulated Production History Match with Bottomhole Pressure Buildup Data	86
Figure 60	Base Map of Echo Springs Field	88
Figure 61	Example "PROMAT" History Match of Production.....	89
Figure 62	Production Indicator Correlated to 10-Year Cumulative Production, Echo Springs Field	93
Figure 63	Contour Map of Production Indicator, C.I. = 10 MSCFM.....	94
Figure 64	Contour Map of 10-Year Cumulative Production, C.I. = 0.5 BCF	95
Figure 65	Average Production Rate for Wells Comparable to NE 4 Sec. 23, T20N, R93W	96
Figure 66	Distribution of Productivity Indicators in Echo Springs Field	97

Tables

Table 1	Core-Based Maximum Stress Direction Determinations	23
Table 2	High Pressure Mercury Injection Test Results, Champlin 254 Amoco B 2-H (data from K&A Laboratories).....	35
Table 3	Semi-Quantitative X-Ray Diffraction Mineralogy	37
Table 4	Number of Measurements (n), Average In Situ Fracture Widths and Geometric Averages of the Calculated Permeabilities (k) for Natural Fractures, Champlin 254 Amoco B 2-H	43
Table 5	Standard Core Analysis, Champlin 254 Amoco B 2-H (K&A Laboratories).....	52
Table 6	Air Permeabilities at Varying Confining Pressure, Champlin 254 Amoco B 2-H (K&A Laboratories)	54
Table 7	Formation Factor Test Results, Champlin 254 Amoco B 2-H (K&A Laboratories)	58
Table 8	Resistivity Index Test Results, Champlin 254 Amoco B 2-H (K&A Laboratories)	60
Table 9	Initial Parameters for Reservoir Model	75
Table 10	Final Parameters for the Naturally-Fractured Reservoir Model.....	78
Table 11	Results of Pre-Fracture Analyses.....	91
Table 12	Results of Post-Fracture PBU Analyses	91
Table 13	Results of Post-Fracture Production Matching.....	92
Table 14	Comparison of Pre- and Post-Fracture Analyses.....	93
Table 15	Comparison of Long-Term Production Performance	97
Table 16	Basic Cost Information for Economic Evaluation.....	98
Table 17	Economic Evaluations - Wells in NE Sec 23, T20N, R93W	99
Table 18	Economic Evaluation with Higher Fracture Flow Capacity.....	100

AN ENGINEERING AND GEOLOGIC EVALUATION OF A HORIZONTAL GAS WELL COMPLETION IN THE ALMOND SANDSTONE, ECHO SPRINGS FIELD, GREATER GREEN RIVER BASIN, WYOMING

PREFACE

The Gas Research Institute (GRI) and the Department of Energy (DOE) have long recognized the Greater Green River Basin (GGRB) as a significant gas resource for the United States; separately and together, they have funded numerous programs in the basin. In addition to studying vertical well enhancements, horizontal completions have been investigated as a potential method for improving gas well productivity, especially in low-permeability, naturally fractured reservoirs (e.g., Myal and Frohne, 1992; CER, 1993a, 1993b and 1993c; and Middlebrook and others, 1993).

Amoco's Northwest Business Unit independently developed a program to collect high-quality geoscience data and evaluate horizontal completions in the Almond sandstone at the north-eastern margin of the Echo Springs Field, Wyoming. Amoco's high-quality data acquisition program included data that would further GRI's near-term goals for the Greater Green River Basin; therefore, a multi-disciplinary team under contract to GRI was formed to evaluate the results and a cost-sharing agreement was made with Amoco to acquire the data. Two horizontal wells, the Champlin 254 Amoco B 2-H, and Champlin 320 C-1A-H, were drilled. Their locations in the Greater Green River Basin are shown in Figure 1. A complete listing of the data acquired from these wells is presented in Appendix 1.

Initial results of the investigations were presented at the "Horizontal Well Drilling and Completions in the Greater Green River Basin" meeting on November 7, 1994, in Denver, that was co-sponsored by GRI, DOE and the Independent Petroleum Association of Mountain States (IPAMS).

This GRI topical report is a compendium of the papers prepared by Amoco and members of the GRI team using primarily the data acquired from the Champlin 254 Amoco B 2-H well. Some results are included for the Champlin 320 C-1A-H well; however, since this well is not an Almond producer, production and economic evaluations were not performed. The information in this volume will augment the existing knowledge base of the Almond sandstone and potentially lead to improved horizontal well siting and completions in the GGRB.

REFERENCES

CER Corporation, 1993a: "Horizontal Well Completion Technology in the Mancos B - Analysis of the Chandler & Associates Southwest Rangely Federal 8H-1-2, Rio Blanco County, Colorado," Topical Report No. GRI-93/0037, prepared for GRI Contract No. 5091-212-2242 and 5091-212-2249, June.

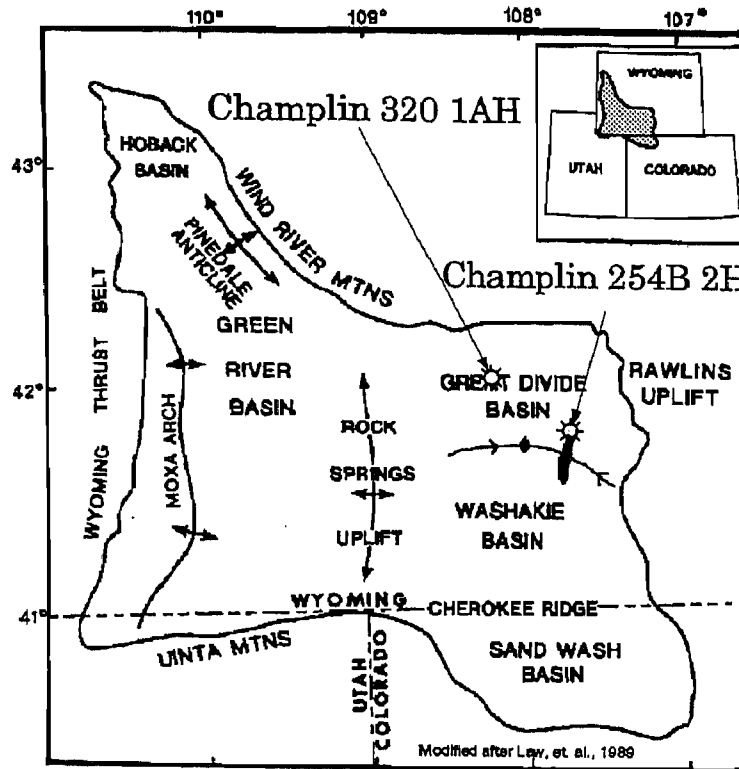


Figure 1 Greater Green River Basin Map Showing the Amoco Horizontal Well Locations

CER Corporation, 1993b: "Horizontal Well Completion Technology in the Davis Sandstone - Analysis of the Dallas Production Inc. Merrill No. 1, Parker County, Texas," Topical Report No. GRI-93/0153, prepared for GRI Contract No. 5091-212-2242 and 5091-212-2241, June.

CER Corporation, 1993c: "Horizontal Gas Well Completion Technology in the Davis Sandstone, - Analysis of the Mitchell Energy Corporation T.P. Sims B No. 1, Wise County, Texas," Topical Report GRI-93/0282, prepared for GRI Contract Nos. 5091-212-2242 and 5091-212-2231.

Myal, F.R. and K-H. Frohne, "Slant-Hole Completion Test in the Piceance Basin," SPE 21866, presented at the Rocky Mountain Regional Meeting and Low-Permeability Reservoirs Symposium, Denver, Colorado, April 15-17.

Middlebrook, M.L., P.T. Branagan, R.E. Hill, G.C. Kukal, R.E. Peterson, T.S. McDonald and J.K. Aslakson, 1993: "Reservoir Evaluation and Completion Results from a Horizontal Well in the Mancos B, Douglas Creek Arch, Northwest Colorado," SPE 25924, presented at the SPE Rocky Mountain Regional/Low Permeability Reservoirs Symposium, Denver, Colorado, April 12-14.

Design, Implementation, and Completion of a Horizontal Tight Gas Wellbore Case Study: Green River Basin, Wyoming

*Lesley W. E. Reinert and Randy Billingsley
Amoco Corporation, E&P Sector*

INTRODUCTION

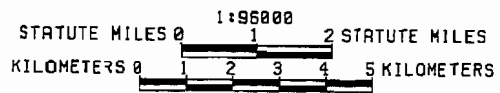
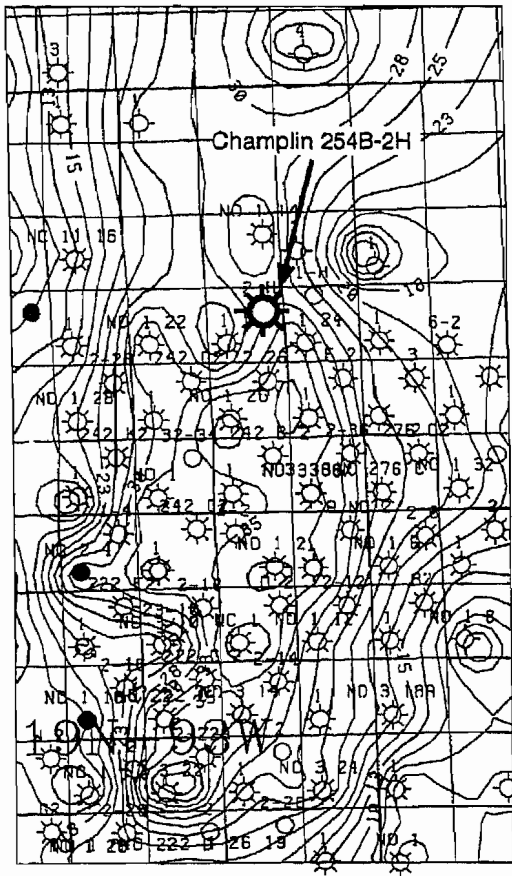
In September 1993, Amoco Production Company spud the Champlin 254 Amoco B 2-H, the first horizontal well drilled on the east flank of the Greater Green River Basin, southwestern Wyoming. The purpose was to test horizontal well technology as a way to accelerate gas recovery in areas of known resource potential and low conventional productivity. This effort was an extension of the prior research performed by the Department of Energy (DOE) at the Multiwell Experiment (MWX) and Slant Hole Completion Test (SHCT) projects and in analogous Gas Research Institute (GRI) projects. Within Amoco, it represents the culmination of an extensive multi-disciplinary investigation into the production characteristics of the Mesaverde tight-gas reservoirs in the Green River Basin, and the identification of natural fractures as a previously unrecognized reservoir element. The Champlin 254 Amoco B 2-H was designed to test the contribution of natural fractures in this reservoir and to test the economic viability of horizontal wellbores for Mesaverde tight gas recovery.

LOCATION

The Champlin 254 Amoco B 2-H well is located on the north end of the Standard Draw area in the Echo Springs Field (Sec. 23, T20N, R93W). This location was chosen for two reasons: good geologic control and below-average vertical well performance. Figure 2 shows there is a high density of wells in the vicinity of the Champlin 254 Amoco B 2-H, and Figure 3 shows a natural fracture in the Almond core from the Champlin 254 B No. 1 well. Fractures in this vertical offset, or *parent* well, to the Champlin 254 Amoco B 2-H were a positive indication that a horizontal well might be successful at this location. The high-density well control allows formation dip to be reliably determined, a prerequisite for planning a horizontal well.

In addition to the good geologic control, the location was also selected because of the below-average production of the Champlin 254 B No. 1 parent well. Basin-wide, Almond production is highly variable. There are "sweet spots" (areas with excellent well productivity), and other areas with lower well productivity. The estimated ultimate recovery (EUR) for the Champlin 254 B No. 1 is 5.24 BCF, about half the field-wide average of 10 BCF per well. It was hoped that horizontal completions could improve the per well productivity in areas not in the "sweet spots".

Figure 2 Upper Almond (Marine) Net Sandstone Isopach Map



Post-lithification reverse fault with quartz mineralization along fault related porosity.

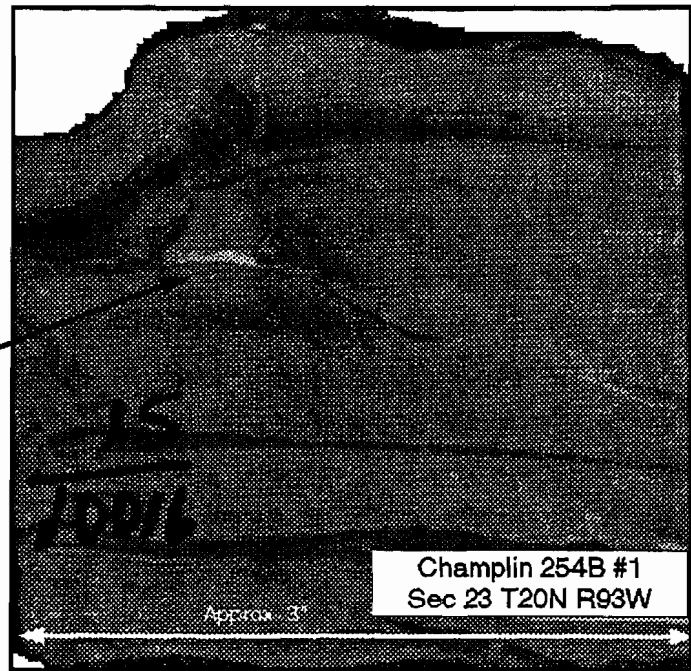


Figure 3 Brittle Deformation in the Champlin 254 B 1 Core

DRILLING AND GEOSCIENCE PROGRAM

Pilot Hole

The drilling program was designed to encounter and minimize damage to as many vertical natural fractures as possible. It was also imperative to preserve directional flexibility until the dominant fracture orientation could be identified. A disposable, deviated (30°) pilot hole was initially drilled to the northwest and penetrated 390 ft vertically into the Almond Formation. A deviated pilot hole was chosen to increase the likelihood of crossing vertical natural fractures. A salt-based mud was chosen over conventional water-based muds to reduce the possibility of having weighting agents, such as barite, block fracture permeability. The total depth of the pilot hole was 10,456 ft (10,340 ft true vertical depth).

The geoscience program in the pilot hole was designed to determine the predominant fracture direction before kickoff of the horizontal leg, and to acquire sufficient data to post-appraise the well. Data acquisition in the pilot hole included: MWD gamma ray, 60 ft of oriented core, Formation MicroImager, Induction, Density-Neutron, Dipole Sonic, and a three component vertical seismic profile (VSP). Log data were "log-netted" back to a Denver computing center for processing and interpretation. On-site electromagnetic goniometer measurements (EMG) were made on the oriented core in a mobile, core-description trailer to determine fracture orientation. In addition to EMG measurements, Anelastic Strain Recovery (ASR) measurements were also made on the core at the wellsite.

Core and log information confirmed the presence and predominant direction of natural fractures. Seven natural fractures were observed in the core, six were partly open. Initial quartz and later calcite cementation is observed on the open fracture faces. The closed natural fracture is completely occluded by calcite. Core EMG measurements indicate that fractures strike between N60° to 70°E, and, on average, dip 87°. Formation MicroImage analysis revealed 20 superior quality fractures which also strike N60° to 70°E and dip 84°. There was little difficulty relating features seen in the core to images on the workstation. The dominant fracture direction trends northeast-southwest, and the horizontal leg was drilled to the south to cross these fractures. Figure 4 illustrates the well's surface location, pilot hole direction and target area (i.e., constrained area based on lease line considerations).

Horizontal Hole

The initial drilling program for the horizontal well called for drilling the build section with a 12-1/4-in. drilling assembly to 90°, penetrating the upper 3 ft into the Upper Almond reservoir, setting 9-5/8-in. casing, and drilling horizontally for 2,000 ft. Three cores were planned for the horizontal leg, as well as MWD gamma ray, and drillpipe-conveyed Formation MicroScanner and LDT/CNL/GR logs. Unfortunately, the 12-1/4-in. assembly encountered severe drag near 78° deviation from vertical, which resulted in penetrating too far into the Upper Almond without reaching horizontal. There was no indication from samples or gas shows when the Upper Almond was penetrated. Nine and 5/8-in. casing was set 12 vertical feet into the Upper Almond, and drilling continued with the more flexible 8-1/2-in. drill string. Even with the more flexible drill string, the borehole could not be turned sharply enough to avoid penetrating 300 ft laterally into the underlying marine shale. The rest of the drilling program proceeded according to plan, with 1,700 ft of horizontal leg in the objective zone as shown in Figure 5. The wellbore was drilled to a measured depth of 12,310 ft (9,970 ft TVD).

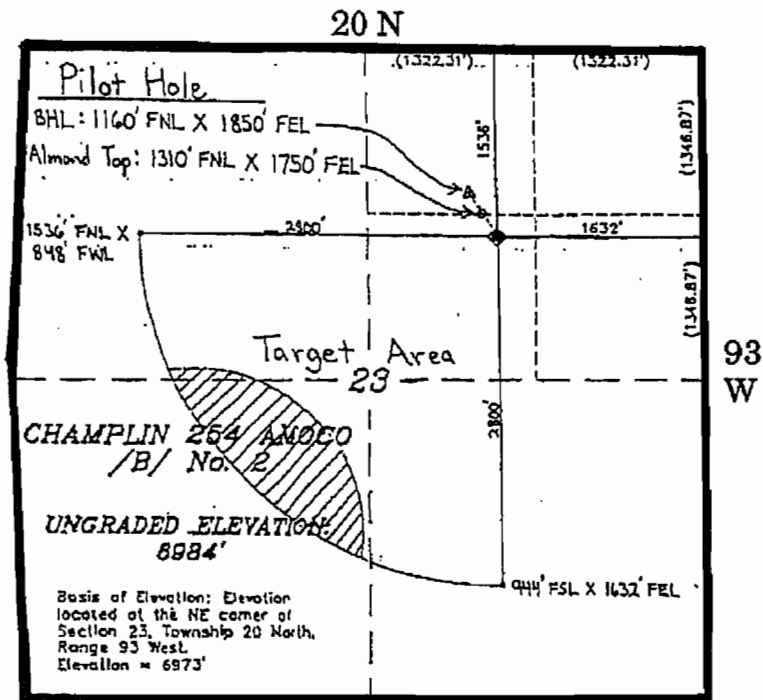


Figure 4 Drilling Plat for Champlin 254 Amoco B 2-H Showing Target Area

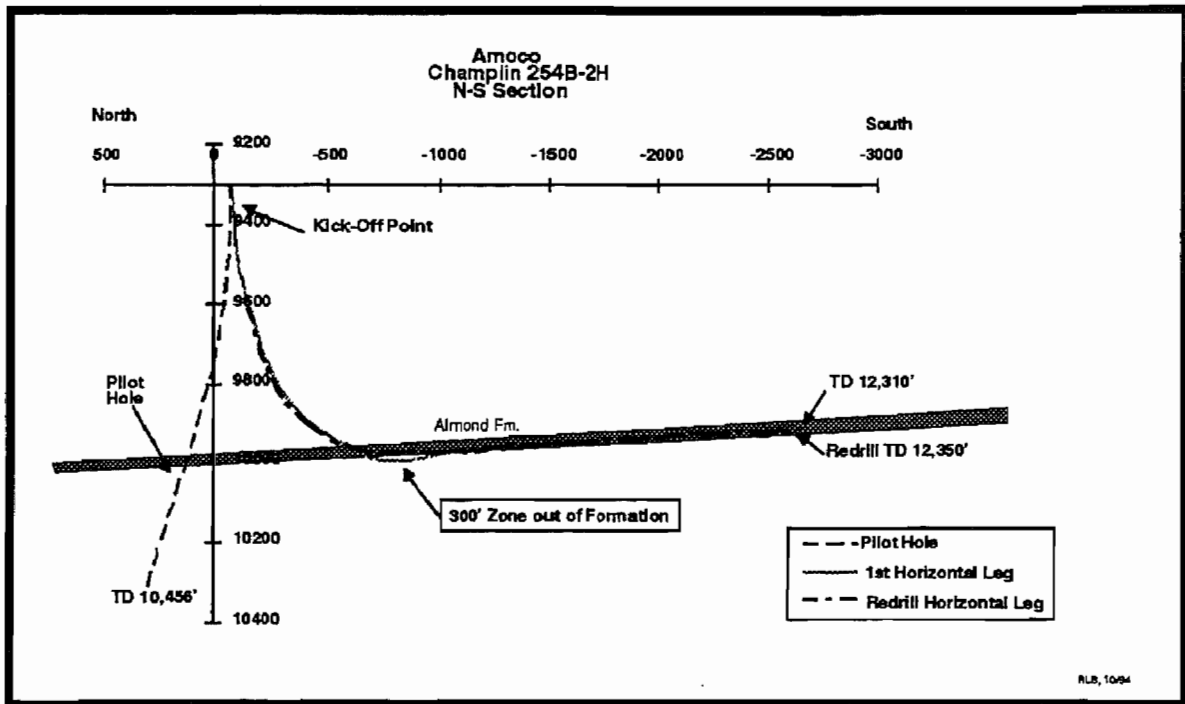


Figure 5 Pilot and Horizontal Wellbore Diagram

The success of the geoscience program was not hindered by the drilling problems encountered in the early phase of the horizontal leg. Three 30-ft cores were cut and retrieved with 100 percent recovery in the horizontal leg. Two cores were cut back to back (10,781 to 10,842 ft) in which three natural fractures were observed. As in the pilot hole, these fractures were lined with quartz and calcite and were oriented N60° to 70°E, dipping 86° to 89°. Four natural fractures were observed in the last core (11,091 to 11,122 ft). These fractures appeared to be only cemented with quartz. Strikes and dips were the same as the two previous cores. One-hundred and forty two superior quality MicroScanner fracture images had a mean azimuth of N67.9°E and a mean dip of 87.1°. ASR measurements were also made on these cores. Density-Neutron logs indicated a homogenous sandstone with 11 percent cross-plot porosity.

COMPLETION

The completion of the horizontal leg was designed to be as simple as possible. Four completion options were initially considered, the ultimate choice depending largely on perceived borehole stability. Option 1 was an open-hole completion with tubing hanging at the lowest spot in the wellbore. Option 2 was to place a slotted liner without cement. Option 3 was to place a slotted liner with external casing packers (i.e., without cement). Option 4 (least preferable) was to cement conventional casing and perforate. There were no indications that the borehole would collapse so Option 1 was chosen; 2-7/8-in. tubing was hung by the drilling rig, the location was cleared, and the wellbore was reverse circulated with nitrogen. The well had initial production of 1.6 MMSCFD that rose to 2.1 MMSCFD within one week.

PRODUCTION HISTORY

From the maximum of 2.1 MMSCFD, the rate stabilized at 1.0 MMSCFD for approximately two months, as shown in Figure 6. Line pressure was fluctuating greatly during the last month of production due to a field-wide compression installation. The relatively modest production rate from the horizontal wellbore was inferred to be an indication of possible formation damage. An attempt was made to flush the wellbore to improve production, during which the marine shale at the lowest point of the wellbore collapsed and 45 ft of tubing was lost in the hole. The drilling rig was brought back to clean out the wellbore, set a liner, and reestablish production. The original borehole eventually completely collapsed in the shale, and the decision was made to plug back the original wellbore and redrill another horizontal leg.

RE-DRILL HISTORY

The redrill horizontal leg was kicked off after the original wellbore was plugged back and a whip stock set. Figure 7 is a plan view showing the relative positions of the pilot and two lateral boreholes. The redrill horizontal was drilled under-balanced with oil-based mud

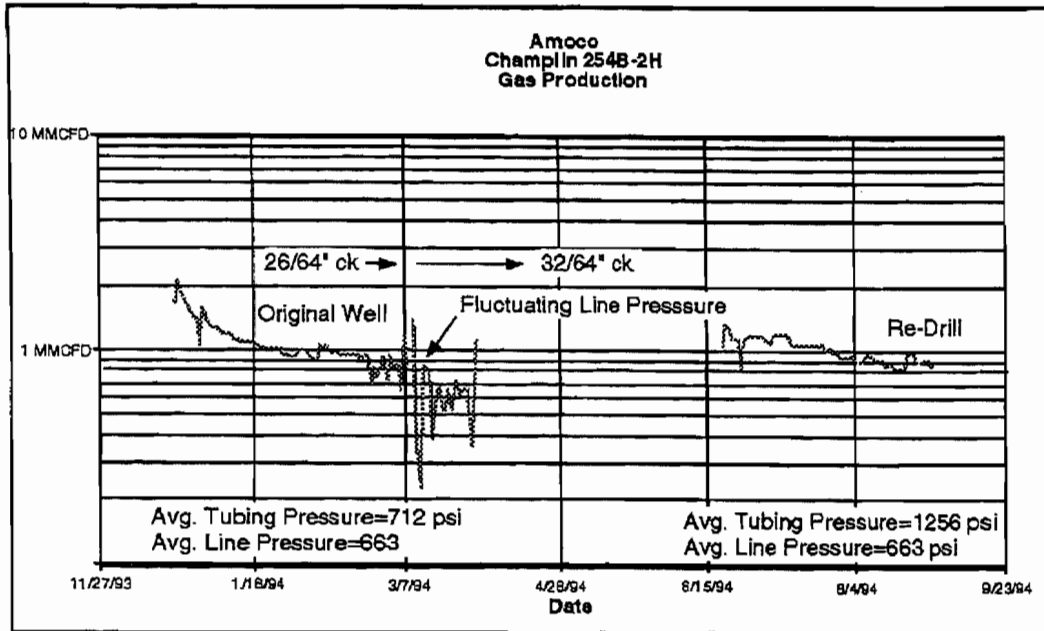


Figure 6 Production History for the Champlin 254 Amoco B 2-H

because minimization of formation damage remained a priority. The remediation of salt-based muds made it cost effective to use oil-based mud in this case. The new wellbore was drilled successfully to a measured depth of 12,350 ft (9,960 ft TVD) with the entire 2,100-ft lateral in zone. The initial production of the original borehole caused near-wellbore depletion, resulting in balanced drilling of the redrill horizontal at 8.9 lb/gal invert mud. Maximum mud weight in the original horizontal wellbore was 9.8 lb/gal.

The redrill completion consisted of a 5-1/2-in. pre-perforated liner (pre-perforated every third joint, 1 shot-per-ft, 90° phasing) placed without cement, and 2-7/8-in. tubing hung in the low point of the wellbore. The redrill had initial production of 1.0 MMSCFD which rose to 1.3 MMSCFD within one week. Production stabilized at 1.0 MMSCFD as shown in Figure 6.

COST

The Champlin 254 Amoco B 2-H initial AFE cost was \$2,100,000 and was drilled for \$1,975,000. Approximately \$600,000 was spent on geoscience-related costs. The redrill AFE cost was \$370,000 and was drilled for that amount. A third well was re-designed to employ the under-balanced technology and the oil-based mud system. Without the \$600,000 in geoscience costs, this well is projected to cost \$1,400,000. Ultimately, the goal is to bring costs down to \$1,000,000.

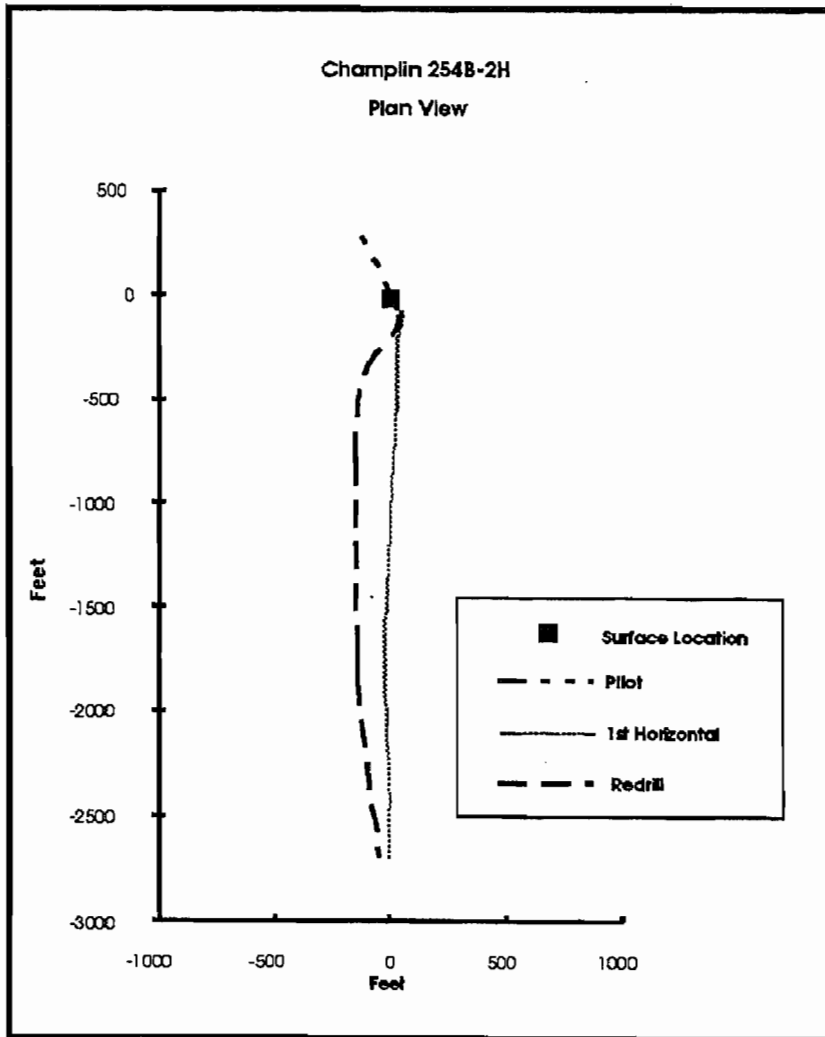


Figure 7 Plan View Showing the Trajectory of the Redrilled Horizontal Lateral

CONCLUSIONS

Amoco demonstrated the ability to drill and complete horizontal wellbores in tight-gas reservoirs in the Greater Green River Basin. The geoscience program for this well was successfully completed in its entirety. Open natural fractures are present, as predicted, in the subsurface at this location and are lined with quartz and calcite cements. There is excellent agreement between log and core fracture measurements. Fractures strike N60° to 70°E and dip nearly vertical. It is the lateral continuity of the natural fractures and their contribution to production that remains unresolved. Formation damage and remediation remains an important issue in the drilling and completion of tight formation horizontal gas wells. For the Wamsutter area, the best practice appears to be drilling under-balanced with invert mud and completing with a slotted liner.

Natural Fractures and Stress Orientations in the Almond Formation, Wamsutter Area, Green River Basin

*Robin E. Hill
CER Corporation*

INTRODUCTION

Collecting geologic information from the Almond Formation was one of the primary objectives of Amoco's Green River Basin Project team in charge of drilling and evaluating the two horizontal wells described in this report, the Champlin 254 Amoco B 2-H (Sec. 23, T20 N, R93W) and the Champlin 320 C-1A-H (Sec. 1, T22N, R96W). Natural fractures were thought to have a significant impact on Almond reservoir permeability prior to starting this project; therefore, characterizing natural fractures was the focus of the geologic data collection efforts. Inclined cores were cut to improve the probability of crossing natural fractures, Formation MicroImager (FMI) logs were run in both pilot holes, and cores and Formation MicroScanner (FMS) logs were obtained from the horizontal laterals of both wells. The wells were drilled in a direction to maximize the number of natural fractures crossed, although lease line constraints were also a consideration in determining hole azimuths.

Where natural fractures are an important part of the reservoir permeability, understanding the in situ stress conditions and their effect on the properties of the fracture system is critical (Laubach and others, 1994; Lorenz and others, 1993). In situ stress affects the measurement and interpretation of geophysical data, petrophysical properties (such as porosity and permeability), rock strength and ductility. In addition, the stress field can change as the reservoir pressure is depleted; this can severely impact reservoir and fracture permeability (Teufel and others, 1991). For these reasons, a significant effort was applied to interpreting in situ stress direction. Specifically, cores were examined for drilling-induced fractures, FMI calipers were examined for borehole breakouts, and anelastic strain recovery data were obtained from the cores.

This report presents the results of the natural fracture and in situ stress characterizations that were performed on the two wells using the core and log data that were collected by Amoco. Related geologic studies of mineralogy and microscopic analysis of fracture characteristics is presented by Dunn (this volume).

REGIONAL SETTING

Figure 8 shows the locations of the Champlin 254 Amoco B 2-H and Champlin 320 C-1A-H wells within the Greater Green River Basin. The basin consists of four intrabasin uplifts (Cherokee Arch, Moxa Arch, Rock Springs Uplift, and Wamsutter Arch) and four subbasins (Great Divide, Green River, Sandwash, and Washakie). The wells are located north of the

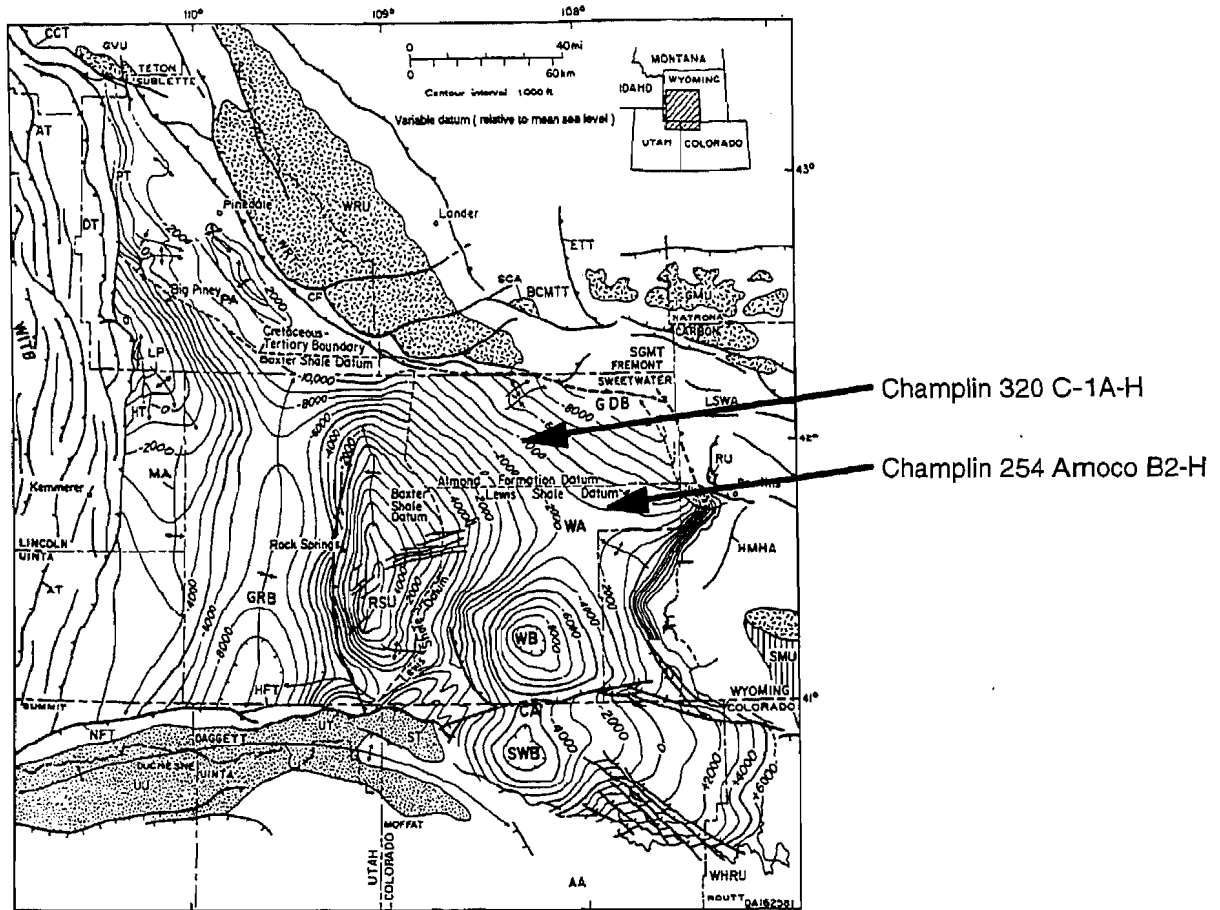


Figure 8 Regional Geologic Map of the Greater Green River Basin (from Dutton and others, 1993)

Wamsutter Arch between the Washakie Basin to the south and the Great Divide Basin to the north. The faults shown on the east flank of the Rock Springs Uplift (RSU on the map) strike about N80°E.

There are two dominant fault orientations in the vicinity of the two wells, as shown on a commercially available structure map of the Wamsutter Arch (based on a Lewis Shale datum). Two large faults located about 15 miles east of the Champlin 254 Amoco B 2-H well strike N45°E and produce mappable offset of the Lewis Shale. The second orientation is from numerous minor faults in the vicinity with strikes that range from N45° to 75°E; however, none of these faults offset the Lewis Shale at the map scale.

The regional tectonic stress map of the continental United States shows that the western part of the Greater Green River Basin lies in the Cordilleran extensional stress province where the maximum horizontal stress direction (σ_H) trends north-northwest. However, the eastern portion of the basin may be in the mid-continent compressional stress province that has an east-northeast to east σ_H (Zoback and Zoback, 1989). In a study of five Frontier Formation wells, located along the Moxa Arch, Laubach and others (1992) found wells with σ_H

that were compatible with both stress provinces. In fact, different sands within the same well often have different orientations. The variable results for σ_H were attributed to the influence of natural macro- and microfractures and low horizontal-stress anisotropy in the area.

Since the Champlin 254 Amoco B 2-H well is more than 100 miles east of the Moxa Arch study area, it is more likely that this well is in the mid-continent stress province with σ_H being east-northeast to east. However, local structural complexities and previous work suggest that regional stress data may be quite variable in the Greater Green River Basin, and for this reason, a significant effort has been made to interpret σ_H in the two study wells.

FRACTURE CHARACTERIZATION

Champlin 254 Amoco B 2-H Core Results

Four oriented cores were taken from the Champlin 254 Amoco B 2-H well as follows:

- Core No. 1 - 10,025.0 to 10,076.0 ft (51 ft recovered)
- Core No. 2 - 10,781.0 to 10,811.5 ft (30.5 ft recovered)
- Core No. 3 - 10,811.5 to 10,841.8 ft (30.25 ft recovered)
- Core No. 4 - 11,091.0 to 11,121.8 ft (30.8 ft recovered)

Seven natural fractures were oriented from pilot Core 1 which was inclined 30° from vertical in the direction N15°W. These fracture strikes are shown in Figure 9, and these data, along with the anelastic strain recovery (ASR) orientations, were used to select the direction to drill the subsequent lateral.

Cores 2 and 3 were cut in the production lateral (azimuth S2°W and inclined 92° from vertical), and Core 4 was cut in the same azimuth as Cores 2 and 3 but up-dip in the formation. Only three fractures were observed in Cores 2 and 3, but there were six fractures described in Core 4, four natural fractures and two "possibly induced" fractures. The fracture strikes from Cores 2, 3 and 4 are shown in Figure 10.

Champlin 254 Amoco B 2-H FMI Analysis

In addition to the deviated core taken from the pilot hole, a Formation MicroImager (FMI) log was also run in the pilot hole prior to plugging-back and kicking-off the horizontal lateral. The results of the FMI workstation analysis of the pilot well are shown in Figure 11. Twenty fractures were identified which have a mean strike of N66°E. All but two of the fractures dip to the southeast. These results are consistent with the oriented core fractures shown in Figure 12 which have a mean strike of N57°E, and, if the two shallow-dipping fractures are excluded, the mean strike is N63°E, just 3° less than FMI results.

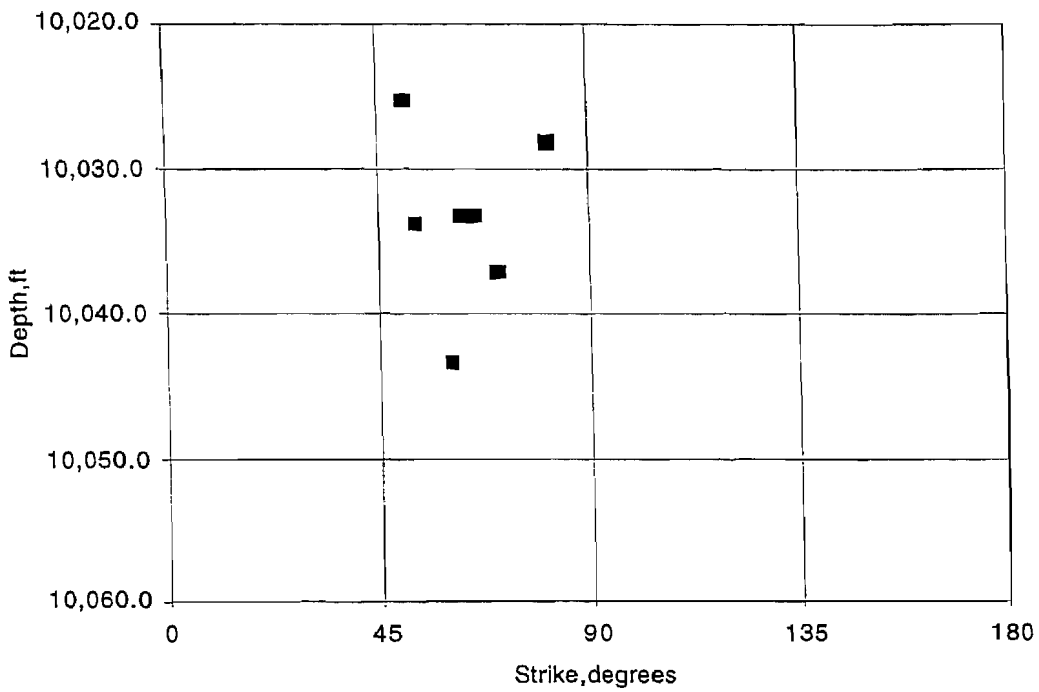


Figure 9 Natural Fracture Strikes from Core No. 1 (Pilot Hole), Champlin 254 Amoco B 2-H Well

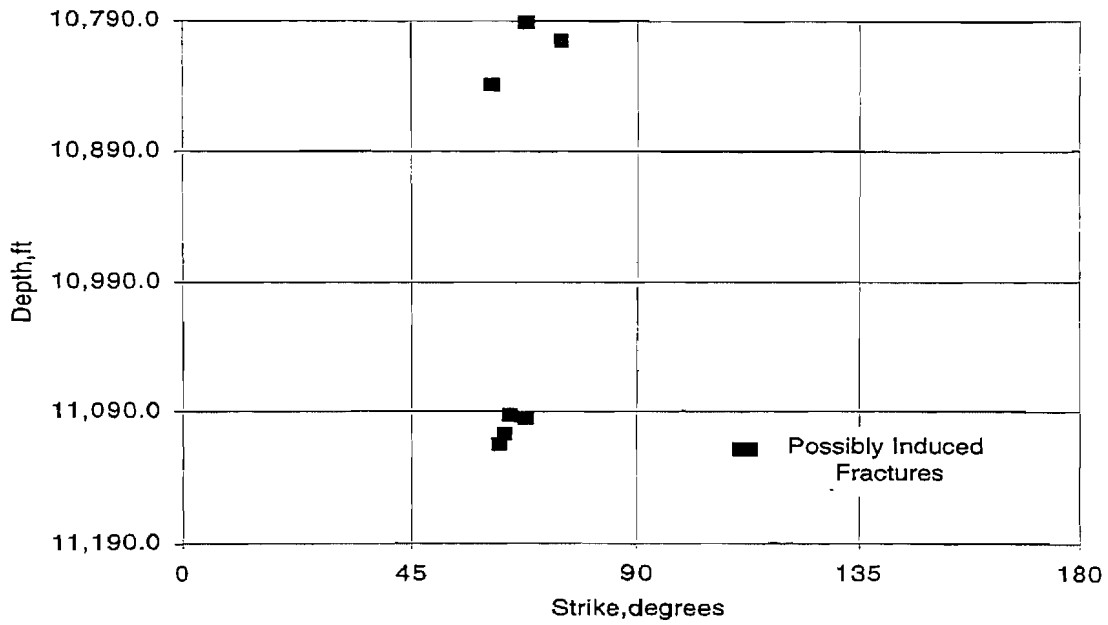


Figure 10 Natural Fracture Strikes from Cores 2, 3 and 4, Champlin 254 Amoco B 2-H Well

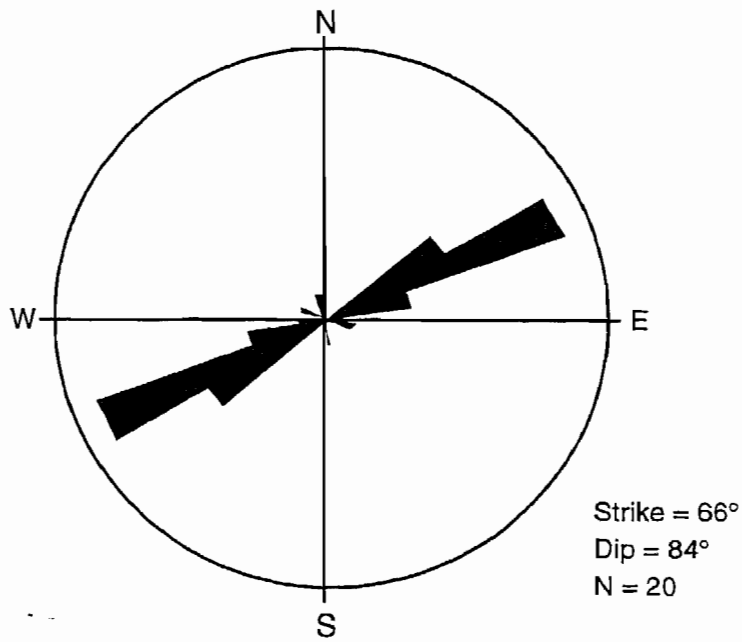


Figure 11 Rose Diagram of FMI-Interpreted Fractures from Pilot Hole, Champlin 254 Amoco B 2-H Well

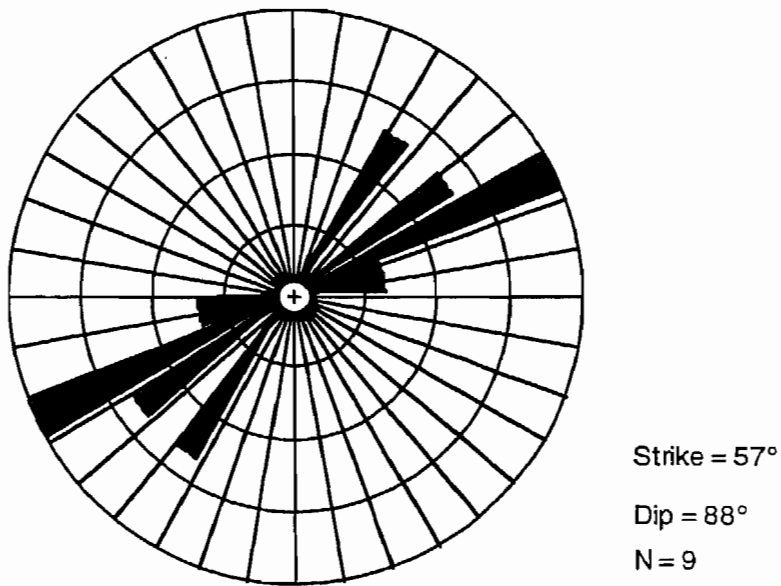


Figure 12 Rose Diagram of Core Fractures from Pilot Hole, Champlin 254 Amoco B 2-H

Champlin 254 Amoco B 2-H FMS Analysis

Orientation

Figure 13 is a rose diagram showing the 263 fracture strikes measured on the FMS workstation analysis of the horizontal lateral in the Champlin 254 Amoco B 2-H well. These fractures have an average strike of N68°E and an average dip of 87°; thus, the fractures are nearly vertical.

These FMS results are consistent with core results from the three horizontal cores. Figure 14 is a rose diagram of natural fracture strikes from the three horizontal cores for comparison.

Spacing

Fracture spacing information was obtained by digitizing the depths where fractures were identified on the Formation MicroScanner (FMS) imagery. Figure 15 shows the spacings as they appear in the borehole, not corrected to true spacing. Since the angle of incidence of the borehole to the fractures is about 66°, the spacings tabulated can be multiplied by 0.913545 ($\sin 66^\circ$) to approximate true spacing. The mean fracture spacing as seen in the borehole is 11.16 ft which is approximately 10.2 ft true spacing. The distribution is strongly skewed toward closer spacings. The median spacing is 7.6 ft (6.9 ft true spacing), and the highest frequency of spacings is the interval from 4 to 5 ft. This indicates the data is strongly skewed toward closer spacings, a characteristic of fractures which has been described in Mesaverde cores from another Rocky Mountain basin (Lorenz and Hill, 1994).

These spacing data are based on FMS interpretation and are not directly comparable to core or outcrop spacing measurements. This is because fractures that are very closely spaced may not be distinguishable on the FMS imagery, and, when over 250 fractures are being measured, it becomes too tedious to try to measure every single fracture. Therefore, it is probable that the fracture spacings for the Champlin 254 Amoco B 2-H well are maximum values. Fracture spacings are likely even more skewed toward closer spacings as has been observed in other studies of core and outcrop (Lorenz and Hill, 1994; Lorenz and Laubach, 1994).

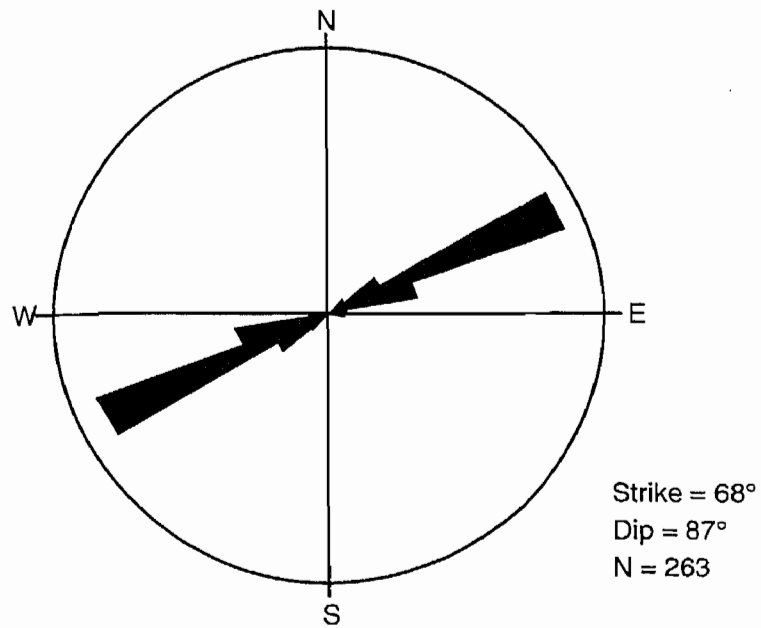


Figure 13 Rose Diagram of FMS-Interpreted Fracture Strikes in the Horizontal Well, Champlin 254 Amoco B 2-H

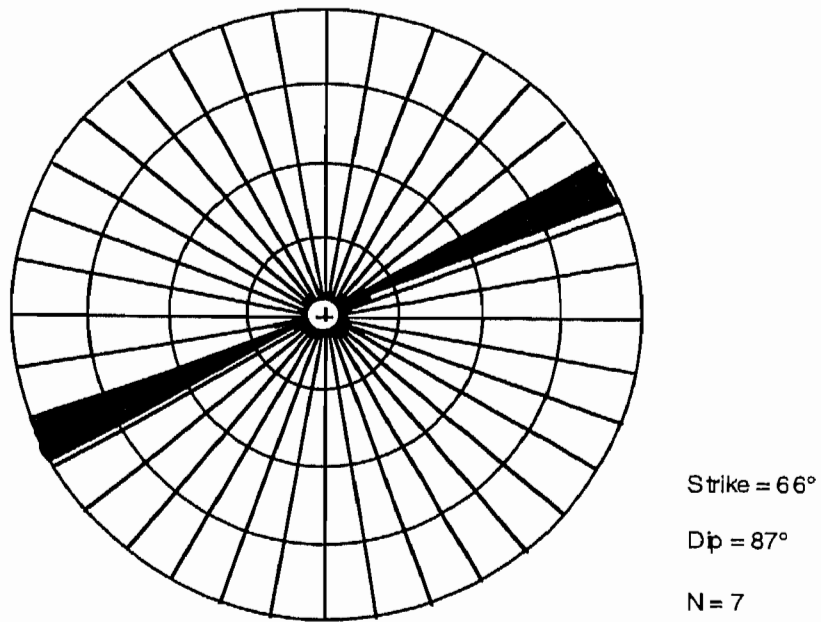


Figure 14 Rose Diagram of Natural Fractures in Horizontal Core, Champlin 254 Amoco B 2-H

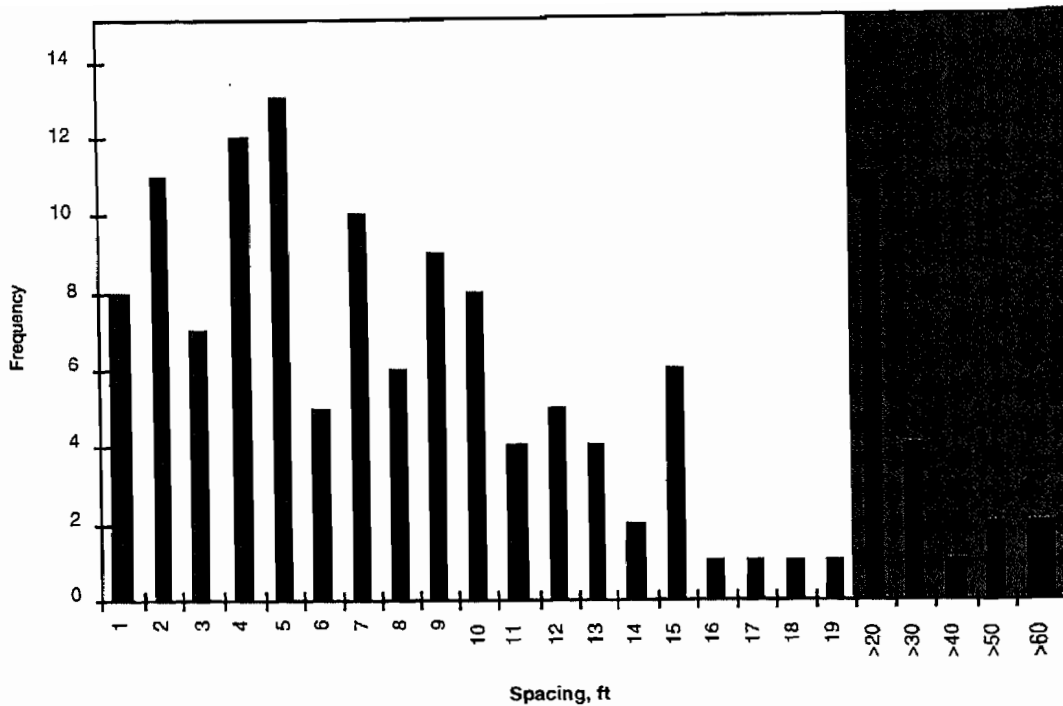


Figure 15 Frequency Histogram of Fracture Spacing, Champlin 254 Amoco B 2-H

Champlin 320 C-1A-H Core Results

Similar to the Champlin 254 Amoco B 2-H well, four oriented cores were taken from the Champlin 320 C-1A-H well as follows:

- Core No. 1 - 10,345.0 to 10,406.0 ft (61 ft recovered)
- Core No. 2 - 10,474.0 to 10,505.0 ft (31 ft recovered)
- Core No. 3 - 12,220.0 to 12,250.5 ft (30.5 ft recovered)
- Core No. 4 - 12,250.5 to 12,281.8 ft (30.8 ft recovered)

Core 1 was cut in the pilot well which was deviated about 30° to the south to increase the probability of crossing natural fractures. Unfortunately, only one fracture, classified as "possibly induced", was observed in the core. With this limited data, the well was drilled to the north since this would cross easterly striking natural fractures as had been seen in the Champlin 254 Amoco B 2-H well and was also good for lease line considerations.

The Almond is nearly 200 ft thick in this well, much thicker than in the Champlin 254 Amoco B 2-H well. Because of the greater thickness, the well was designed to slant through the entire section at about 70° before building angle to about 95° (i.e., reversing angle to intentionally drill up into the pay zone). Core 2 was cut in the 70° slant portion of the well

in the direction N10°E, and Cores 3 and 4 were cut from the 95° portion of the well at an azimuth of 0° (due north).

Macroscopic natural fractures were not obvious in the cores from the Champlin 320 C-1A-H well. One fracture in Core 2 and two fractures in Core 3 were classified as natural fractures, but these were not mineralized and their classification is uncertain. The other 12 fractures encountered are classified as “possibly induced.” The core fracture strikes are shown in Figures 16 and 17.

Champlin 320 C-1A-H FMI Analysis

The results of the FMI interpretation for the pilot hole of the Champlin 320 C-1A-H well are shown in Figure 18. Of the 37 interpreted fractures, only 4 are in the Almond. All four of these fractures are classified as “C-Quality” fractures; their strikes are N82°, 83°, 84°, and 90°E. The 18 “A-Quality” fractures have a mean strike of N77°E and are all from the overlying sands within the Lewis Shale. Of the 263 fractures described from the Champlin 254 Amoco B 2-H well, 142 are classified as “A-quality” which means the fracture’s presence is obvious from the imagery, and the orientation is reliable. “C-Quality” implies the fracture’s presence and orientation cannot be ascertained from the imagery. “C-Quality” is the lowest quality that can be discerned on the workstation. Only 54 of the 263 fractures measured in the Champlin 254 Amoco B 2-H well were classified as “C-Quality.” However, because of the large number of fractures in the well, there are probably many more “C-Quality” fractures that were not measured.

Champlin 320 C-1A-H FMS Interpretation

Nearly 200 fractures were interpreted from the FMS log run in the Champlin 320 C-1A-H lateral. However, these had poor expressions on the imagery. In fact, only three fractures of similar quality to the 142 fractures measured in the Champlin 254 Amoco B 2-H well were observed in the Champlin 320 C-1A-H well. The mud system for both wells had similar conductivity, so if fractures of comparable quality were present in the Champlin 320 C-1A-H well, they would have been observed on the FMS imagery. Thus, the contribution of natural fractures to reservoir permeability in the Champlin 320 C-1A-H well is less apparent than in the Champlin 254 Amoco B 2-H well (see Branagan, this volume). The Almond was eventually plugged back in the Champlin 320 C-1A-H to implement a completion in the overlying Lewis.

INTERPRETATION OF IN SITU STRESS DIRECTION

Numerous techniques have been used for interpreting maximum horizontal stress direction (σ_H) (Hill and others, 1993). The techniques applied to the Champlin 254 Amoco B 2-H and Champlin 320 C-1A-H wells are anelastic strain recovery (ASR), borehole breakouts, and drilling-induced fractures.

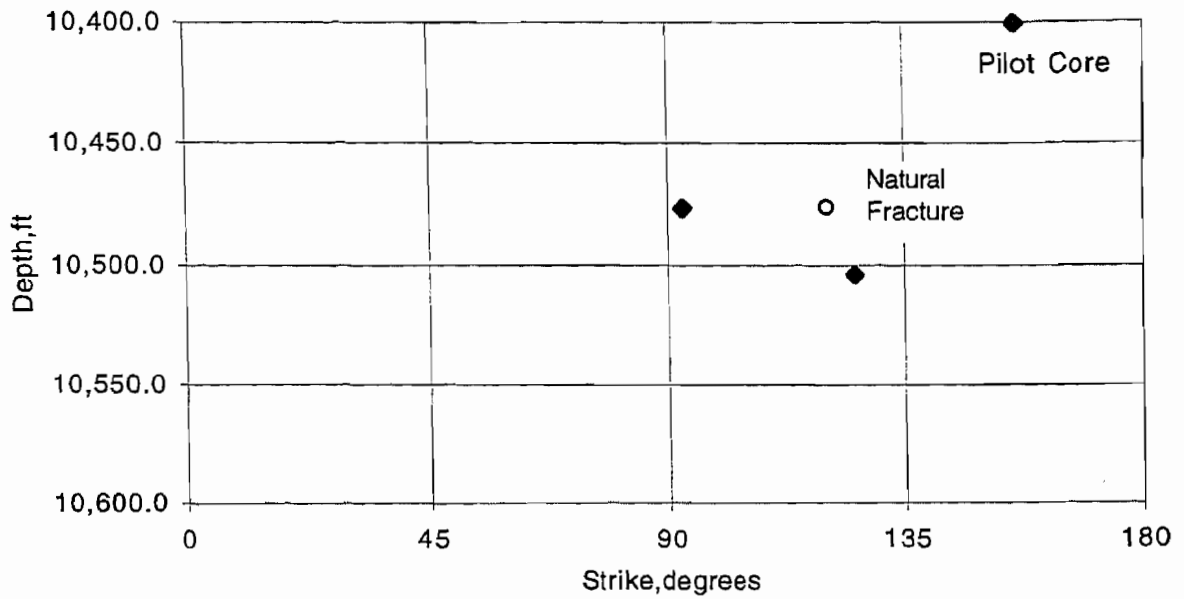


Figure 16 Fracture Strikes from Cores 1 and 2, Champlin 320 C-1A-H

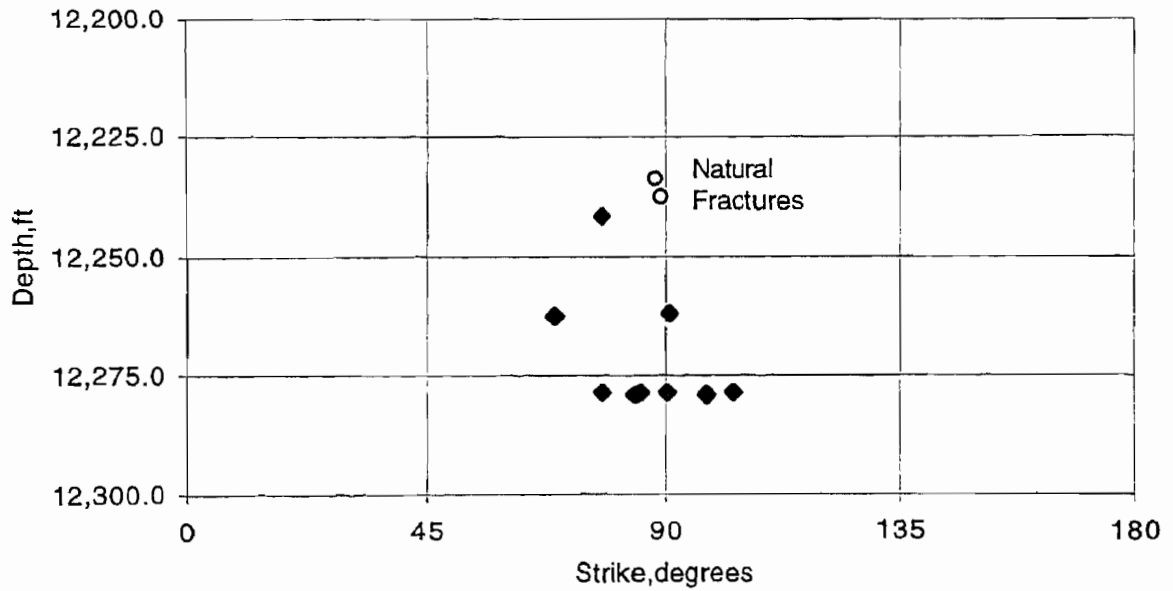


Figure 17 Fracture Strikes from Cores 3 and 4, Champlin 320 C-1A-H

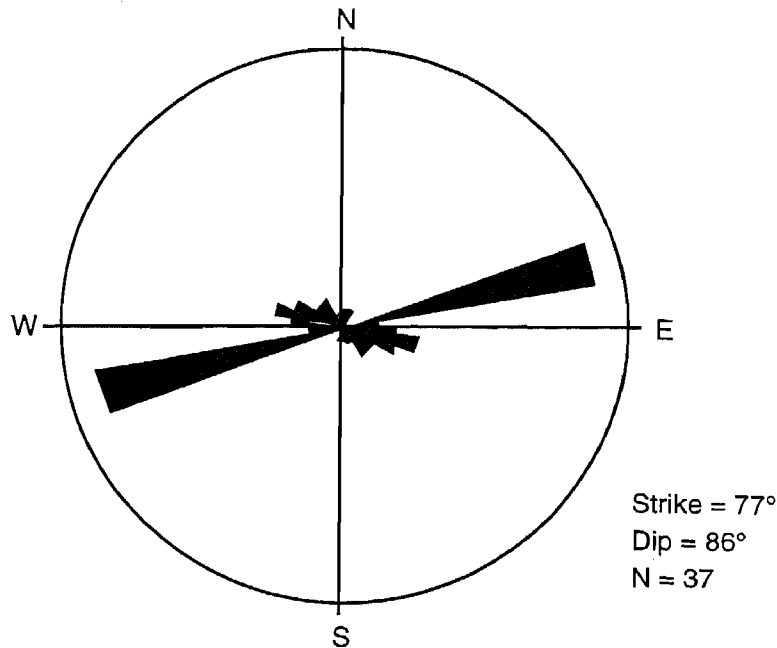


Figure 18 Rose Diagram of FMI Interpretation of Pilot Hole, Champlin 320 C-1A-H Well

ASR Results from Champlin 254 Amoco B 2-H Pilot Core

Anelastic strain recovery is a stress orientation technique where the core is instrumented with strain gauges as soon as possible after a core is recovered at the surface. The gauges record the strain relaxation over a 12- to 48-hour time period; and these data are then used to interpret σ_H . For the Champlin 254 Amoco B 2-H core, Sandia National Laboratories analyzed three ASR samples from the 30° pilot core, and Amoco Research analyzed a sample adjacent to Sandia Sample No. 1. Sandia Sample No. 2 had a gauge failure; however, the data from the other gauges are compatible with the result from Sample No. 1. The σ_H directions interpreted from Samples 1 and 3 are S59°E and N83° to 94°E, respectively. Sample No. 3 has a range value because the sample was still relaxing when the gauges were turned off. The Amoco sample adjacent to Sandia Sample No. 1 yielded a σ_H direction of S66°E.

A memorandum to Amoco indicates that the axial strains are intermediate to the horizontal strains, suggesting that overburden stress is the intermediate stress; however, shale laminations may be affecting the axial readings (Warpinski, 1994). Sandia also attempted velocity anisotropy, a technique for measuring σ_H based on directional variations in acoustic velocity, on one of the core samples, but there was insufficient anisotropy to interpret σ_H .

Horizontal Core ASR Results

Amoco also analyzed two horizontal core samples from Champlin 254 Amoco B 2-H, but only one of these had useable data. The good data was obtained from Core No. 4, and the results are as follows:

- Maximum Stress N66°W (294° azimuth) dip 45°
- Intermediate Stress N35°E (35° azimuth) dip 9°
- Minimum Stress S46°E (134° azimuth) dip 44°

ASR results from the Champlin 320 C-1A-H are based on the average results of four tests, two samples from 70° core and two samples from 95° core. Samples were instrumented to record strain in ten directions, and the orientations were calculated using a least squares method. The orientation of the three principal stresses interpreted from the ASR samples are as follows:

- Maximum Stress S30°W (210° azimuth) dip 60°
- Intermediate Stress N60°E (60° azimuth) dip 30°
- Minimum Stress N30°W (330° azimuth) dip 20°

These results are significantly different from the Champlin 254 Amoco B 2-H results, and both well's results indicate the principal stress axes are inclined. That is, the vertical stress is not one of the principal stress axes.

Drilling-Induced Fractures

Drilling-induced fractures are fractures that are initiated as a result of the drilling or coring of the well. The strike of these fractures can be used to infer the σ_H direction (Kulander and others, 1978; Kulander and others, 1990)

Two fractures from the Champlin 254 Amoco B 2-H Core No. 4 are classified as "possibly induced". The strikes of these fractures are S67°E and S69°E. There were 12 "possibly induced" fractures from the Champlin 320 C-1A-H cores, and Figure 19 shows these have a vector mean strike of S88°E (92° azimuth).

The σ_H orientations interpreted from the core-based techniques are summarized in Table 1.

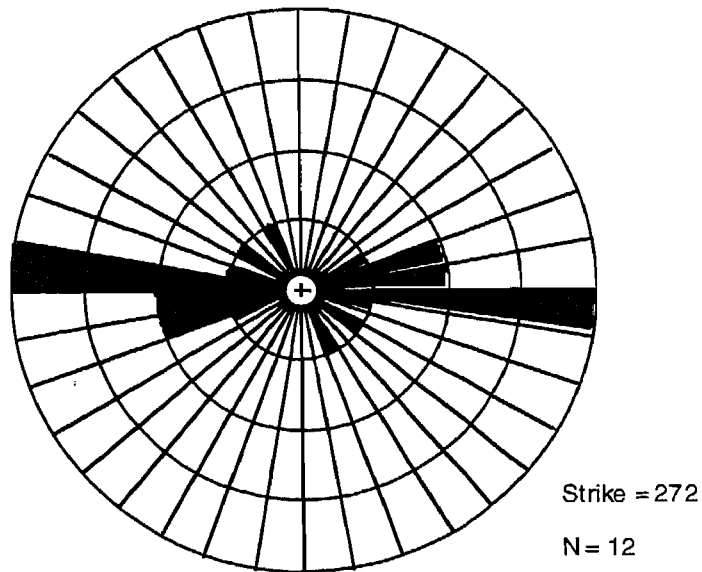


Figure 19 Rose Diagram of Drilling-Induced Fracture Strikes, Champlin 320 C-1A-H

Table 1 Core-Based Maximum Stress Direction Determinations

Data Type	Sample ID	Source	Results
ASR	No. 1	SNL	$\sigma_H = 121^\circ$
ASR	No. 2	SNL	Supports No. 1 Result
ASR	No. 3	SNL	$\sigma_H = 83^\circ$ to 94°
ASR	Adjacent to SNL No. 1	Amoco	$\sigma_H = 114^\circ$
ASR	Core 2	Amoco	Poor Data Quality
ASR	Core 4	Amoco	$\sigma_H = 294^\circ$, 45° dip Intermediate Stress - 35° , 9° dip Minimum Stress - 134° , 44° dip
ASR	Champlin 320 C-1A-H 4 samples	Amoco	$\sigma_H = 210^\circ$, 60° dip Intermediate Stress - 60° , 30° dip Minimum Stress - 330° , 20° dip
Velocity Anisotropy	Unknown	SNL	Insufficient Anisotropy
Induced Fractures	Champlin 254 Amoco B 2-H	Core Lab	$\sigma_H = 112^\circ$
Induced Fractures	Champlin 320 C-1A-H	Core Lab	$\sigma_H = 92^\circ$

FMI Breakout Analysis

Borehole breakouts are elongations created in the borehole in response to the in situ stress field and can be used to interpret σ_H (Gough and Bell, 1978). Oriented calipers from the Formation MicroImager (FMI) log were digitized from the FMI Acquisition Record paper log. The caliper data were then analyzed using a computer algorithm that applies the Plumb and Hickman (1985) criteria for recognizing breakouts from borehole elongations resulting from other phenomenon.

Calipers from the Champlin 254 Amoco B 2-H well were analyzed over the interval from 6,940 to 9,200 ft. The borehole conditions are poor for breakout analysis due to an enlarged borehole. The bit size is 8-1/2 in., but the hole size is never less than 12 in., even for the smaller caliper reading. For good breakout detection, one of the caliper diameters should be within an inch of bit size (Plumb and Hickman, 1985). This criterion was not applied to the Champlin 254 Amoco B 2-H well in order to get some stress information from the caliper data.

Because of the overall enlarged hole, several ellipticity cut-off values were tried in order to get a better statistical result. The general guide for good data is to use an ellipticity cutoff of 0.03 where ellipticity is defined by the equation:

$$Ellipticity(R) = \frac{C1 - C2}{BitSize}$$

where C1 and C2 are the two caliper measurements of hole diameter.

An ellipticity cutoff of 0.03 corresponds to a 0.25 in. difference between the two caliper values in an 8-1/2-in. borehole. Using this value, there is so much scatter to the data that it is difficult to interpret a preferred orientation. Several larger values for ellipticity discrimination were tried and resulted in an ellipticity cutoff of 0.10. This change in ellipticity cutoff reduces the number of breakouts from 66 to 11. The maximum horizontal stress direction interpreted from breakouts (orthogonal to breakout direction) for the Champlin 254 Amoco B 2-H well is shown in Figure 20. The dominant σ_H orientation interpreted from breakouts is N40°E to N50°E. There is also a subdominant σ_H orientation in the S60°E to S70°E which is more compatible with the σ_H interpreted from pilot core ASR results and the two drilling-induced fractures from Core 4.

Oriented calipers from the Champlin 320 C-1A-H were analyzed over the interval 6,990 to 10,520 ft. These data could be analyzed using the Plumb and Hickman (1985) criteria without modification. The interpreted σ_H from the 74 breakouts detected is shown in Figure 21. Although this breakout data is considered excellent quality, the interpreted σ_H is not compatible with the other stress data from this well.

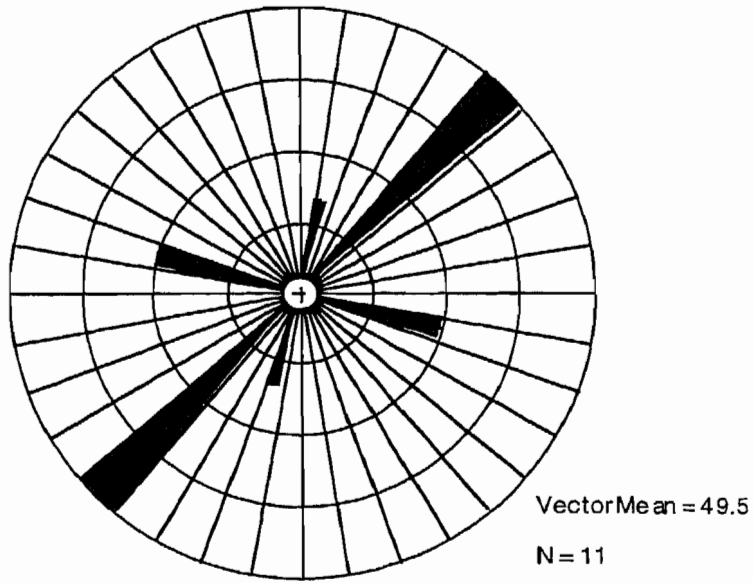


Figure 20 σ_H Interpreted from Borehole Breakouts, Champlin 254 Amoco B 2-H

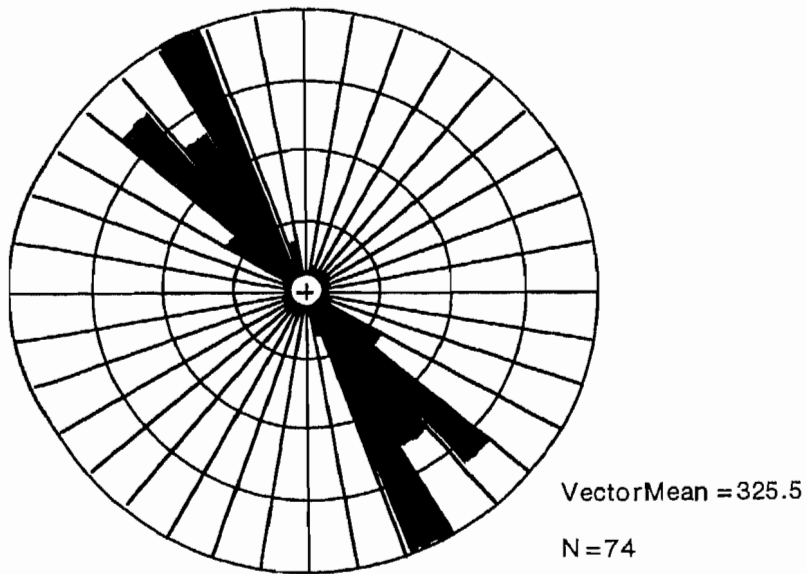


Figure 21 σ_H Interpreted from Borehole Breakouts, Champlin 320 C-1A-H

CONCLUSIONS

Based on the core and image log results for the Champlin 254 Amoco B 2-H well there appears to be a well-developed natural fracture set that strikes N65° to 70°E. These fractures were present in core, and more than 250 were measured in the horizontal well FMS log.

In contrast, natural fractures are interpreted to be poorly developed in the Champlin 320 C-1A-H well. The fractures classified as natural in the core were not mineralized, so their origin remains ambiguous; the image log analysis of the Champlin 320 C-1A-H well only identified three fractures of a comparable quality to the Champlin 254 Amoco B 2-H well. It is inferred therefore, that natural fractures are poorly developed in the Champlin 320 C-1A-H well Almond section. The Almond was eventually plugged-back in the well, and it currently produces gas from sands within the Lewis Shale where fractures are observed in the image logs.

In situ stress directions for the Champlin 254 Amoco B 2-H well and cored natural fractures are shown in Figure 22. The ASR stress azimuths and fractures are shown on a stereographic projection that is overlain on a rose diagram of breakout orientation. The intermediate stress axis, which has a shallow dip, is oriented nearly perpendicular to the natural fractures. This stress alignment could permit hydraulic fractures to grow in an orientation that crosses natural fractures at an oblique angle.

Figure 23 is a similar plot for the Champlin 320 C-1A-H. The principal stress axes are poorly aligned with the east-west striking natural fractures as measured from low quality FMS fractures. This poor alignment of stresses may keep natural fractures from having significant apertures which may account for the poorer production from wells in this area.

The overall poor compatibility of borehole breakouts with the three-dimensional ASR results could be explained by the effect that a deviated stress field can have on breakouts. Conventional breakout analysis is based on the assumption that the vertical stress is one of the principal stress axes, and when this condition is not true, breakout orientation is not aligned with the minimum horizontal stress (Mastin, 1988). This could undermine the use of borehole breakouts for stress interpretation in this area, assuming the ASR results are correct.

ACKNOWLEDGMENTS

The information presented in this paper was collected from numerous sources. The FMI and FMS workstation interpretation was performed by David Thorn (Schlumberger Well Services) and Lesley Reinert (Amoco). The ASR data from Sandia was taken from a memorandum by Norm Warpinski (Sandia National Laboratories) and the Amoco ASR data was measured by Jason Zhang (Amoco Research). The core fracture orientation data was taken from a Core Lab report prepared by David Foster (Core Lab). Wayne Rowe (Schlumberger Well Services) was a great help in acquiring the log data for the breakout study and copies of FMS workstation results. I also want to thank Tom Dunn (Univ. of Wyoming), John Lorenz (Sandia National Labs) and Lesley Reinert (Amoco) for sharing their knowledge regarding the core fractures and Greater Green River Basin geology.

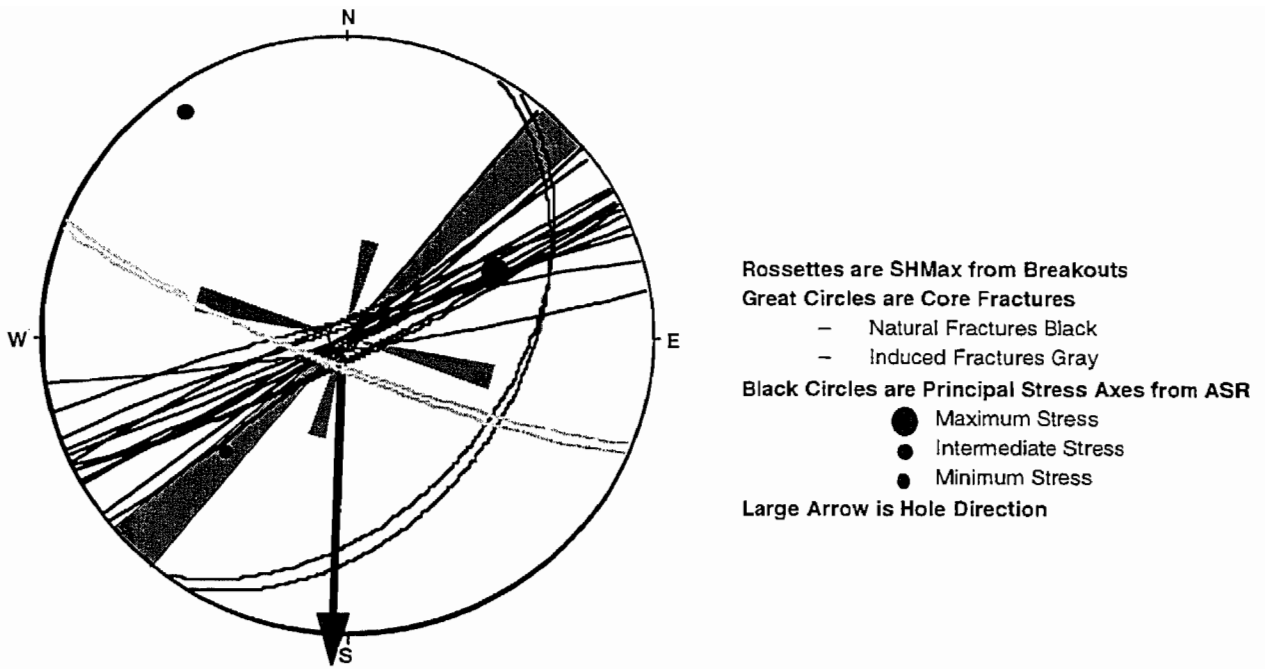


Figure 22 Composite Figure of Fractures, Breakouts, and Stress Directions in the Champlin 254 Amoco B 2-H Well

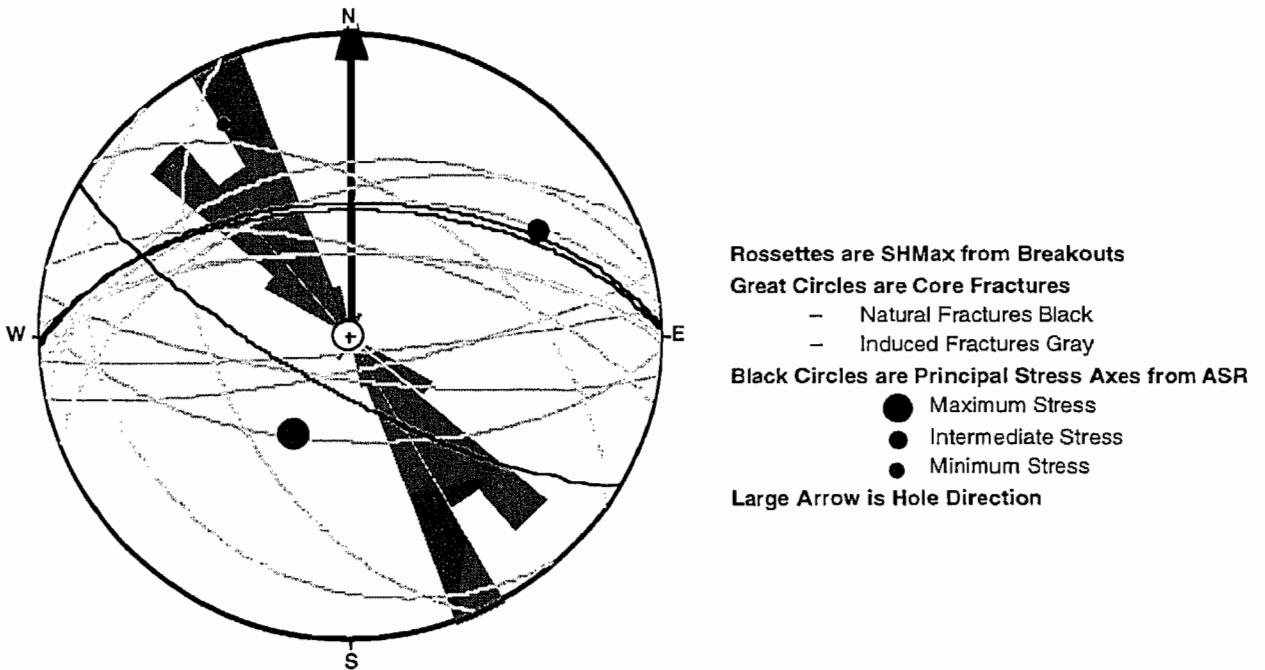


Figure 23 Composite Figure of Fractures, Breakouts, and Stress Directions in the Champlin 320 C-1A-H Well

REFERENCES

Dutton, S.P., S.J. Clift, D.S. Hamilton, H.S. Hamlin, T.F. Hentz, W.E. Howard, M.S. Akhter, and S.E. Laubach, 1993: "Major Low-Permeability-Sandstone Gas Reservoirs in the Continental United States," Bureau of Economic Geology, Report of Investigations No. 211, 221 p.

Gough, D.I. and J.S. Bell, 1981: "Stress Orientations from Oil-Well Fractures in Alberta and Texas," Canadian Journal of Earth Science, V. 18, p. 638-645.

Hill, R.E., R.E. Peterson, N.R. Warpinski, J.C. Lorenz and L.W. Teufel, 1993: "Techniques for Determining Subsurface Stress Direction and Assessing Hydraulic Fracture Azimuth," Gas Research Institute Topical Report, GRI-93/0429, 133 p.

Kulander, B.R., C.C. Barton and S.L. Dean, 1979: "The Application of Fractography to Core and Outcrop Investigations," Morgantown Energy Technology Center, METC/SP-79/3, 174 p.

Kulander, B.R., S.L. Dean and B.J. Ward, 1990: "Fracture Core Analysis: Interpretation, Logging, and Use of Natural and Induced Fractures in Core.," American Association of Petroleum Geologists Methods in Exploration Series, No. 8, 88 p.

Laubach, S.E., S.J. Clift, H.S. Hamlin, S.P. Dutton, T.F. Hentz, H. Baek and B.A. Marin, 1994: "Geology of a Stratigraphically Complex Natural Gas Play: Canyon Sandstones, Val Verde Basin, Southwest Texas," Gas Research Institute Topical Report, GRI -94/0167, 135 p.

Laubach, S.E., S.J. Clift, R.E. Hill and J. Fix, 1992: "Stress Directions in Cretaceous Frontier Formation, Green River Basin, Wyoming," Wyoming Geological Society, Annual Meeting

Lorenz, J.C. and R.E. Hill, 1994: "Subsurface Fracture Spacing: Comparison of Inferences from Slant/Horizontal and Vertical Core," SPE Formation Evaluation, V. 9, No. 1, p. 66-72.

Lorenz, J.C. and S.E. Laubach, 1994: "Description and Interpretation of Natural Fracture Patterns in Sandstones of the Frontier Formation Along the Hogsback, Southwestern Wyoming," Gas Research Institute Topical Report, GRI-94/0020, 89 p.

Lorenz, J.C., N.R. Warpinski and L.W. Teufel, 1993: "Rationale for Finding and Exploiting Fractured Reservoirs, Based on the MWX/SHCT-Piceance Basin Experience," Sandia Report, SAND93-1342, UC-132,150 p.

Mastin, L., 1988: "Effect of Borehole Deviation on Breakout Orientation," Journal of Geophysical Research, V. 93, p. 9187-9195.

Plumb, R. A. and S.H. Hickman, 1985: "Stress-Induced Borehole Elongation: A Comparison Between the Four-Arm Dipmeter and the Borehole Televiwer in the Auburn Geothermal Well," Journal of Geophysical Research, V. 90, N. B7, p. 5513-5521.

Teufel, L.W., D.W. Rhett and H.E. Farrell, 1991: "Effect of Reservoir Depletion and Pore Pressure Drawdown on In Situ Stress and Deformation in the Ekofisk Field, North Sea," in Roegiers, J.C. Ed., *Rock Mechanics as a Multidisciplinary Science*, Proceedings of the 32nd U.S. Symposium, A.A. Balkema, Rotterdam, Netherlands, p. 62-72.

Zoback, M.L. and M.D. Zoback, 1989: "Tectonic Stress Field of the Continental United States," *Geological Society of America Memoir 172*, Chapter 24, p. 523-539.

Improvements to Reservoir Evaluation and Characterization, Almond Formation, Green River Basin, Wyoming

*Thomas L. Dunn, William P. Iverson, Bernabe Aguado,
John Humphreys and Ronald C. Surdam
The Institute for Energy Research, University of Wyoming*

INTRODUCTION

A joint field test by Amoco Production Company and the Gas Research Institute of a horizontal well has provided an opportunity to investigate a number of properties important to improved tight gas sand reservoir evaluation. The well, Champlin 254 Amoco B 2-H, shown in Figure 24, is in the Almond Formation of the Mesaverde Group in the Greater Green River Basin. This study has focused particularly on field-specific and formation-specific evaluation and description procedures, and characterization of fracturing and permeability anisotropy. This included a close examination of the properties of the rock matrix and the fractures, including the new application of scanning electron microscopy to measuring fracture widths from samples prepared at in situ horizontal effective stress.

The Almond Formation is the uppermost member of the Mesaverde Group and accounts for a significant portion of the total gas production from the Mesaverde. Of the cumulative 2 TCF of gas produced from the Mesaverde in the entire Greater Green River Basin (GGRB), over 80 percent has come from three "sweet spots": the Patrick Draw - Table Rock area, the Standard Draw - Echo Springs trend, and the Canyon Creek - Trail area. Patrick Draw and Trail are older fields, significantly depleted at present, so the largest gas reserve is in the Standard Draw area (Figure 24).

Four oriented cores were taken by Amoco (one from the slant hole: 10,025 to 10,076 ft and three from the horizontal leg: 10,781 to 10,811 ft, 10,812 to 10,842 ft, and 11,091 to 11,122 ft); a brief core description is presented in Appendix 2. The slant (or pilot) core was taken at 30° from vertical. This core traverses Almond Formation shoreface sandstones which also appear in the horizontal cores. The upper portions of the core contain well-defined small-scale low-angle and planar cross-stratification with *Ophiomorpha* burrows at the top. Shell fragments and oyster shells increase in abundance downward in the sandstone as it assumes a more massive character. The horizontal cores contain generally massive to faintly bedded sandstones with low-angle stratification. The path of the horizontal well-bore places these cores in the lower portion of the shoreface sands as well.

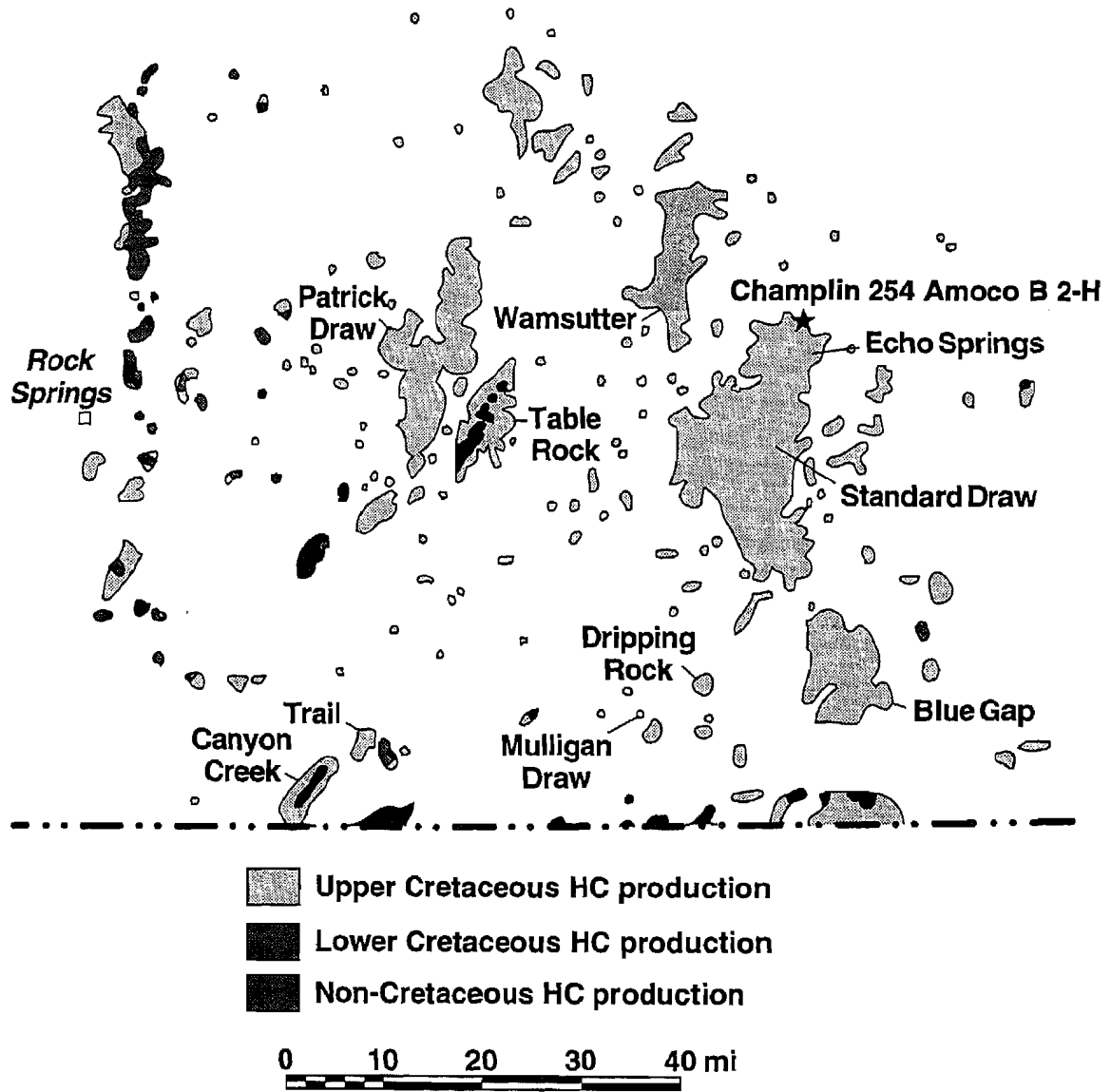


Figure 24 Location Map of the Champlin 254 Amoco B 2-H on the Northern Edge of the Echo Springs Field (Modified from Gregory and DeBruin, 1991)

PETROLOGY

The petrology and mineralogy of these sandstones were examined to determine the reservoir matrix. This analysis included transmitted light microscopy, scanning electron microscopy, and x-ray diffractometry.

The Almond Formation sandstone at the Champlin 254 Amoco B 2-H is a fine- to very-fine-grained, well-sorted lithic arenite (Q72 F3 L25, including chert as lithic fragments) containing undulose monocrystalline quartz with lesser amounts of chert, polycrystalline quartz, and nonundulose monocrystalline quartz as shown in Figures 25 and 26.

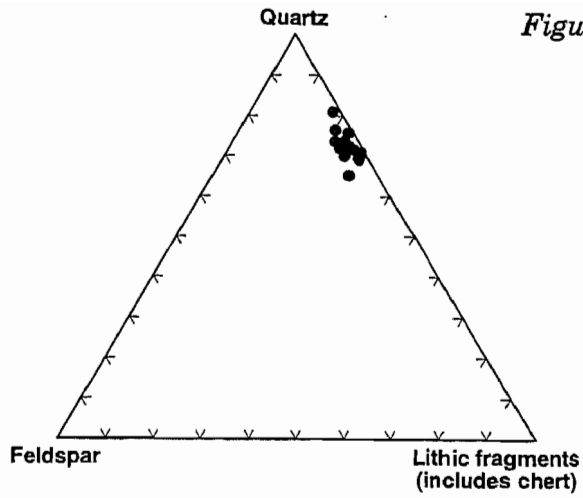


Figure 25 Model Compositions of Almond Formation Sandstones from the Champlin 254 Amoco B 2-H Slant and Horizontal Core

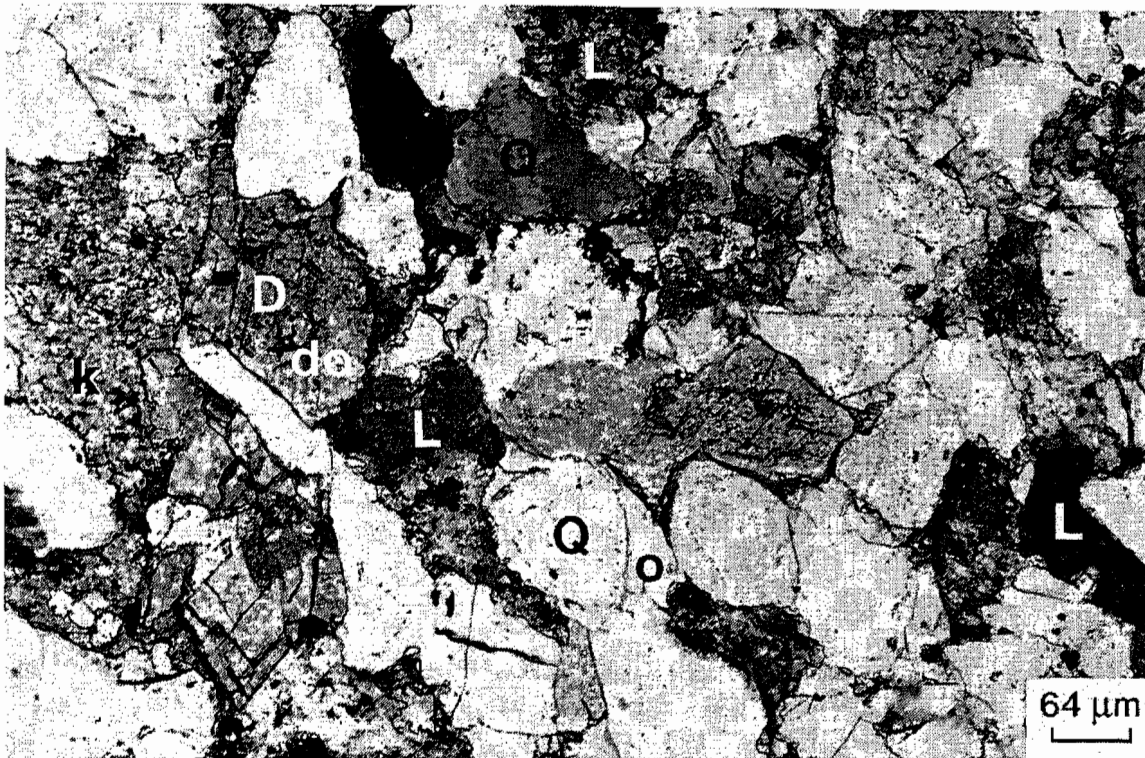


Figure 26 Photomicrograph of the Almond Formation (Partially Crossed Polars)

Figure 26 shows quartz grains (Q) that have extensive overgrowths (o) which form the most abundant cement. The lithic fragments (L) are primarily argillaceous. Detrital carbonate (dolomite) clasts (D) also show overgrowths (do). A moldic pore now filled with kaolinite (k) and carbonate is shown in the far left. Minor detrital components include argillaceous and volcanic lithic fragments and feldspar. Minor amounts of detrital carbonate are present, both micrite and rounded, inclusion-filled sparry forms, which are common to the Almond Formation. Most of the feldspar originally present has been altered to kaolinite and albite. The feldspar that remains is mostly plagioclase, typically sericitized.

The sandstones are extensively cemented with quartz that formed as overgrowths on monocrystalline grains and as annealing cements within broken quartz grains (Figure 26). Dolomite is present as sparry cement and as overgrowths on detrital carbonate (Figure 26). Kaolinite occurs within the small remnant intergranular pores and in moldic pores, which commonly show relict traces of the replaced feldspar. Trace amounts of barite and pyrite are also present.

Point-count intergranular porosity averages 2 percent. The majority of the diagenetic intergranular clay, the lithic fragments, and small amounts of the chert are microporous, showing the characteristic blue-green colors in planar transmitted light indicative of finely disseminated blue-dyed epoxy. Boyle's law helium porosity measurements obtained from conventional core analysis average 10.3 percent. Hence, roughly 80 percent of the porosity in these sandstones is within micropores. Capillary pressure measurements shown in Table 2 indicate that an average of 93 percent of the porosity is behind pore radii of 0.54 mm.

Overall, these samples are petrographically typical of the Greater Green River Basin Almond Formation sandstones as described by prior workers (e.g., Keighin and others, 1989; Yin and others, 1992; and Yin and Surdam, 1993).

CLAY MINERALOGY

Procedures

Two samples were prepared for x-ray diffractometry from the horizontal core and another two from the slant core, as identified in Table 3. The samples were mechanically disaggregated by hand grinding using mortar and pestle and treated with warm acetic acid-acetate to dissolve carbonate minerals; hydrogen peroxide was used to remove organic matter, and a sodium citrate treatment was used to remove iron oxides. Size fractionation was accomplished by sieving and centrifugation. Oriented slides were prepared with the <2 μ m size fraction and run on a Scintag 3000 X-ray diffractometer at 30 mA and 40 Kv, using a Cu anode. The slides were then placed in an ethylene glycol atmosphere for 72 hours and run again to detect the presence of expandable clay minerals. Two samples were selected for separation of a 0.01 μ m size fraction to characterize the mixed-layer clays.

*Table 2 High Pressure Mercury Injection Test Results, Amoco
Champlin No. 254B-2H (K&A Laboratories)*

Sample Number:	2M	3M	16M
Depth, feet:	10,030.6	10,034.6	10,043.6
Air Permeability, md.:	0.0588	0.0659	0.00860
Porosity, percent:	9.7	11.9	7.6

Injection Pressure, psia	Mercury Saturation, %PV	Mercury Saturation, %PV	Mercury Saturation, %PV
0	0.0	0.0	0.0
1	0.2	0.1	0.2
3	2.3	1.4	1.5
5	2.8	1.8	1.9
7	3.0	1.9	2.2
10	3.1	2.1	4.4
15	3.3	2.2	4.6
20	3.5	2.3	4.7
40	3.5	2.3	4.7
60	3.5	2.3	4.7
80	3.5	2.3	4.7
100	3.5	2.3	4.7
150	3.5	2.6	4.9
200	3.6	2.9	4.9
300	7.5	4.1	5.1
500	35.1	45.8	5.8
750	47.5	60.2	16.8
1,000	55.1	67.8	38.7
1,250	60.4	72.7	54.6
1,500	64.2	76.2	60.7
1,750	67.3	79.0	64.3
2,000	69.6	81.0	67.5
3,000	75.8	85.6	75.3
5,000	81.3	89.5	82.2
7,500	84.6	92.1	86.0
10,000	86.6	93.5	88.2
15,000	89.1	95.1	90.6
20,000	90.3	95.8	91.8

Table 2, Continued

Sample Number:	17M	45M	46M
Depth, feet:	10,047.6	10,061.6	10,065.6
Air Permeability, md.:	0.200	0.0141	0.00280
Porosity, percent:	12.0	7.1	3.6

Injection Pressure, psia	Mercury Saturation, %PV	Mercury Saturation, %PV	Mercury Saturation, %PV
0	0.0	0.0	0.0
1	0.7	0.5	0.2
3	2.3	3.1	2.7
5	3.9	3.5	3.7
7	4.1	3.8	8.0
10	4.2	4.0	8.4
15	4.6	4.3	8.6
20	4.7	4.5	8.8
40	4.7	4.5	8.8
60	4.9	4.5	9.3
80	5.1	4.5	9.4
100	5.3	4.5	9.4
150	6.5	4.6	9.5
200	13.0	4.7	9.5
300	41.1	5.0	9.8
500	57.5	5.4	10.2
750	66.7	6.7	10.5
1,000	72.0	13.7	10.7
1,250	75.8	27.3	11.0
1,500	78.5	35.2	11.2
1,750	80.6	40.3	11.5
2,000	82.2	44.1	11.7
3,000	86.4	55.0	12.4
5,000	90.0	66.8	14.0
7,500	92.3	74.7	16.3
10,000	93.7	79.0	20.5
15,000	95.3	83.8	38.2
20,000	96.1	86.4	49.5

Table 3 Semiquantitative X-Ray Diffraction Mineralogy (Weight Percent of the < 2 μm Size Fraction, ± 15%

Depth, ft	Kaolinite	Illite	Mixed-Layer Clays
10,791.00	75	18	7
11,093.50	82	10	8
10,025.75	89	7	4
10,033.25	78	14	8

Results

The amounts of the clay minerals present were semi-quantified using methods modified from those described by Reynolds and Hower (1970) and Moore and Reynolds (1989) (Table 3). Figure 27 shows that the clay mineralogy of all samples is dominated by kaolinite, which forms an average of more than 80 percent of the <2μm size fraction. The solid trace is that of the ethylene glycol solvated sample. The dotted trace is that of the air dried sample. The narrow peaks of the 7.0 and 3.53Å reflections indicate that the kaolinite is well crystallized (Figure 27).

Illite is the second most abundant clay mineral, forming an average of 12 percent of the total clay present. The last column in Table 3 refers to the mixed-layer clay minerals, which could not be separated quantitatively into the various species present. The mixed-layer clay minerals form an average of only 7 percent of the <2 μm fraction. This combination of two different mixed-layer clay minerals can be properly identified in diffractograms of the <0.01 μm size fraction as shown in Figure 28. The solid trace is that of the ethylene glycol solvated sample. The dotted trace is that from the air-dried sample. This diffractogram clearly shows the two mixed-layer clays that are present in the Almond Formation sandstones at the Champlin 254 Amoco B 2-H. The sample contains a mixed-layer illite/smectite and a mixed-layer 50:50 chlorite/smectite (corrensite). Both of these minerals are regularly ordered, as indicated by the characteristic glycolated d-spacings and by the presence of superlattice reflections. Corrensite is more abundant in these samples than illite/smectite. The corrensite occurs within and upon lithic fragments, as shown in Figure 29. Where these fragments are adjacent one another, little or no quartz overgrowth occurs. Hence, the macroscopic pores are commonly partially lined with a chloritic clay. Because of the position of the corrensite in the pore structure and the knowledge that chlorite is sensitive to acid well-cleanup treatments, sensitivity tests were ordered. The results of those tests indicated little or no acid sensitivity.

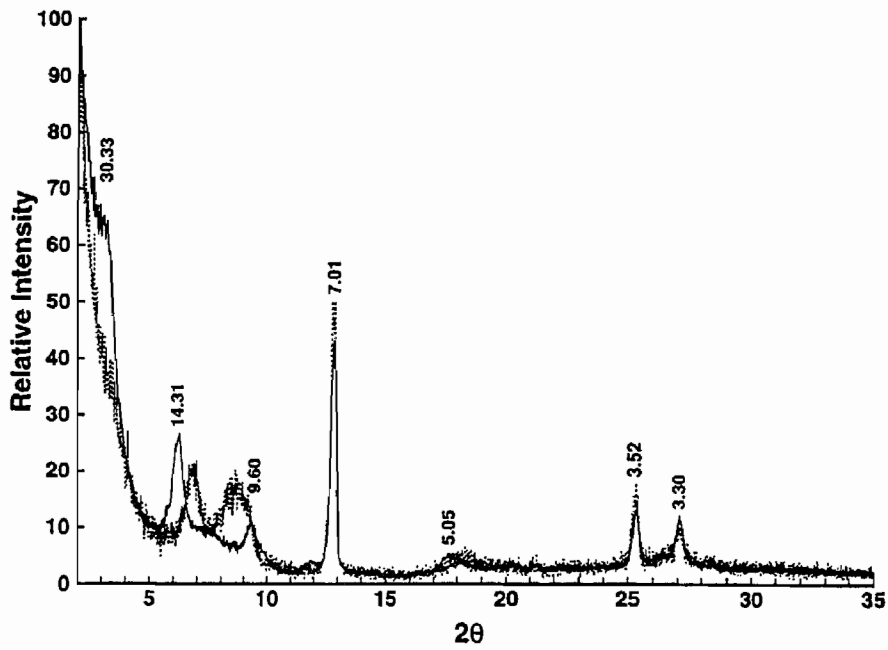


Figure 27 X-Ray Diffractogram of the <2 μ m Size Fraction of Sample 10,791.5 ft

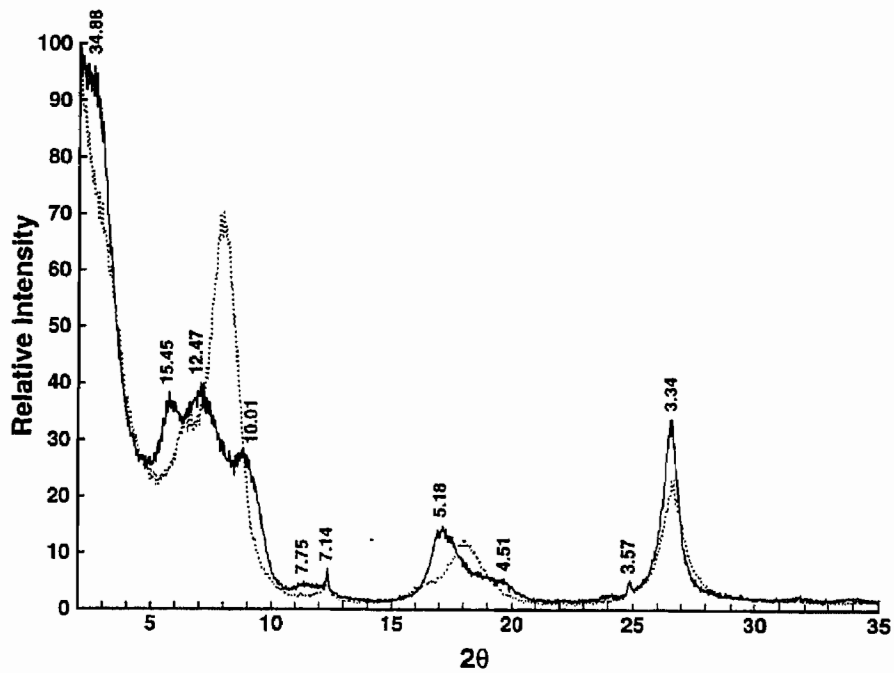


Figure 28 X-Ray Diffractogram of the <0.01 μ m Size Fraction of Sample 10,791.5 ft, Sandstone from the Horizontal Core

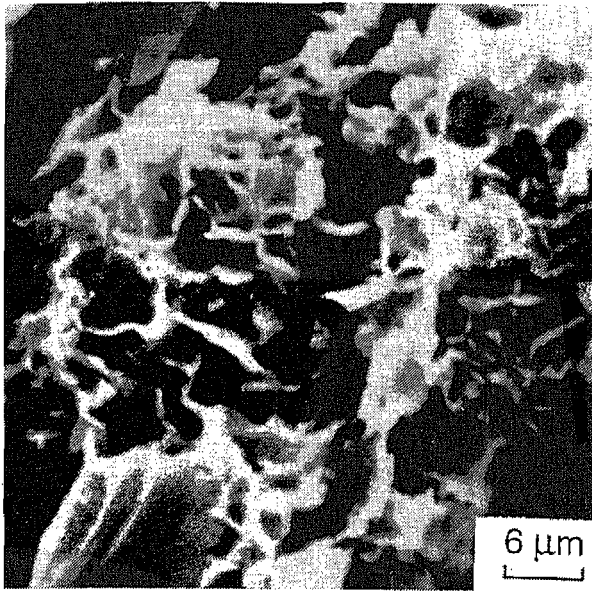


Figure 29 Scanning Electron Photomicrograph of Crenulated Flakes of Corrensite Which are Typically Attached to Lithic Fragments

FRACTURES

Spacings and Orientation

Hill (this volume) and Reinert and Billingsley (this volume) separately describe the observed spacing and direction of the natural fractures in the Champlin 254 Amoco B 2-H well. These determinations were derived from FMI log response and core inspection. The orientation of the near-vertical fractures was consistently N50 to 70°E. Evans and Thorn (1995) found that the spacings are not uniform and typically are representative of fracture swarms with spacings of less than two feet. The observed spacing of a few feet in the pilot core is consistent with a fracture swarm, also observed by Evans and Thorn (1995). Lorenz and Hill (1994) found similar irregular distributions of fracture spacings in the Mesaverde Group in the Department of Energy's SHCT-1 well, northwestern Colorado.

Fracture Apertures

This cooperative study provided a unique opportunity to combine a number of analytical techniques for characterizing the natural fractures of the upper Almond Formation. One aspect of the study was to attempt to measure the in situ fracture apertures using the scanning electron microscope to image fractures present in pressure-impregnated thin sections.

Prior Work

There are few studies containing measured apertures of natural fractures occurring in the subsurface. Nelson (1985) compiled published values for near-surface natural fracture widths. These included values calculated from pressure tests at dam sites and the Rocky Mountain Arsenal well (Snow, 1968a, b). These ranged from 10 to 500 μm . Nelson (1985) also provides experimental data for simulating deeply buried rocks of various lithologies. For sandstones, these experimental values range from 10 to 100 μm (Nelson, 1985). Lorenz

and Hill (1994) report remnant (partially mineralized) fracture apertures from the Mesa-verde of the SHCT-1 well averaging between 0.004 and 0.02 in. (about 100 and 500 μm). These values were derived from unstressed samples. Recent work by Hyman and others (1991), Soeder (1990), Gies (1987), and Brower and Morrow (1985) suggest other approaches to directly measure fracture apertures using fluorescent dyes and transmitted light microscopy of samples prepared at in situ pressures. The use of back-scattered scanning electron digital imaging of microfractures is possible through the use of polished thin sections impregnated with epoxy while under confining pressure. The difficulty in resolving small variations in width at high magnifications experienced using fluorescence is not experienced using scanning electron microscopy.

Champlin 254 Amoco B 2-H Natural Fractures

Branagan (this volume) uses values of 12 to 25 μm for the Champlin 254 Amoco B 2-H fracture apertures in his modeling of the pressure and flow behavior of the well. Evans and Thorn (1995 and personal communication) calculate similar fracture apertures for the Almond sandstones from the Formation MicroImager and Dual Induction log responses.

Fracture Aperture Measurements

Procedures

The samples were collected as one-inch core plugs oriented to include the fracture trace, as shown in Figure 30. The core plugs were pressure-impregnated with epoxy at Core Laboratories in Carrollton, Texas. A confining pressure of 2,500 psi was imposed on the samples to simulate an in situ minimum effective horizontal confining stress. The true effective confining stress may be higher; however, 2,500 psi represents a level at which fracture closure due to higher stress will not be appreciable. The samples were evacuated, impregnated with epoxy, and allowed to harden while under confining pressure.

The fracture apertures were measured using a Robinson backscattered electron detector mounted on a JEOL-35CF scanning electron microscope (SEM). The backscattered electron detector provides for differentiation of pore space and minerals by responding to the average atomic number of the part of the specimen under the beam. The average atomic number contrast between epoxy and normal rock forming minerals is sufficient to provide strong gray-level contrast. The backscattered electron detector has been used in the past to determine both porosity (Nadeau and Hurst, 1991) and, coupled with other spectroscopy, mineralogy (Hall and Lloyd, 1981, among others). The SEM is linked to a Noran Voyager[®] image analysis system, which provides digital processing of the image. The Voyager system allows simple and rapid measurement of fracture width through the "Measure Distance" function in the "Image Process and Analysis" window, which provides a moveable and adjustable ruler. Up to 20 measurements were obtained across a single image in this way. The width of each fracture was measured perpendicular to the tangent of the fracture trace. A minimum of 240 measurements were obtained for each thin section. Each thin section contained approximately 3 cm of fracture trace. Clearly, this technique provides

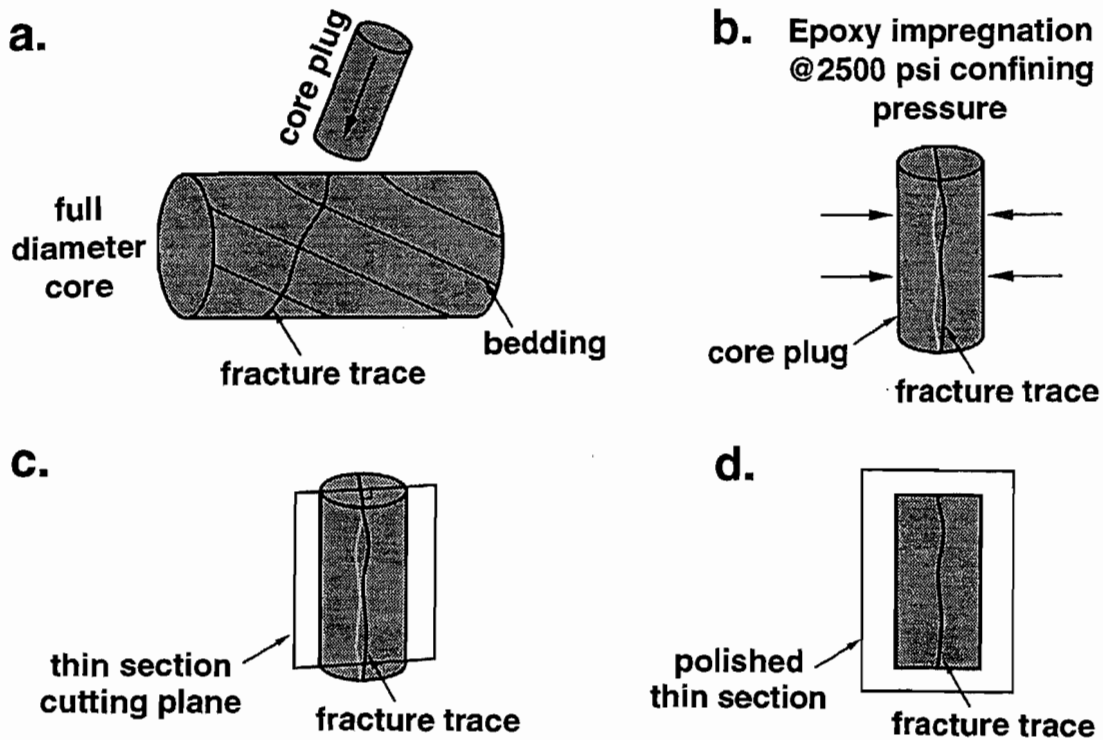


Figure 30 Sequence of Procedures for Producing Polished Thin Sections Containing Natural Fracture Traces

detailed measurements over a small portion of a natural fracture trace. It should be noted that fracture aperture can vary drastically over short intervals. For example, Lorenz and Hill (1994) found width variations up to 100 percent due to mineralization and fracture surface roughness within "several inches." This study found similar fracture aperture variations over even shorter lengths.

Measured Values

Eight thin sections were prepared in the manner described above from four samples, three from the slant hole core (at 10,028, 10,033.5 and 10,051 ft) and one from the horizontal core (at 11,106 ft). Longitudinal and axial sections were made from each sample. There was no visible difference in the fracture aperture between the longitudinal and axial sections. Figure 31 and Table 4 present the aperture data for the longitudinal sections. Because the 10,028 ft sample showed a roughly 20 percent fracture dilation that was the result of handling and preparation, the aperture data from that sample was not used in this analysis. On this very fine scale of examination, the fracture openings for 11,106.5-ft and 10,051-ft samples appear log-normally distributed; the data for the 10,033.5-ft sample appear to be more normally distributed (Figure 31).

Figure 31 In Situ Fracture Aperture Distributions in Microns (μm) for Three Samples from the Champlin 254 Amoco B 2-H

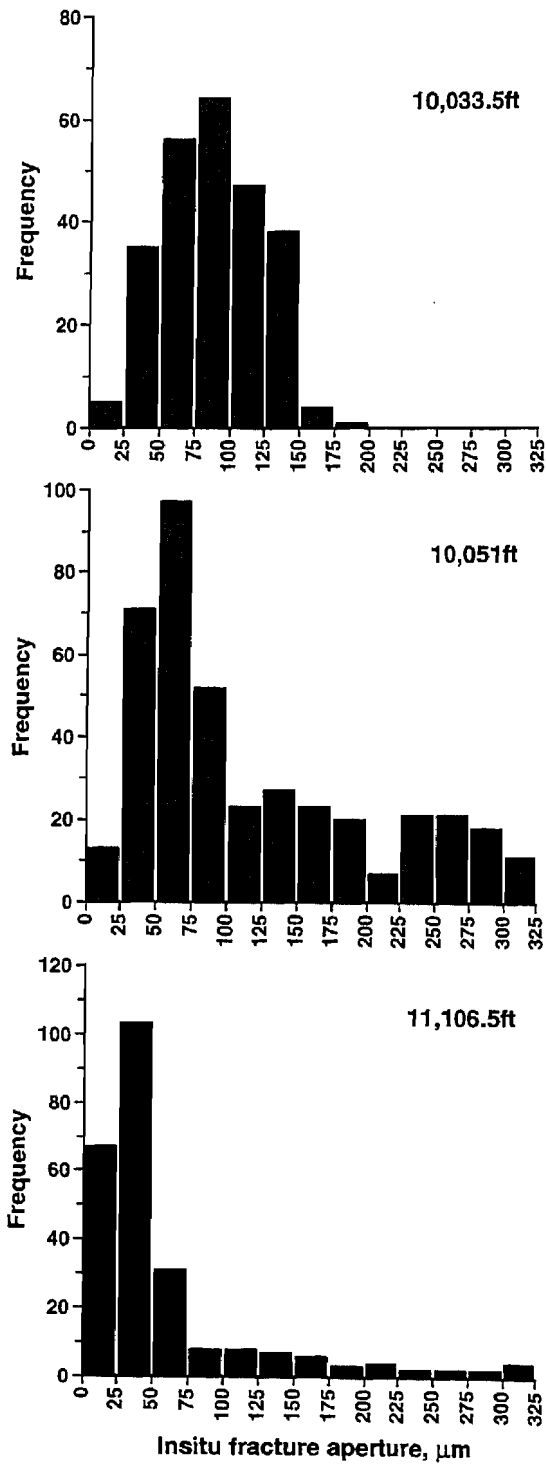


Table 4 Number of Measurements (n), Average In Situ Fracture Widths and Geometric Averages of the Calculated Permeabilities (k) for Natural Fractures, Amoco Champlin No. 254B-2H

Sample, ft	n	Width, μm	k, md
10,033.5	249	87	2,151
10,051.0	403	118	3,108
11,106.5	246	59	297

Apparent one-inch plug permeabilities were calculated for each measurement using the equation shown on Figure 32. The calculated permeabilities are shown in Figure 33 and Table 4.

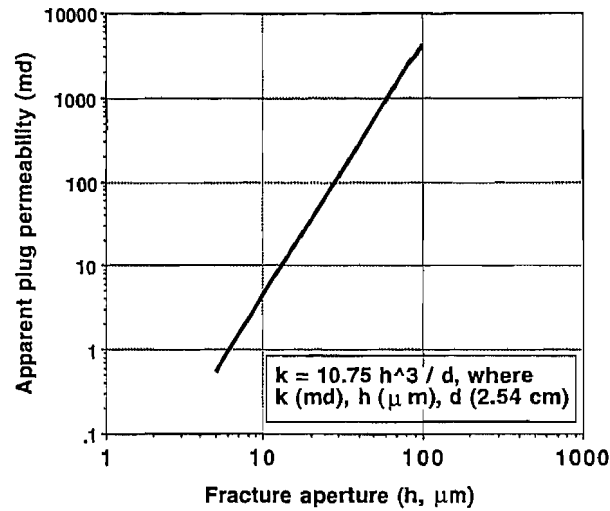
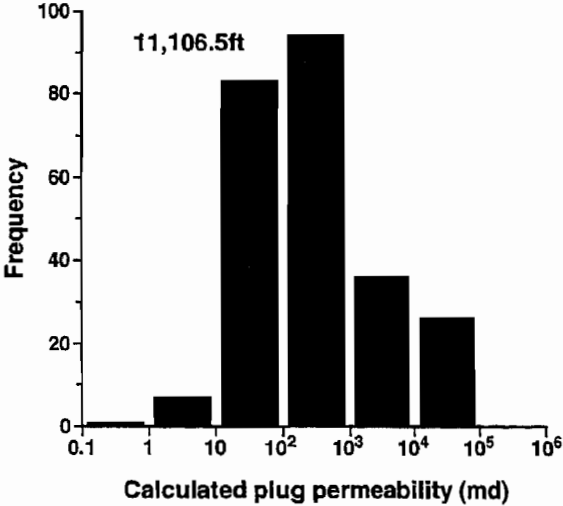
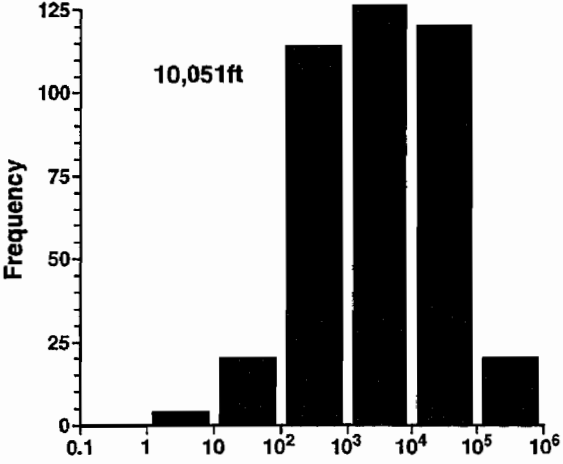
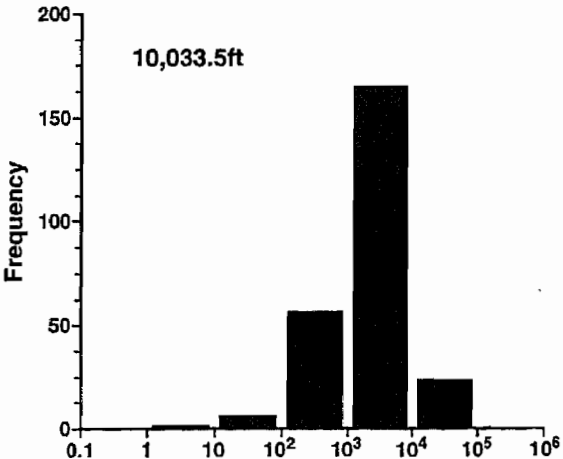


Figure 32 Plot of Apparent Plug Permeability for Different Fracture Apertures (μm) (Modified from Morrow and others, 1990)

Figure 33 Calculated Plug Permeabilities from the Measured In Situ Fracture Aperture Data



Discussion

The fracture apertures observed in thin section are considered to represent in situ widths because of textural evidence as well as the reasonableness of the effective horizontal stress applied. In the 10,033.5-ft sample, small patches of barite are found as fracture fill, as shown in the two magnifications in Figure 34. The bright material in the fracture is barite (b). The fine particles in the fracture, adjacent to the barite, are kaolinite (k). The photo on the right is a close-up showing the barite enclosing the kaolinite. Also, note the euhedral quartz overgrowth (og) which grew into the pore and was subsequently enclosed by the barite. The barite completely bridges the fracture and neatly locks into the surrounding matrix. It appears intact and undisturbed by preparation. The open fracture widths immediately adjacent to the barite are equal to the widths of the cemented zone. From these observations, it is concluded that the samples have retained the appropriate in situ fracture widths. Fracture cementation is discussed below.

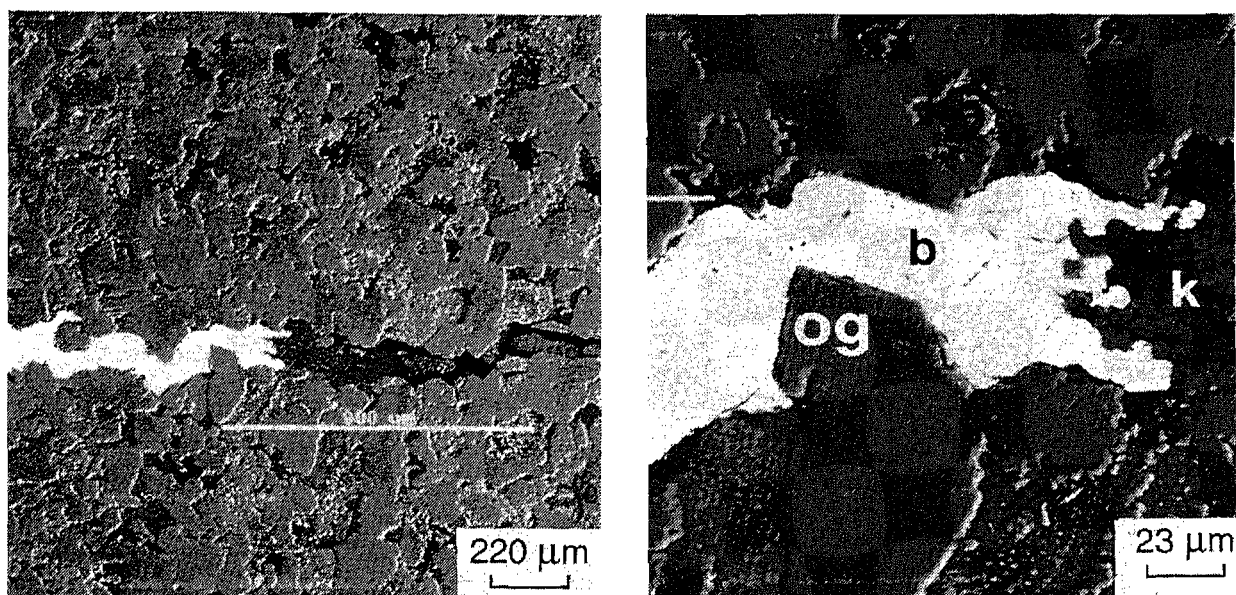


Figure 34 Backscattered Electron Photomicrographs of a Fracture in the 10,033.5-ft Sample

Fracture Cementation

Mineralizations were found in thin section to partially or completely bridge the fractures. The need to examine these rests in the decrease in average fracture width and reduction of permeability accompanying cementation. In addition to these cements, the mineral constituents of the matrix, described above, are all present along the walls of the fractures, including dolomite, mixed-layered clays, and microporous lithic fragments.

Mineralogy

Quartz, calcite, barite and kaolinite are present as fracture fillings, as shown in Figure 35 (and Figure 34). Photo 35A is a backscattered electron image of a polished thin section,

10,033.5 ft. It shows a euhedral overgrowth on a quartz grain (Q) adjacent to the fracture, which contains kaolinite (k) and drilling mud (dm). The dark areas are epoxy and therefore porosity. Note the partially dissolved microporous chert in the upper left. Photo 35B is a secondary electron image of the fracture surface showing the small euhedral quartz overgrowths covered and surrounded by the kaolinite (k). Photo 35C is a backscattered electron image of a polished thin section, 10,028 ft. This photo shows euhedral quartz (q) growing into the fracture, which has been filled with barite (b) and calcite (c). This sample contains abundant dolomite (d) as a cement in the rock matrix. The barite is euhedral against the calcite, indicating that it was formed first. The sample 10,028 ft experienced some fracture dilation during preparation as evidenced by the broken and missing calcite in the fracture. Photo 35D is a secondary electron image of calcite (c) enclosing the top of a quartz overgrowth (q) that formed on the fracture face.

The quartz occurs as euhedral overgrowths, which only very rarely bridge the fracture openings. On a very small scale, the overgrowths likely reduce wall roughness by covering small irregularities with smooth surfaces. A sparry calcite is the most abundant fracture filling (Figures 35C and 35D). Where present, it always completely bridges the fracture apertures. Barite (BaSO_4) is present in minor amounts, and also always completely bridges the fractures (Figures 34 and 35C). Kaolinite is present only in the sample from 10,033.5 ft (Figures 34, 35A and 35B). It occurs as booklets of hexagonal plates, 10 to 40 μm across, which are inhomogeneously distributed in the fractures. Microporosity values for these masses range from 15 to 40 percent, based on backscattered electron imagery methods similar to those described by Nadeau and Hurst, 1991.

Pitman and Dickinson (1989) found these same cements within fractures in Mesaverde sandstones of the MWX sites in the Green River Basin, Wyoming, and the Piceance Basin, Colorado. The kaolin-group polymorph dickite was identified rather than kaolinite. Dickite is generally found in rocks that have experienced elevated temperatures; however, the conditions for its formation are not well characterized. Pitman and Dickinson (1989) also found bitumen in the MWX Mesaverde sandstones. No bitumen was observed in the samples examined from the Champlin 254 Amoco B 2-H.

Paragenesis

The textural relationships of these cements clearly indicate their sequence of formation, as shown in Figure 36. The quartz overgrowths are euhedral and enclosed by the calcite and the barite (Figure 34 and 35C), indicating that they were formed prior to either barite or calcite cementation. The quartz is also euhedral to adjacent masses of kaolinite, indicating that the kaolinite did not impede quartz growth, and hence that the quartz formed prior to the formation of the kaolinite (Figure 34 and 35A). The sample from 10,028 ft contains calcite and barite (Figure 35C), which are in contact. The barite is euhedral to the calcite, indicating that it formed prior to the enclosing calcite. Barite and kaolinite are

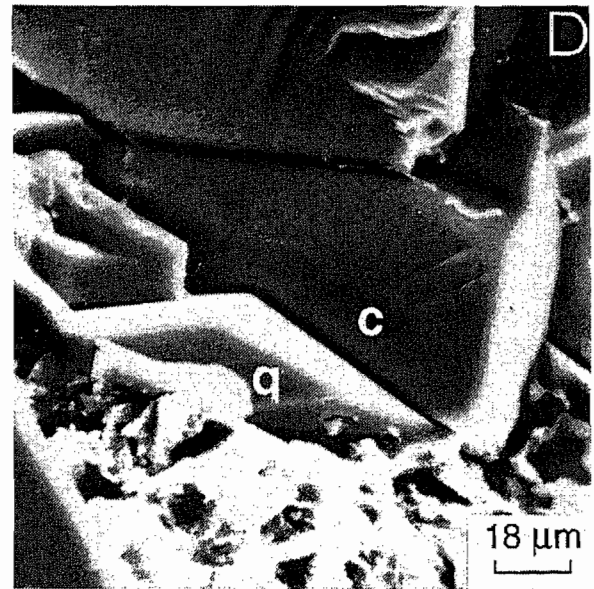
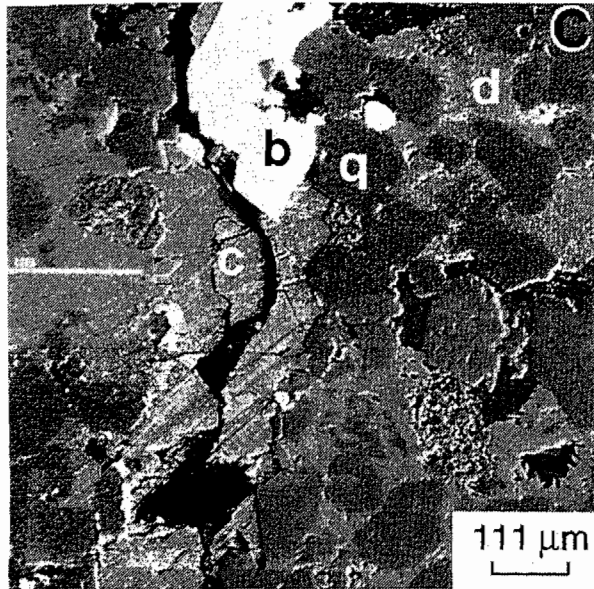
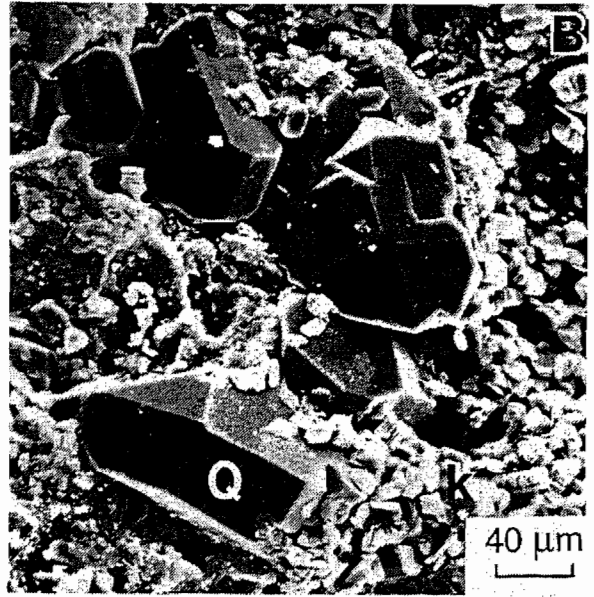
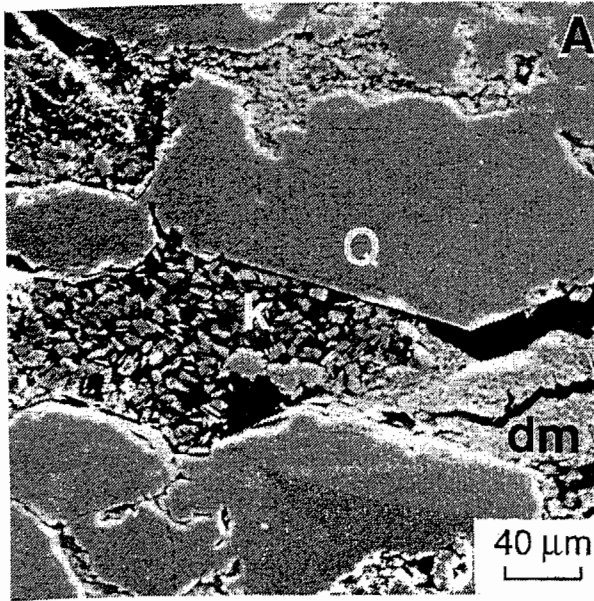


Figure 35 Photomicrographs of Natural Fracture Filling and Lining Cements

Fracture Mineralization Sequence

Quartz --

-- Kaolinite --

-- Barite --

-- Calcite

—————→
Time

*Figure 36 Paragenetic Sequence
for the Champlin 254
Amoco B 2-H Fracture Fill*

found in contact in the sample for 10,033.5 ft (Figure 34). There, the kaolinite is partially enclosed by the barite, indicating that the kaolinite was formed prior to barite precipitation.

From these paragenetic textural relationships, the sequence of fracture filling was constructed (Figure 36), with quartz forming first, followed by kaolinite, then the fracture-bridging barite and calcite. Hence, it is the later-formed cements that are likely the most damaging to permeability in the Champlin 254 Amoco B 2-H Almond Formation sandstones. Pitman and Dickinson (1989) describe a slightly different paragenetic sequence. They observed replacive textures by the barite which were not observed in the Champlin 254 Amoco B 2-H samples. Taken together, these textures indicate that barite and calcite formed fracture fillings in the Mesaverde sandstones of the Green River Basin penecontemporaneously.

Discussion

In half of the samples examined, drilling mud was present in the fractures similar to that shown in the backscattered electron images of polished thin sections in Figure 37 (A: 10,051 ft and B: 10,033 ft). Drilling mud (dm) is present in each of these fractures. Kaolinite (k) is present in the 10,033.5-ft sample. Should this prove to be true fracture plugging, then such damage would reduce flow rates along the fractures.

FORMATION EVALUATION AND CHARACTERIZATION

Reservoir evaluation of the Standard Draw "sweet spot" has resulted in specific questions that can only be answered by acquiring additional data. Sandstone cores from the Champlin 254 Amoco B 2-H well have provided an opportunity to obtain some of these data. Although the questions posed below appear to address very specific petrophysical constants, their context in a larger reservoir framework must first be reviewed. The Standard Draw area is a prolific producer, considering the generally tight matrix of most other Mesaverde sands in the region. In fact, the volume of gas plus condensate produced from some of the Standard Draw (and Echo Springs) wells just south of the Champlin 254 Amoco B 2-H exceed the volume of gas-in-place for the Almond bar sand alone. This single bar sand has

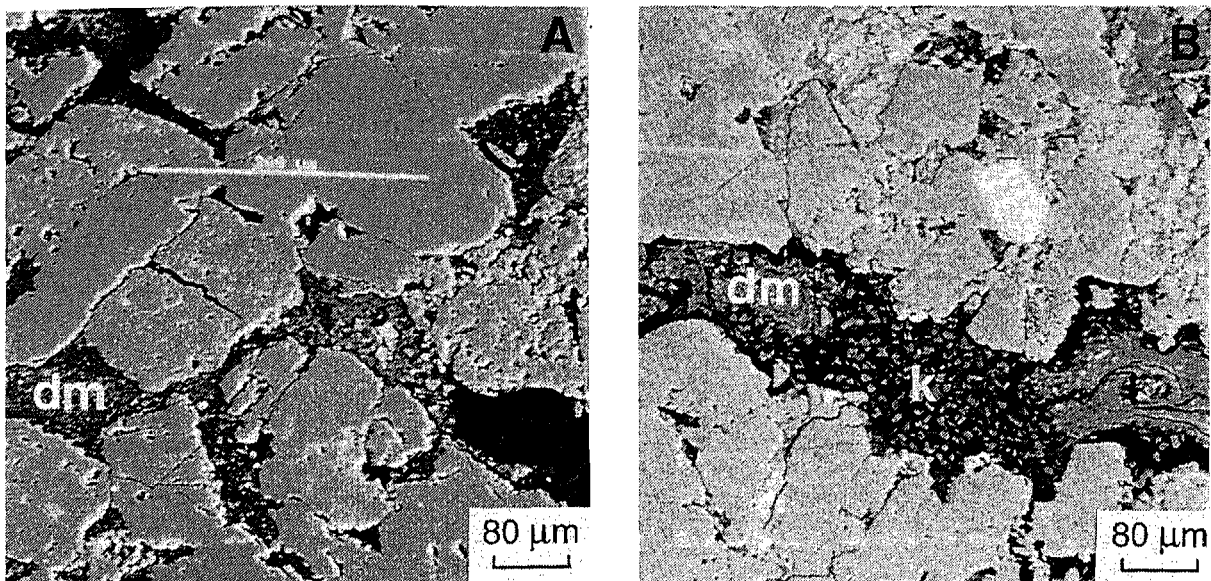


Figure 37 *Backscattered Electron Images of Polished Thin Sections Showing Drilling Mud in the Fractures*

attracted considerable development into the Standard Draw region since 1978. The Champlin 254 Amoco B 2-H well was drilled horizontally through this one bar sand and now provides a unique opportunity for further analysis.

Need for Permeability Versus Confining Stress Data

Almond sandstones are generally very tight (< 0.1 md) with some good sands in the 1 to 10 md range. Considerable data on sandstone permeability has been acquired by many different operators over the past decades. Some of these data are summarized by Yin and Surdam (1993). The normal procedure is to measure Klinkenberg gas permeability at laboratory conditions with low (400 psi or less) confining pressure. In situ permeability will be much less, (e.g., Morrow and others, 1990), but more Mesaverde data is needed to accurately quantify permeability reduction with confining stress. Sattler (1989) presented the permeability reduction of Mesaverde fluvial and coastal sands from the Department of Energy MWX site in Colorado. Is there a similar permeability reduction, characteristic of the Almond sands?

Need for Petrophysical Constants

Gas production from the Almond at Standard Draw is significant. Discovery of a relatively high-permeability sandstone (up to 10 md) in 1978 spurred development of the area and many completions at the depth of this sandstone. Subsequent analysis has indicated that this sandstone was deposited as a barrier bar, and it is often referred to as "the bar sand." It has a maximum thickness of 40 ft, averages 20 ft thick, and tapers to zero at the edges of Standard Draw, over 6 miles east to west. Over 400 BSCF has been produced to date from over 30 wells in the heart of the field. One well in particular, the Champlin No. 226 - Amoco F-1, has produced over 25 BSCF. This large volume of gas cannot be explained simply by volumetric depletion of the bar sand (Iverson and Surdam, 1995). Further, the

bar sand can be correlated 20 miles farther to the north, yet is not productive outside the Standard Draw field. These observations lead us to question whether the calculations of gas-in-place from well logs are accurate. In particular, is the water saturation calculated from Archie's rule accurate?

This question is particularly important for gas volumetrics in the producing trend, and also for verification of large amounts of gas-in-place at the nonproductive locations. The applicability of Archie's rule is questionable, as the Almond Formation sandstones have a significant fraction of clays that can strongly affect clean sand analysis. Open-hole logs from the vertical Champlin 254 Amoco B-1 well are shown in Figure 38. Note that the productive Almond Formation sandstone appears fairly "clean," with a gamma ray average at 40 APIU. The porosity logs, however, show no gas cross-over, yet the well produces mostly gas. This lack of gas cross-over can be explained partly by the high density of gas in the reservoir, but the major effect is the presence of clays, as demonstrated by Mesheryakova (1993). This leads us to again question the accuracy of log-based calculations, since the effects of the clay minerals are so prominent on these porosity logs.

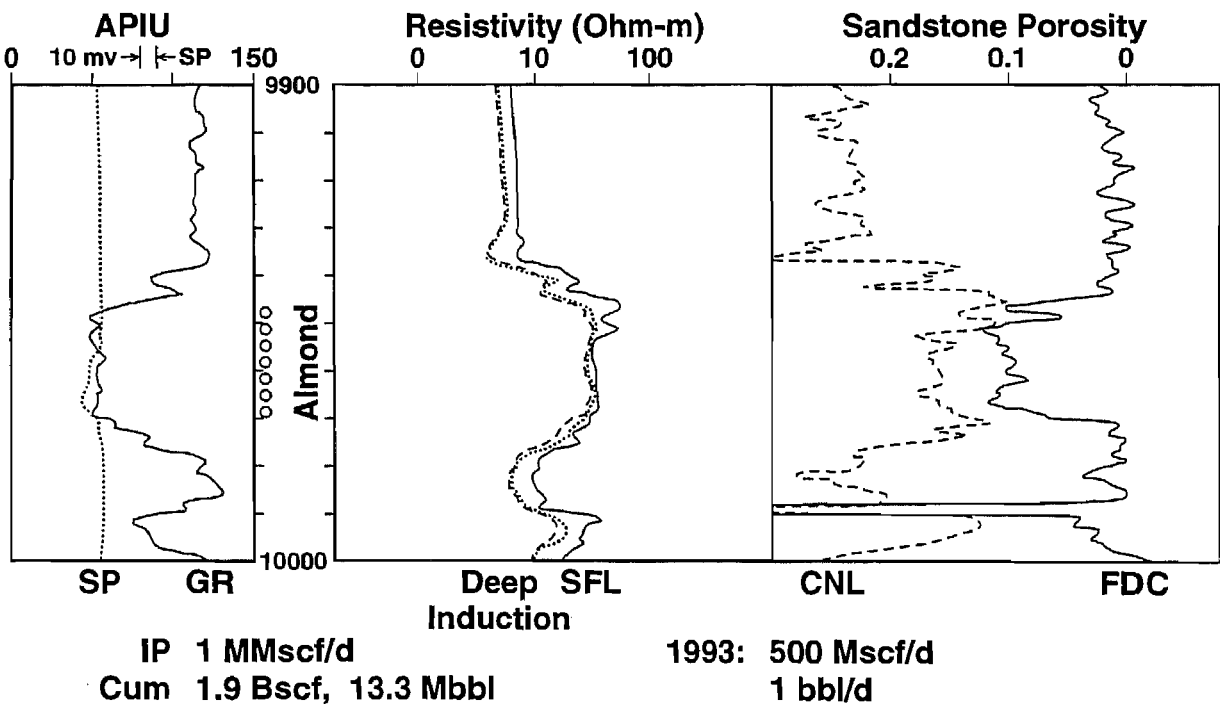


Figure 38 Open-Hole Logs for the Champlin 254 Amoco B-1 (Vertical Well)

Need for Capillary Pressure Data

Previous work (Iverson and others, 1992) has demonstrated that sandstones can act as both reservoirs and seals under two-phase fluid-flow conditions. This phenomenon occurs whenever matrix permeability is so low that a capillary seal is created under two-phase flow. A common name for this effect is the stratigraphic trap, where a permeable sand grades into an impermeable unit. The Almond sand, however, is of such low permeability

that it is entirely possible for the sandstone to act as both reservoir and seal. Such sealing capacity is normally evaluated with the use of capillary pressure curves. The only way to obtain reliable capillary pressure data in such tight rock is to use high-pressure mercury injection testing. Six samples were selected from the Almond Formation sandstone core plugs for such laboratory experiments.

Laboratory Experiments

Core plugs from the Almond Formation sandstone were made available by Amoco. Forty-six plugs had already been cut from the samples obtained on the Champlin 254 Amoco B 2-H pilot hole. Standard porosity and permeability measurements were available. Plugs were selected from this set to generate data addressing the questions summarized above. K&A Laboratories of Tulsa performed the laboratory experiments described below.

Table 5 summarizes the standard core analysis performed prior to selecting plugs for the specific studies outlined in this report. Note that the Almond sandstone in this well covers a range from 10,026 to 10,065 ft (measured depth). Approximately ten plugs were taken at various orientations with respect to true horizontal. All sample sets show relatively high permeability and porosity at depths of 10,027 and 10,047 ft. No anisotropy is apparent from these data. Sample numbers from Table 5 will be used throughout the remainder of this report.

Laboratory Results: Permeability Versus Confining Stress

All 46 samples were used to determine dry gas permeability at confining pressures of 400, 3,000, 6,000, and 9,000 psi, as shown in Table 6. The pore pressure in the laboratory is approximately 1 atm for these gas permeability measurements; hence, the confining pressures are essentially equal to effective stress. In situ conditions at Standard Draw are thought to be about 5,000 psi original effective stress (10,000 psi confining or overburden pressure minus 5,000 psi pore or gas pressure), now depleted to about 7,000 psi effective stress (10,000 minus 3,000 psi remaining pore pressure).

Porosity versus permeability for all 46 plugs at two different confining stresses is plotted in Figure 39. The zero and 6,000 psi confining stress sets are selected for this plot to demonstrate the amount of permeability reduction with increasing pressure. Least-squares lines are fit through each dataset. Note that the slope of this line is consistently parallel for the two confining stresses, indicating a uniform decrease in permeability at all porosities. In addition, the very tight samples (less than 5 percent porosity) show a marked decrease in permeability when confining stress is applied. From these observations, it is apparent that standard laboratory measurements of permeability (usually no confining stress) are indicative of in situ conditions within about one order of magnitude. Thus, cores that show up to 1 md in the lab indicate about 0.1 md in the subsurface. In the past, 8 percent porosity was considered to correspond to the extreme lower limit of productive permeability. These data verify that 8 percent porosity corresponds to about 0.01 md in situ, a reasonable permeability cut-off.

Table 5 Standard Core Analysis, Champlin 254 Amoco B 2-H (K&A Laboratories)

Sample Number	Depth, ft	Air Permeability, md	Porosity, percent	Grain Density, gm/cc
<u>True Horizontal 0°</u>				
1	10,026.3	0.11200	11.8	2.66
2	10,030.6	0.05870	9.9	2.66
3	10,034.6	0.05390	12.1	2.67
4	10,038.7	0.02990	11.7	2.70
5	10,042.7	0.03460	10.8	2.68
6	10,046.7	0.10600	11.3	2.65
7	10,050.7	0.06350	10.7	2.65
8	10,054.7	0.06090	11.6	2.67
9	10,058.7	0.03230	9.4	2.66
10	10,063.3	0.00865	3.5	2.68
<u>True Horizontal 45°</u>				
11	10,026.5	0.05810	9.6	2.66
12	10,027.6	0.14700	12.4	2.65
13	10,031.6	0.15100	12.4	2.65
14	10,035.6	0.03180	11.8	2.67
15	10,040.6	0.04630	12.4	2.68
16	10,043.6	0.00917	7.9	2.71
17	10,047.6	0.18400	12.7	2.67
18	10,051.6	0.08030	12.4	2.67
19	10,054.6	0.06050	11.7	2.67
20	10,055.6	0.06870	11.7	2.66
21	10,060.6	0.01720	8.6	2.68
22	10,064.6	0.24700	3.1	2.69
<u>True Horizontal 90°</u>				
23	10,026.2	0.14900	12.3	2.65
24	10,028.6	0.02390	8.8	2.70
25	10,032.4	0.08110	10.5	2.66
26	10,036.6	0.02890	10.2	2.68
27	10,039.6	0.02690	11.7	2.70

Table 5, Continued

Sample Number	Depth, ft	Permeability, md	Air Porosity, percent	Grain Density, gm/cc
<u>True Horizontal 90°, Continued</u>				
28	10,044.7	0.09140	10.3	2.65
29	10,048.7	0.06640	10.9	2.65
30	10,052.3	0.06680	12.0	2.67
31	10,055.1	0.05360	10.3	2.67
32	10,056.6	0.06380	11.7	2.67
33	10,059.6	0.01180	4.2	2.70
34	10,063.6	0.06200	3.8	2.66
<u>True Horizontal 135°</u>				
35	10,026.2	0.16300	12.5	2.65
36	10,029.3	0.12600	11.9	2.66
37	10,033.6	0.03710	10.2	2.66
38	10,037.3	0.03490	11.7	2.68
39	10,041.6	0.04610	11.3	2.66
40	10,045.6	0.08580	11.2	2.65
41	10,049.6	0.19000	12.0	2.65
42	10,053.9	0.05260	11.8	2.69
43	10,055.2	0.06230	12.1	2.67
44	10,057.4	0.03870	10.9	2.70
45	10,061.6	0.01460	7.4	2.69
46	10,065.6	0.00223	3.0	2.68

Table 6 Air Permeabilities at Varying Confining Pressure, Champlin 254 Amoco B2-H
(K&A Laboratories)

Sample Number	Depth, ft	Air Permeability, md at Confining Pressure, psi			
		400	3,000	6,000	9,000
<u>True Horizontal 0°</u>					
1	10,026.3	0.1160	0.06160	0.04820	0.04300
2	10,030.6	0.0571	0.02110	0.01170	0.00904
3	10,034.6	0.0659	0.03500	0.02540	0.02100
4	10,038.7	0.0325	0.02030	0.01540	0.01370
5	10,042.7	0.0468	0.02040	0.01220	0.00980
6	10,046.7	0.1200	0.04810	0.03180	0.02570
7	10,050.7	0.0813	0.03030	0.01940	0.01580
8	10,054.7	0.0672	0.02940	0.01990	0.01540
9	10,058.7	0.0517	0.01430	0.00447	0.00319
10	10,063.3	0.0161	0.00148	0.00027	0.00013
<u>True Horizontal 45°</u>					
11	10,026.5	0.06140	0.02460	0.01140	0.00925
12	10,027.6	0.15100	0.09840	0.08370	0.07680
13	10,031.6	0.15600	0.06920	0.05040	0.04350
14	10,035.6	0.03470	0.01870	0.01300	0.01110
15	10,040.6	0.05380	0.02560	0.01720	0.01390
16	10,043.6	0.00827	0.00369	0.00241	0.00163
17	10,047.6	0.20000	0.07470	0.05370	0.04410
18	10,051.6	0.10300	0.04710	0.03270	0.02790
19	10,054.6	0.06860	0.03580	0.02440	0.02090
20	10,055.6	0.08660	0.03740	0.02670	0.02300
21	10,060.6	0.02230	0.00979	0.00280	0.00192
22	10,064.6	0.26900	0.02240	0.00500	0.00179
<u>True Horizontal 90°</u>					
23	10,026.2	0.15400	0.10600	0.08810	0.08020
24	10,028.6	0.02930	0.01790	0.01370	0.01280
25	10,032.4	0.08490	0.04240	0.02950	0.02490
26	10,036.6	0.03530	0.01240	0.00539	0.00385

Table 6, Continued

Sample Number	Depth, ft	Air Permeability, md at Confining Pressure, psi			
		400	3,000	6,000	9,000
<u>True Horizontal 90° Continued</u>					
27	10,039.6	0.02970	0.01920	0.01420	0.01280
28	10,044.7	0.09910	0.03450	0.02100	0.01700
29	10,048.7	0.06820	0.03330	0.02390	0.02050
30	10,052.3	0.07520	0.03890	0.02860	0.02440
31	10,055.1	0.05640	0.02230	0.01260	0.00972
32	10,056.6	0.07120	0.03710	0.02590	0.02220
33	10,059.6	0.01200	0.00185	0.00039	0.00021
34	10,063.6	0.06430	0.00625	0.00116	0.00050
<u>True Horizontal 135°</u>					
35	10,026.2	0.16200	0.11000	0.09210	0.08400
36	10,029.3	0.12700	0.06700	0.05160	0.04660
37	10,033.6	0.04110	0.01640	0.00932	0.00596
38	10,037.3	0.03910	0.01850	0.01190	0.06400
39	10,041.6	0.04680	0.02170	0.01300	0.01020
40	10,045.6	0.09060	0.03920	0.02540	0.02120
41	10,049.6	0.18400	0.08310	0.05730	0.04880
42	10,053.9	0.05570	0.02910	0.02060	0.01730
43	10,055.2	0.06890	0.03250	0.02250	0.01940
44	10,057.4	0.04180	0.02190	0.01470	0.01240
45	10,061.6	0.01770	0.00509	0.00146	0.00098
46	10,065.6	0.00280	0.00018	0.00008	0.00032

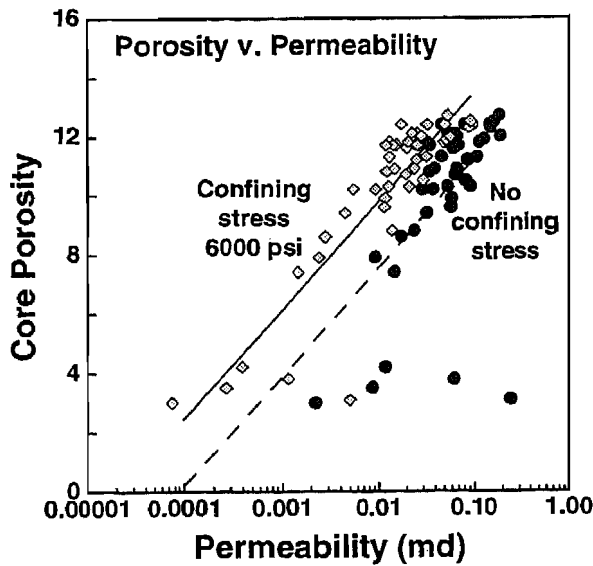
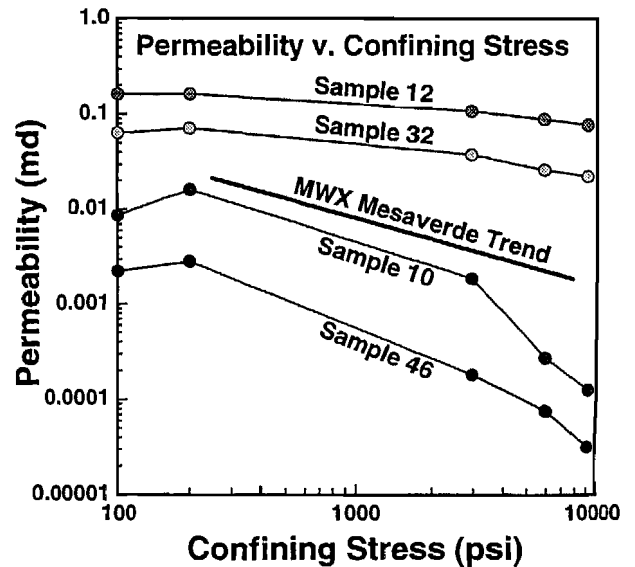


Figure 39 Porosity vs. Log Permeability for Samples at Two Confining Pressures from the Pilot Core of the Champlin 254 Amoco B 2-H Well

It has also been suggested in the past that 12 percent porosity is where the real “sweet spot” begins in these sandstones. These data again verify this concept that 0.1 md and above in situ permeability is reached at 12 percent porosity and above.

Permeability versus confining stress for a few individual samples is shown in Figure 40. Also shown is a line corresponding approximately to the permeability decrease shown by Sattler (1989) as the MWX Mesaverde trend. Sands at MWX lack the permeability “sweet spot” that the Echo Springs Almond Formation displays. It is also apparent that the MWX Mesaverde sands consistently show less permeability decrease than the very tight Almond Formation sandstones. Yet the sweet spot of the Almond Formation sandstones has relatively less permeability decrease with confining stress than the MWX Mesaverde sandstones. Again, this shows that the standard permeability analyses that has been used for the Almond Formation are good indicators of relative variations in permeability.

Figure 40 Permeability vs. Confining Stress for Four Samples from the Champlin 254 Amoco B 2-H Well



Laboratory Results: Petrophysical Data

Samples 3 through 10 and 17 through 22 were used in an attempt to estimate the Archie constants "a" and "m" of the saturation equation,

$$S_w^n = (aR_w)/(\phi^m R_t)$$

where S_w = water saturation

n = saturation exponent

a = cementation constant

R_w = water resistivity

m = cementation exponent, and

R_t = true formation resistivity.

Table 7 lists these analyses. Water resistivity R_w is established at 0.1395 ohm-m at 74°F by using a constant-salinity brine in the measurements. This R_w approaches actual connate water resistivity in the Standard Draw gas field. The core plug samples selected represent an attempt to obtain the widest possible variation in porosity, as this is what is needed for cross-plotting techniques. Unfortunately, the porosity spread is not sufficient for precise determination of the cementation exponent, m . The samples were saturated with a selected brine, and resistivity R_t was measured. Each sample was also partially desaturated to a lower S_w , and resistivity R_t and S_w were measured again. A plot of porosity versus resistivity is shown in Figure 41. A line of 100 percent water saturation and fixed cementation constants (Figure 41) is drawn for reference to see how close this line fits the data. A second line of 50 percent water saturation, with the same cementation constants, is also drawn for reference. This 50 percent saturation line goes through the cluster of data approximating 50 percent saturation as measured in the laboratory. It is difficult to precisely control water saturation in such tight sandstones, so a window of $S_w = 45$ to 55 percent was used to estimate $S_w = 50$ percent. Within the precision of these measurements, it appears that the saturation calculations are valid for the Almond sandstone.

Initially, an "m" value was calculated for each individual sample, and an average of $m=1.8$ was estimated (Table 7). The two tight samples (10 and 22 at porosities under 4 percent) have individual "m" values of 1.4 and 1.3, respectively. Two hypotheses are presented to explain these low "m" values. First, these tight samples are siltstones containing a high fraction of clay minerals. The clay minerals contribute excessive conductivity, thus lowering the measured resistivity below the value expected by Archie's rule. Secondly, these siltstones probably contain microfractures, which again contribute to higher conductivity as compared to completely intergranular porosity. This idea is also verified by the large permeability reduction observed with confining stress (Figure 39) for these samples. If these points are removed from the average "m" calculation, then $m = 1.9$ is obtained. Due to the scatter of the data, and the limited range of permeability, $m = 2.0$ is a good fit to these data.

Table 7 Formation Factor Test Results, Champlin 254 Amoco B 2-H (K&A Laboratories)

Sample Number	Depth, ft	Air Permeability, md	Confining Pressure, psig	Porosity, percent	Formation Factor	Phase Angle, degree	Individual Cementation Exponent, "m"
3	10,034.6	0.053907	0.00	12.1	65.56	0.70	1.98
4	10,038.7	0.029900	0.00	11.7	73.05	0.60	2.00
5	10,042.7	0.034600	0.00	10.8	72.68	0.80	1.93
6	10,046.7	0.106000	0.00	11.3	57.29	0.70	1.86
7	10,050.7	0.063500	0.00	10.7	62.43	0.70	1.85
8	10,054.7	0.060900	0.00	11.6	58.35	0.70	1.89
9	10,058.7	0.032300	0.00	9.4	61.50	0.70	1.74
10	10,063.3	0.008650	0.00	3.5	142.1	0.80	1.48
17	10,047.6	0.184000	0.00	12.7	53.97	0.70	1.93
18	10,051.6	0.080300	0.00	12.4	51.84	0.70	1.89
19	10,054.6	0.060500	0.00	11.7	58.38	0.70	1.90
20	10,055.6	0.068700	0.00	11.7	60.24	0.70	1.91
21	10,060.6	0.017200	0.00	8.6	82.26	0.60	1.80
22	10,064.6	0.247000	0.00	3.1	95.42	0.90	1.31

Water Resistivity, "Rw" = 0.1395 ohm-meters at 73.8°F
 Composite Cementation Exponent, "m" = 1.79 at 0.00 psi confining pressure

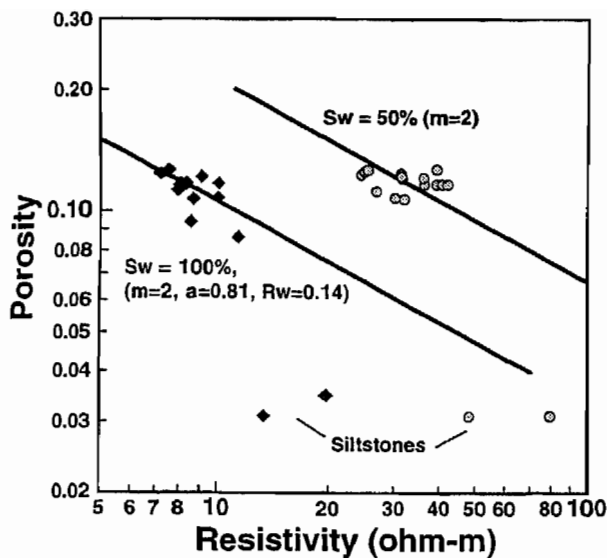


Figure 41 Pickett Plot for Samples from the Champlin 254 Amoco B 2-H Showing that $m=2$ Provides a Good Match for Varying Water Saturation

Calculation of the saturation exponent, n , is also accomplished by plotting resistivity versus water saturation. Table 8 lists the saturation and resistivity values measured for these samples. Figure 42 shows resistivity versus saturation based on the core plugs used in Figure 41. In Figure 42, the whole range of measured saturations is used to estimate the exponent n . A least-squares line yields a value of $n=2.04$, which is considered close enough to 2.0 to assume $n=2.0$.

With n , a , and m defined, the Archie equation simplifies to

$$S_w = (0.9/\phi) (R_w/R_t)^{1/2},$$

which is the equation commonly used for sandstones.

Laboratory Results: Capillary Pressure Curves

Capillary pressure curves were obtained for six selected plugs in the Almond Formation sandstone. Samples 2, 3, 16, 17, 45 and 46 were selected for these experiments. Complete results are listed in Table 2. Mercury is a nonwetting phase, so pressure increases rapidly with increasing mercury saturation in all six samples. Two sample curves are shown in Figure 43. The samples begin gas saturated (dried), and mercury is slowly injected. Pressure increases rapidly as the mercury initially fills the larger pore spaces on the injection end of the core. A break in slope is observed when the mercury begins to fill the entire pore network. If a line is drawn along this slope and extrapolated back to zero saturation, then an estimate of threshold displacement pressure is obtained (Schowalter, 1979).

Table 8 Resistivity Index Test Results, Champlin 254 Amoco B 2-H (K&A Laboratories)

Sample Number	Depth, ft	Air Perm., md	Confining Press., psig	Porosity, percent	At 0.0 psig Confining Pressure			
					Brine Saturation, Percent Pore Volume	Resist. Index, R.I.	Phase Angle, degree	Saturation Exponent, "n"
3	10,034.6	0.0539	0.00	12.1	90.2	1.21	0.71	1.93
					86.8	1.42	0.70	
					75.3	1.77	0.80	
					60.0	2.53	0.51	
					51.9	3.47	0.60	
48.5	3.98	0.61						
4	10,038.7	0.0299	0.00	11.7	94.3	1.14	0.60	2.11
					89.1	1.23	0.70	
					77.3	1.76	0.70	
					64.4	2.53	0.66	
					52.7	3.88	0.50	
5	10,042.7	0.0346	0.00	10.8	91.3	1.18	0.80	1.94
					85.5	1.40	0.70	
					73.4	1.88	0.40	
					62.2	2.54	0.50	
					55.0	3.00	0.50	
6	10,046.7	0.106	0.00	11.3	92.8	1.19	0.70	1.87
					85.1	1.31	0.70	
					76.9	1.75	0.80	
					63.3	2.38	0.70	
					50.6	3.38	0.55	
44.3	4.51	0.50						

Water Resistivity, "Rw" = 0.1395 ohm-meters at 73.8°F

Table 8, Continued

Sample Number	Depth, ft	Air Perm., md	Confining Press., psig	Porosity, percent	At 0.0 psig Confining Pressure			
					Brine Saturation, Percent	Resist. Index, R.I.	Phase Angle, degree	Saturation Exponent, "n"
7	10,050.7	0.0635	0.00	10.7	94.2	1.16	0.70	2.03
						87.9	1.27	0.80
						75.4	1.78	0.70
						63.8	2.51	0.50
						52.2	3.70	0.60
8	10,054.7	0.0609	0.00	11.6	90.7	1.17	0.90	2.12
						85.0	1.46	0.85
						79.2	1.79	0.80
						62.4	2.75	0.60
						56.6	3.08	0.51
9	10,058.7	0.0323	0.00	9.4	92.4	1.20	0.80	2.18
						84.7	1.38	0.80
						76.2	1.97	0.71
						62.9	2.80	0.61
						58.0	3.03	0.60
10	10,063.3	0.00865	0.00	3.5	82.4	1.55	0.90	1.98
						69.3	2.02	0.90
						67.9	2.10	0.85
						66.4	2.22	0.88

Table 8, Continued

At 0.0 psig Confining Pressure									
Sample Number	Depth, ft	Air Perm., md	Confining Press., psig	Porosity, percent	Brine Saturation, Percent Pore Volume	Resist. Index, R.I.	Phase Angle, degree	Saturation Exponent, "n"	
						82.9	1.47	0.80	
						74.4	1.70	0.70	
						65.8	2.25	0.70	
						53.2	3.38	0.68	
						42.7	5.22	0.40	
18	10,051.6	0.0803	0.00	12.4	92.5	1.20	0.80	2.00	
						84.9	1.33	0.80	
						72.0	1.91	0.71	
						66.1	2.37	0.60	
						54.0	3.41	0.50	
						47.7	4.37	0.40	
19	10,054.6	0.0605	0.00	11.7	93.0	1.26	0.76	2.31	
						85.9	1.38	0.71	
						73.2	2.00	0.70	
						67.0	2.74	0.58	
						51.7	4.48	0.50	
						48.6	5.00	0.50	
20	10,055.6	0.0687	0.00	11.7	93.3	1.26	0.90	2.41	
						86.2	1.44	0.80	
						73.0	2.24	0.50	
						60.8	3.03	0.52	
						50.6	5.00	0.40	

Table 8, Continued

Sample Number	Depth, ft	Air Perm., md	Confining Press., psig	Porosity, percent	At 0.0 psig Confining Pressure			
					Brine Saturation, Percent Pore Volume	Resist. Index, R.I.	Phase Angle, degree	Saturation Exponent, "n"
21	10,060.6	0.0172	0.00	8.6	90.9	1.25	0.66	1.99
						82.4	1.41	0.60
						73.4	1.76	0.50
						62.4	2.71	0.50
22	10,064.6	0.247	0.00	3.1	76.5	1.85	0.90	2.12
						64.7	2.55	0.90
						54.7	3.62	0.97
						42.9	5.98	0.98
						32.8	10.1	1.00

Water Resistivity, "Rw" = 0.1395 ohm-meters at 73.8°F

Figure 42 Saturation Exponent Measured on Champlin 254 Amoco B 2-H Pilot Core Samples

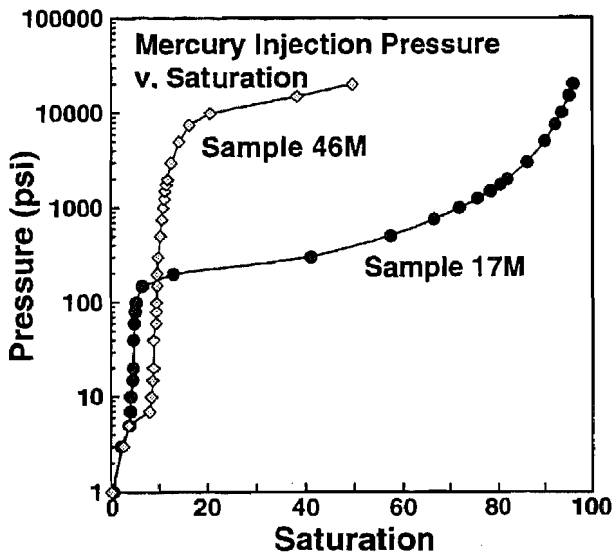
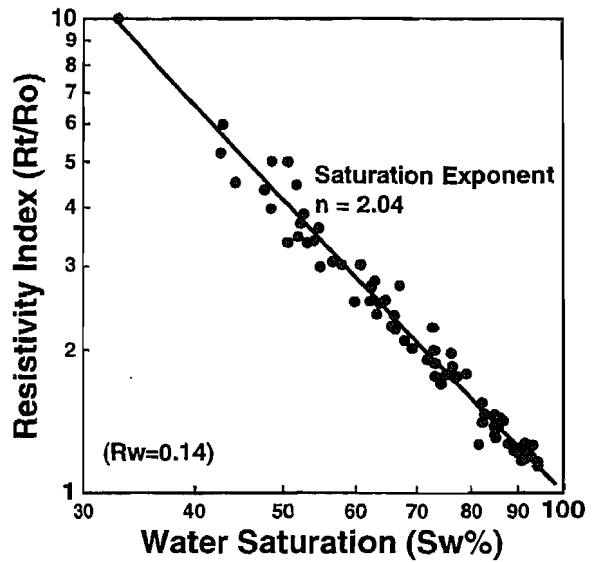


Figure 43 Capillary Pressure Curves for Two Almond Formation Sandstones, Champlin 254 Amoco B 2-H Well

Threshold displacement pressure has been examined in many previous studies to investigate the pressure needed to initiate flow through a porous medium when two fluid phases are present. Calculations follow those presented earlier by Katz and co-workers (Thomas, 1967) in a study of gas storage. The sealing capacity of sandstones in the entrapment of overpressured reservoirs has also been related to this threshold displacement pressure (Iverson and others, 1995). Basically, an effective seal is formed whenever the gas reservoir pressure is below the threshold pressure required to initiate Darcy flow and leakage of gas out of the reservoir. This detail of stratigraphic trapping works under two-phase fluid flow to allow a tight sandstone such as the Almond Formation to act as both a reservoir and a seal. With high gas pressure or low threshold pressure, the sand acts as a reservoir. At high threshold pressures or low gas pressure, the sandstone is effectively a seal.

Threshold displacement pressures were extrapolated for six samples of the Almond Formation sandstone, and are plotted against the reference (zero confining stress) gas permeability in Figure 44. Also shown in Figure 44 are two clusters of data derived from published sources on capillary pressure. One cluster (Reservoirs, Sandstones in Figure 44) with high permeability corresponds to good reservoirs. The other cluster (Seals, Shales) corresponds to seals such as shale, anhydride or dolomite. Such seals do have a finite gas (single-phase) permeability yet very high threshold displacement pressure, causing them to act as seals. The Almond Formation sandstone points fall intermediate between seals and reservoirs. This indicates that tight portions of the reservoir seal the gas into higher-permeability portions. Therefore, good drainage of the Almond Formation sandstones can be achieved only in a very continuous permeable zone, or in a zone where hydraulic fracturing has placed more sands in communication with each other.

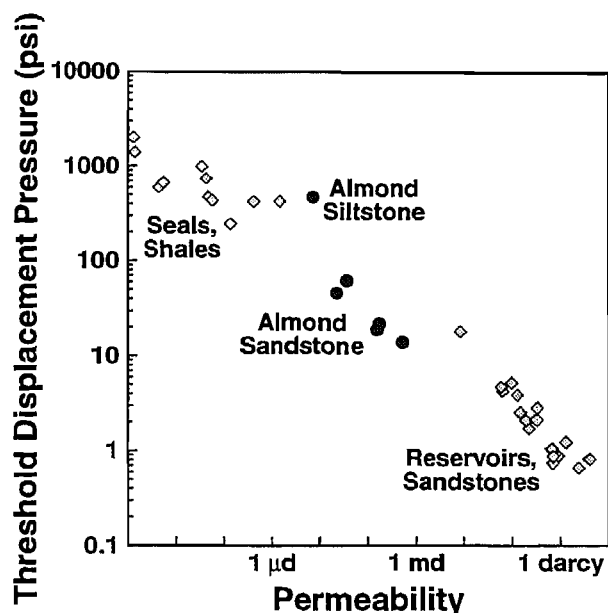


Figure 44 Threshold Displacement Pressures, as Derived Using a Method Described by Schowalter (1979)

Laboratory Results: Effective Permeability

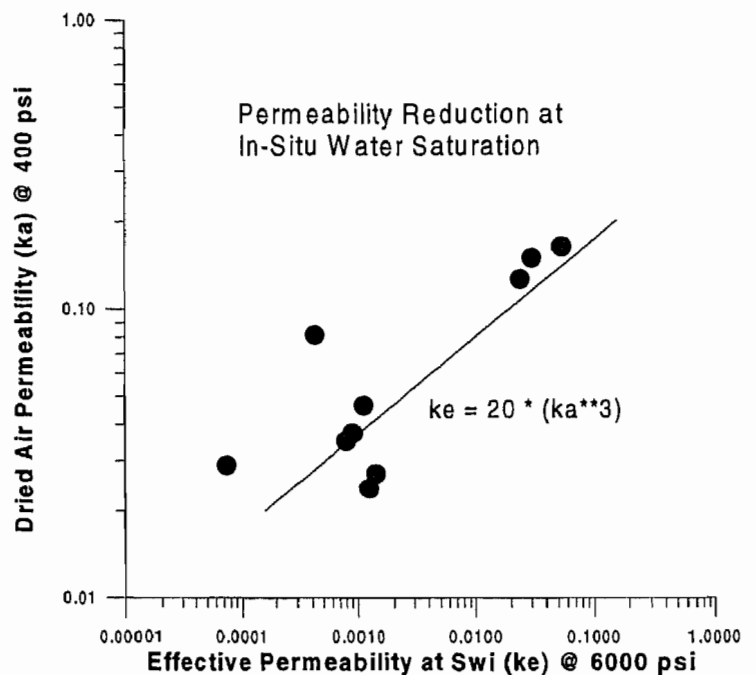
Ten samples were selected for analysis of effective permeability. Each sample was saturated with brine water (as before) to achieve an initial water saturation of approximately 30 to 40 percent. Then gas was forced through each sample at a series of confining stresses. The initial water saturation in each core is variable, depending upon the capillary forces within the core and the ability of the core to hold water during the air permeability experiment. This reference air permeability is identical to that shown in Figure 39 for no confining stress on an air-dried sample. Each of these ten samples was then placed in a permeameter, and gas permeability was measured at confining stress.

Gas permeability decreases as a function of confining stress, just as was shown in Figures 39 and 40. However, the decrease with confining stress is much greater due to the presence of water in the samples. Mild decreases are observed in the more permeable samples but drastic decreases in permeability are observed in the very tight samples.

These results are summarized in Figure 45 where the reference air permeability (as before) is plotted against the effective permeability with water in the sample. The applied confining stress for these samples is 6,000 psi, equivalent to our approximation of Echo Springs effective reservoir stress.

Although there is considerable scatter in these data, a rough correlation can be estimated for calculating effective in situ gas permeability at confining stress (k_e), from a reference air permeability without confining stress (k_a). The line shown in Figure 45 is a power law relationship between k_e and k_a and implies that a 0.1 md sandstone will still have about 0.2 md in the subsurface. However, a very tight sand (0.01 md dry gas permeability) will reduce to 0.0002 md effective gas permeability in the subsurface at 6,000 psi effective stress. Such a relationship should be useful for estimating the appropriate permeability to use in reservoir simulators, where the use of in situ rock properties is required. The importance of fractures (either natural or induced) in such tight rocks is obvious.

Figure 45 Common Air Permeability Vs. In Situ Effective Gas Permeability for Almond Sands



CONCLUSIONS

This analysis finds good evidence for open fractures at depth in the vicinity of the Champlin 254 Amoco B 2-H wellbore. There is demonstrable evidence that using the scanning electron microscope provides a means of measuring fracture apertures at in situ pressures as well as examining small-scale roughness and fracture fillings. Four minerals, quartz, kaolinite, barite and calcite, formed in that order to fill and line the fractures. Because they completely bridge fractures, the later-forming cements (barite and calcite) likely represent the greatest threat to fracture permeability.

The Almond Formation sandstones are fine- to very-fine-grained, have a composition of Q72 F3 L25, and contain an abundance of quartz and dolomite cements, mixed-layer clays such as corrensite, illite/smectite and kaolinite. An average of 93 percent of the porosity is behind pore aperture radii of 0.54 μm .

In the Champlin 254 Amoco B 2-H core, the average fracture apertures range from 59 to 118 μm . These values are higher than those used in the reservoir modeling. The calculated plug permeabilities give geometric averages ranging from 297 to 3,108 md. These values are high in relation to the production history of the well (see Branagan, this volume).

Several factors likely contribute to this discrepancy. First, the areal extent of the fractures is unknown, and may be small. A few of the fractures terminate within the diameter of the whole core as they traverse it at an oblique angle, suggesting that those fractures are of limited extent. Limited areal extent would reduce the open fracture contribution to production flow rate.

Second, the presence of the observed patchy cements reduces the overall permeability; however, the magnitude of the effect is unknown. The presence of kaolinite in the fractures may indicate some sensitivity to permeability reduction as a result of migration of fines and brushpiling. The patches of kaolinite, as stated earlier, have porosities in the range 15 to 40 percent. Should these microporous areas remain stable during production, their permeability would be less than that of an open fracture. Furthermore, the presence of drilling mud in the fractures of core samples may be an indication of wellbore damage.

The formation evaluation data help verify that the Standard Draw gas field as a whole produces gas from more than just the single Almond Formation sandstone. The concept of sweet-spot reservoirs as described by Iverson and Surdam (1993) is entirely consistent with the observations made in these detailed core analysis studies. First, the gas-in-place estimates of Iverson and Surdam (1995) are verified as calculated from Archie's rule and well logs. Second, the permeabilities from standard core analyses are indicative of relative changes of permeability at in situ conditions. Third, Almond Formation sandstones can act as a seal or a reservoir depending on the threshold displacement pressure. Hydraulic fracturing enables the drainage of many layers of sandstone in the upper Almond Formation. Although natural fractures certainly help to achieve high flow rates from any one sand, the individual natural fractures apparently do not tie the Almond Formation sand bodies together.

With the confirmation of Standard Draw draining numerous stacked sandstones, continued focus on hydraulically fractured vertical or slant hole completions in the bar sand may be justified. This idea is verified by the production histories shown in Figure 46. The Champlin 254 Amoco B-1 (vertical) well was drilled in 1981, hydraulically fractured, and put on line for an average of 1 MMSCFD in the first year. To date, about 2 BSCF has been produced, and the Champlin 254 B-1 well is probably an economic success, especially if the low decline rate continues for the next 30 years (the EUR is 5.24 BSCF at year 2025). The Champlin 254 Amoco B 2-H (horizontal) well has not been producing on-line long enough to determine an accurate decline, but it appears to be producing about the same as the 254

B-1. Considering the additional cost of horizontal drilling, the economics likely favor vertical or slant hole completions. The horizontal well probably will recover gas more efficiently from the single Almond Formation bar sand. However, without hydraulic fracturing, the sands beneath are not tapped, and the well cannot be a spectacular producer.

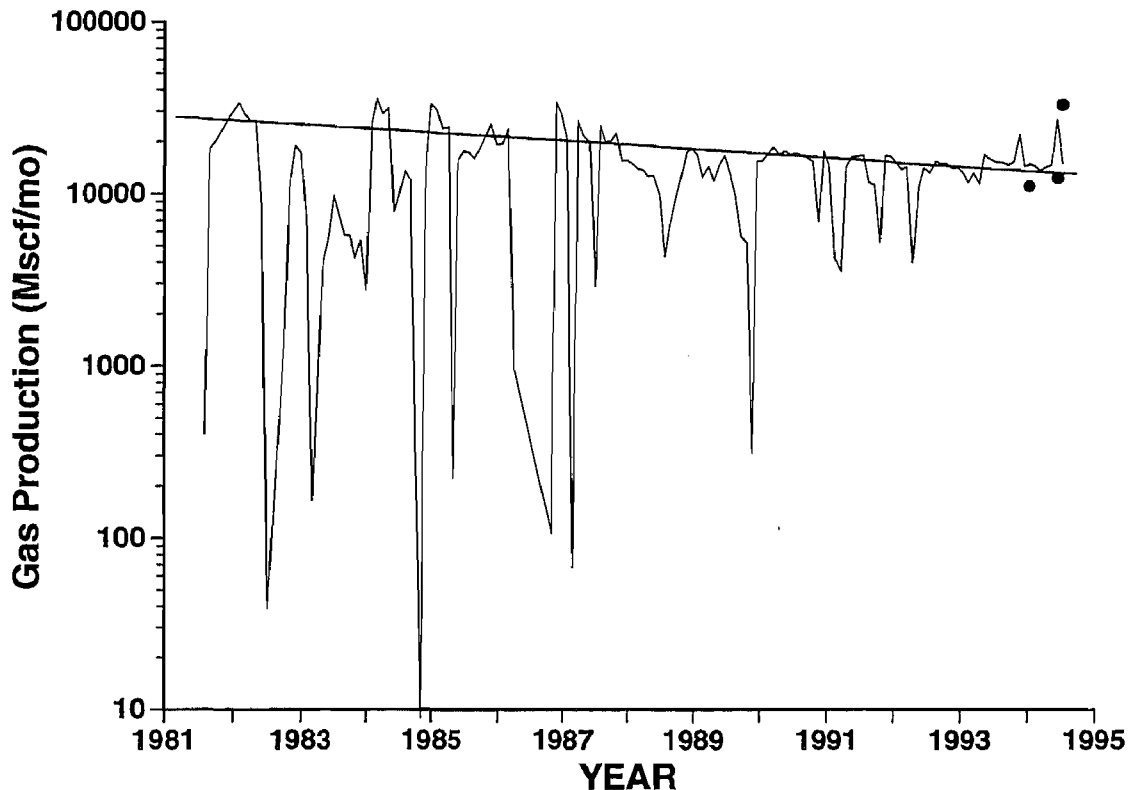


Figure 46 Production Histories for the Champlin Amoco 254B-1 (solid line) and the Champlin 254 Amoco B 2-H (dots) (data obtained from Petroleum Information)

As additional information such as basin paleostresses, fracture areal extent, and distribution of fracture fillings, become known, horizontal well completions may provide an efficient method to access the enormous natural gas resource present in Mesaverde Group of the Greater Green River Basin.

ACKNOWLEDGMENTS

Financial support for this study was provided by the Gas Research Institute (Contract No. 5091-221-2146) and through a subcontract with CER Corporation (Gas Research Institute Contract No. 5093-212-2589). The manuscript was improved with editorial help of David Copeland. Allory Deiss prepared the graphic arts. Scott Stookey provided petrographic

data. The senior author thanks Randy Billingsley, Paul Branagan, Lesley Evans, Robin Hill, and John Lorenz for their thoughtful discussions. The UW microbeam laboratory is kept healthy through the care of Keith Krugh and Susan Swapp.

REFERENCES

Brower, K.R. and N.R. Morrow, 1985: "Fluid Flow in Cracks as Related to Low-Permeability Gas Sands," *Society of Petroleum Engineers Journal*, V. 25, p. 191-201.

Evans, L.W. and D. Thorn, 1995: "Formation MicroImager, MicroScanner, and Core Characterization of Natural Fractures in a Horizontal Tight Gas Wellbore," *American Association of Petroleum Geologists Abstracts for 1995 Rocky Mountain Section Meeting*.

Gies, R. M., 1987: "An Improved Method for Viewing Micropore Systems in Rocks with the Polarizing Microscope," *Society of Petroleum Engineers Formation Evaluation*, V. 2, p. 209-214.

Gregory, R.W. and R.H. DeBruin, 1991: "Oil and Gas Fields Map of the Greater Green River Basin and Overthrust Belt, Southwestern Wyoming," *Wyoming Geological Survey Map Series No. 38*.

Hall, M.G. and G.E. Lloyd, 1981: "SEM Examination of Geological Samples with a Semiconductor Back-Scattered Electron Detector," *American Mineralogist*, V. 66, p. 362-368.

Hyman, L.A., D.J. Malek and C.A. Admire, 1991: "The Effects of Microfractures on Directional Permeability in Tight Gas Sands," *SPE Paper 21873*, *Society of Petroleum Engineers Rocky Mountain Regional Low Permeability Reservoirs Symposium*, Denver, April 15-17.

Iverson, W.P., R.S. Martinsen and R.C. Surdam, 1992: "Pressure Compartments in the Powder River Basin, Wyoming," *SPE Paper 24357*, presented at the *Society of Petroleum Engineers Rocky Mountain Regional Meeting*, Casper.

Iverson, W.P. and R.C. Surdam, 1995: "Tight Gas Sand Production from the Almond Formation, Washakie Basin, Wyoming," *SPE Paper 29559*, presented at the *Society of Petroleum Engineers Rocky Mountain Regional Meeting & Low-Permeability Reservoirs Symposium*, Denver.

Iverson, W.P., R.S. Martinsen and R.C. Surdam, 1995: "Pressure Seal Permeability and Two-Phase Flow," in P. Ortoleva, Ed., *Pressure Compartmentalization in Sedimentary Basins: American Association of Petroleum Geologists Memoir 61*, Chapter 20, p. 313-319.

Keighin, C. W., B.E. Law and R.M. Pollastro, 1989: "Petrology and Reservoir Characteristics of the Almond Formation, Greater Green River, Basin, Wyoming," in E. Coalson, S. Kaplan, C. Keighin, C. Oglesby, J. Robinson, Eds., *Rocky Mtn. Assoc. Geol., Petrogenesis and Petrophysics of Selected Sandstone Reservoirs of the Rocky Mountain Region*, p. 281-298.

Lorenz, J. C. and R.E. Hill, 1994: "Subsurface Fracture Spacing: Comparison of Inferences from Slant/Horizontal and Vertical Cores," *Society of Petroleum Engineers Formation Evaluation*, V. 9, p. 66-72.

- Mesheryakova, G.S., 1993: "Gas Cross-Over Effect in the Tight Gas Sands, Almond Formation, Washakie Basin, Wyoming," M.S. thesis, University of Wyoming, 137p.
- Moore, D.M. and R.C. Reynolds, Jr., 1989: X-Ray Diffraction and the Identification and Analysis of Clay Minerals: New York, Oxford University Press, 332 p.
- Morrow, N. R., K.R. Brower, S. Ma and J.S. Buckley, 1990: "Fluid Flow in Healed Tectonic Fractures," *Journal of Petroleum Technology*, V. 42, p. 1310-1318.
- Nadeau, P.H. and A. Hurst, 1991: "Application of Back-Scattered Electron Microscopy to the Quantification of Clay Mineral Microporosity in Sandstones," *Journal of Sedimentary Petrology*, V. 61, p.921-939.
- Nelson, R.A., 1985: "Geologic Analysis of Naturally Fractured Reservoirs," *Contributions in Petroleum Geology and Engineering*, No. 1, Gulf Publishing Co., Houston, 320 p.
- Pitman, J.K. and W.W. Dickinson, 1989: "Petrology and Isotope Geochemistry of Mineralized Fractures in Cretaceous Rocks—Evidence for Cementation in a Closed Hydrologic System," *U.S.G.S. Bulletin*, No. 1886, p. J1-J15.
- Reynolds, R.C., Jr. and J. Hower, 1970: "The Nature of Interlayering in Mixed-Layered Illite-Montmorillonites," *Clay and Clay Minerals*, V. 18, p.359-367.
- Sattler, A.R., 1989: "Core Analysis: Multiwell Experiment Final Report, Volumes III and IV," *Sandia Laboratory Reports SAND88-3284 and SAND89-2612*.
- Schowalter, T.T., 1979: "Mechanics of Secondary Hydrocarbon Migration and Entrapment," *American Association of Petroleum Geologists Bulletin*, V. 63, p. 723-776.
- Soeder, D. J., 1990: "Application of Fluorescence Microscopy to Study of Pores in Tight Rocks," *American Association of Petroleum Geologists Bulletin*, V. 74, p. 30-40.
- Snow, D.T., 1968a: "Rock Fracture Spacings, Openings and Porosities," *American Society of Civil Engineering Journal, Soil Mechanics and Foundation Division*, V. 94, SM1.
- Snow, D.T., 1968b: "Fracture Deformation and Changes of Permeability and Storage Upon Changes of Fluid Pressure," *Colorado School of Mines Quarterly*, V. 63, p. 201-244.
- Thomas, L.K., 1967: "Threshold Pressure Phenomena in Porous Media," Ph.D. Dissertation, University of Michigan, 148 p.
- Yin, P. and R.C. Surdam, 1993: "Diagenesis and Overpressuring in the Almond Sandstones, Mesaverde Group," in B. Stroock and S. Andrew, Eds., *Wyoming Geological Association Jubilee Anniversary Field Conference Guidebook*, p. 349-358.
- Yin, P., J. Liu. and R.C. Surdam, 1992: "Petrographic and Petrophysical Properties of the Almond Sandstone in the Washakie Basin," in C. Mullen, Ed., *Rediscover the Rockies: Wyoming Geological Association, Forty-Third Annual Field Conference Guidebook*, p. 191-206.

RESERVOIR ENGINEERING STUDY OF THE CHAMPLIN 254 AMOCO B 2-H, WAMSUTTER FIELD, WYOMING

*Paul T. Branagan
Branagan & Associates*

RESERVOIR ENGINEERING SUMMARY

The reservoir engineering portion of this GRI-sponsored study of the Champlin 254 Amoco B 2-H well involves assessing the overall effectiveness of producing gas from the naturally fractured Upper Almond sandstone with a long, near-horizontal wellbore. This engineering effort initially focused on consolidating the various geologic, geophysical and other field data into a comprehensive three-dimensional (3-D) naturally fractured reservoir model; the model was then used to help direct field testing, evaluate the influence and effectiveness of the natural fractures to enhance gas flow, simulate production and pressure histories, and forecast reservoir performance.

The engineering aspects of this study were performed in three basic segments that include:

1. an initial meeting to review existing data and provide recommendations regarding drilling and additional data collection from the Champlin 254 Amoco B 2-H;
2. the formulation of a base reservoir model from which to assess early-time gas production data and recommend further field testing; and
3. the history matching of production data and assessing the role of the natural fractures in enhancing production.

Although the results of this study suggest that production from the Champlin 254 Amoco B 2-H (averaging about 900 MSCFD) is above normal for vertically stimulated wells in the area, it is a relatively modest rate for this naturally-fractured reservoir setting coupled to an open horizontal borehole with an effective length of 1,500 ft. (*Editor's Note: 1,500 ft is the effective borehole length that crosses the primary natural fracture set; the actual wellbore is 1,700 ft in zone or 2,100 ft in zone in the redrill.*)

Furthermore, natural fractures do not appear to significantly influence present day gas production even though they are apparently well developed in this area. Outcrop and well data suggest that natural fractures occur as a predominately unidirectional set (see Hill, this volume); however, this interpretation cannot be validated by the reservoir modeling. The production data can be simulated with a uniform-permeability reservoir without invoking an anisotropic production process as would be the case if flow were controlled by a predominately unidirectional fracture set.

Since the modest production rates indicate that gas flow in the natural fractures is impeded, it may be the result of a series of complex damage mechanisms or simply that liquids are present in the horizontal portion of the well. The presence of liquids would not only severely limit gas flow through natural fractures near the wellbore, it would also significantly reduce production through the "open" but liquid-filled wellbore.

These engineering study results are applicable to both the original well and the second, or "redrill", well which is parallel and about 200 ft west of the original well.

RESERVOIR DESCRIPTION

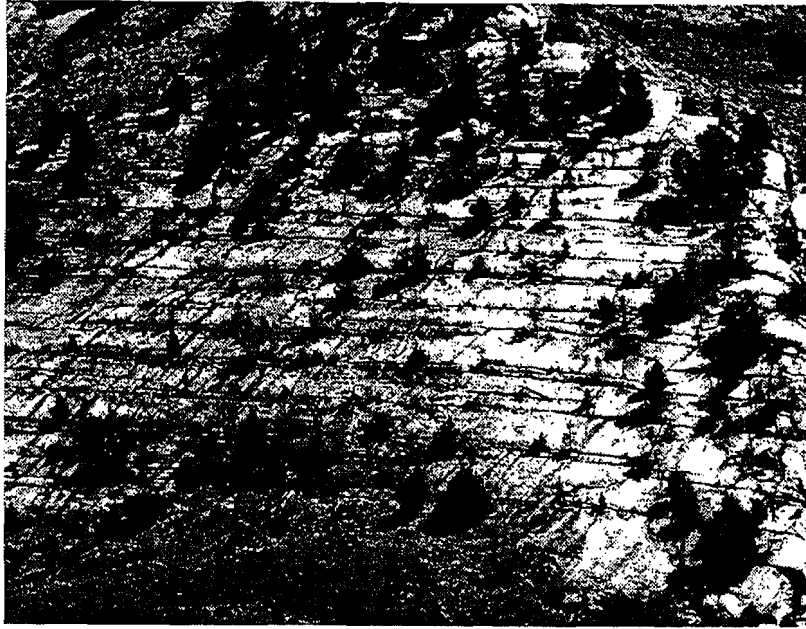
Natural Fractures

Initial reservoir properties including natural fracture data used to develop the 3-D naturally-fractured reservoir model for the Champlin 254 Amoco B 2-H were taken from several sources. These sources include prior Greater Green River Basin outcrop studies (Lorenz and Laubach, 1994; Lorenz, 1994), core and log data from the vertical and horizontal portions of the Champlin 254 Amoco B 2-H well, and production information from nearby wells. These data were used to build a descriptive reservoir model of the naturally-fractured Upper Almond sandstone that would be drained by an open horizontal wellbore with an effective length of 1,500 ft.

Outcrop data described by Lorenz (1994) indicate that natural fractures in the Greater Green River Basin often occur as a regularly-spaced, unidirectional set. An example of this natural fracture pattern is shown in Figure 47. The dominant, evenly-spaced fracture set is intersected by an irregularly-spaced cross set of fractures. Production from this fracture pattern could create an elliptical drainage pattern with its major axis following the direction of the dominant fracture set assuming that fracture spacing controls average system permeability and that fracture conductivity is directionally independent. The latter assumption has considerably more relevance for a vertical well and is less of an issue for a horizontal well that presumably crosses the closer, evenly-spaced dominant fracture set.

Lorenz (1994) also provided data regarding the lateral extent, or length, of natural fractures observed in outcrops. These data suggest that individual fractures of the dominant set are generally between 50 and 150 ft long. The secondary, or cross fractures, terminate where they intersect fractures of the dominant set; thus, their average lengths are controlled by the dominant fracture spacing which is about 10 ft.

Characteristics of natural fractures in the Champlin 254 Amoco B 2-H borehole are based on image logs (FMI and FMS) and direct observation of cores. Both core and log data show one set of natural fractures that strikes between N57° to 68°E. Average spacing of these fractures is about 10 ft, but the spacing data is strongly skewed toward closer spacings of about 5 ft (see Hill, this volume).



*Aerial Photo: Grand Hogback, SW Wyoming
*from GRI-94/0020 SNL/BEG

Figure 47 Frontier Outcrop Showing Typical Natural Fractures in the Greater Green River Basin

Natural fractures in the Champlin 254 Amoco B 2-H core were extensively studied by the University of Wyoming (see Dunn, this volume). Their results indicate that fracture apertures range from 8 to 466 μm at in situ conditions and the dominant frequency is toward the low end of the range, about 15-25 μm .

Reservoir Matrix Properties

Almond sandstone cores are described as fine-grained sandstone with average porosity of 10 to 12 percent. Air permeability for these samples ranged from 0.030 to 0.150 md. When measured under a confining stress of 6,000 psi, the permeabilities were reduced by a factor of 3 (0.010 to 0.050 md)(Dunn, this volume); corrected for water saturation, the permeability could be further reduced 3 to 5 times. Therefore, in situ matrix permeability is conservatively estimated to range from 0.002 to 0.017 md.

The permeability of a simple planar slot is fracture width squared dependent as seen in the following equation (Amyx and others, 1960):

$$k_f = 54.4 \times 10^6 * w_f^2 \quad \text{Equation 1}$$

where:

k_f = slot or fracture permeability, 1,000 md

w_f = fracture aperture or width, in.

For an average, 25 μm -wide fracture, the open-slot permeability calculated from Equation 1 is about 54,000 md. The fracture's non-planar features and rough walls could further reduce the in situ average k_f to 40,000 md.

Considering then the average reservoir permeability to be given by:

$$\bar{k}_{\text{sys}} = \frac{k_f * w_f + k_m * (S - w_f)}{S} \quad \text{Equation 2}$$

where:

k_{sys} = average reservoir or system permeability, md

k_f = slot or fracture permeability, md

w_f = slot or fracture width, in.

k_m = matrix or rock permeability, md

S = fracture spacing, in.

From Equation 2, the average, or system, permeability with natural fractures at 10-ft spacing and 0.010 md matrix permeability is:

$$\bar{k}_{\text{sys}} = \frac{40,000 * 0.001 + 0.010 * (10 * 12 - 0.001)}{10 * 12}$$

or,

$$\bar{k}_{\text{sys}} = \frac{40 + 1.2}{120} = 0.343 \text{ md} \quad \text{Equation 3}$$

Thus, natural fracture conductivity, 40 md-in. (3.3 md-ft), is 33 times more conductive than an adjacent matrix block, 1.2 md-in. (0.10 md-ft). This indicates that production is critically dependent on the ability of the natural fractures to remain open (0.001 in.) and conductive (3.3 md-ft).

RESERVOIR MODELING

Simulation Results (Original Wellbore)

Figure 48 is an artist's conception of the 3-D naturally-fractured reservoir model, ZETA I NF. This reservoir model was initialized with the values listed in Table 9.

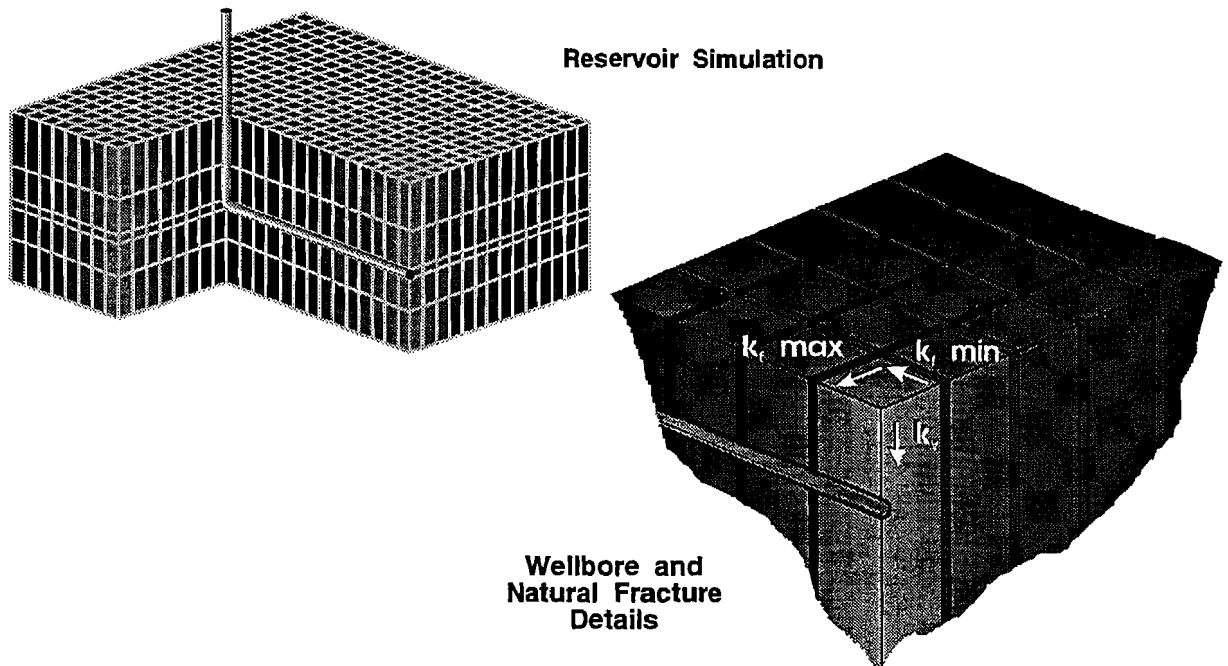


Figure 48 Schematic of the 3-D Naturally Fractured Reservoir Model Used to Simulate the Champlin 254 Amoco B 2-H Field Data

Table 9 Initial Parameters for Reservoir Model

Parameter	Value
Matrix Permeability	0.010 md
Fracture Spacing	10 ft
Fracture Permeability	40,000 md
Fracture Width	0.001 in. (25 μm)
Matrix Porosity	10%
Net Height	30 ft
Horiz Well Length	1,500 ft
Wellbore Diameter	8.5 in.
Depth	10,500 ft

In this initial case, the effects of anisotropic natural fracture permeability were not considered (i.e., $k_{f \max} = k_{f \min}$). These initial modeling runs were, in essence, scoping calculations designed to provide an order of magnitude fit to the field data.

Field production data for the first two months indicated average daily gas rates of about 1,000 MSCFD with surface pressures of nearly 800 psi. Figure 49 shows the measured production rates and surface pressures for the original Champlin 254 Amoco B 2-H well. These are the data that initial model simulations were attempting to match; however, the reservoir simulator predicted production rates in excess of 20,000 MSCFD. Attempts to reduce modeled production rates, including the use of significant permeability anisotropy (50:1), failed to match the lower, measured production by about 1,000 MSCFD.

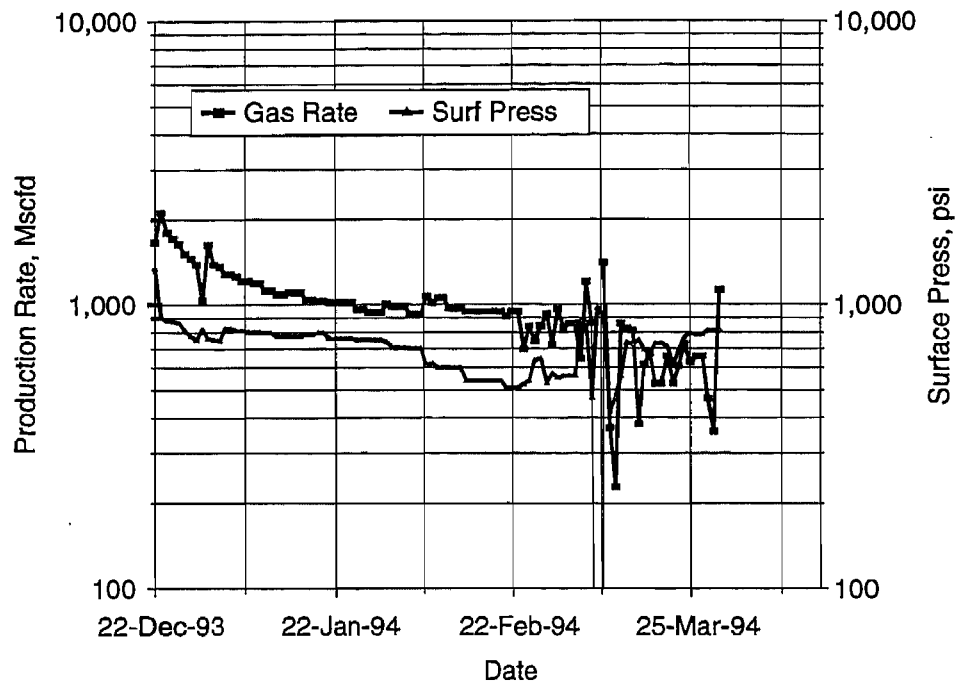


Figure 49 Daily Production Rates and Surface Pressures from the Original Champlin 254 Amoco B 2-H Borehole

A slightly simpler, homogeneous model (ZETA I) was subsequently formulated with the same reservoir values shown in Table 9, but the entire system permeability was confined to the matrix. A series of simulations were then performed where permeability was reduced so as to match the 1,000 MSCFD production rate. Figure 50 shows the model-simulated rates and pressures overlying the measured field data. This is an excellent history match of the field data. However, the average reservoir permeability for this history match was 0.011 md. This result suggests there is little, if any, contribution by natural fractures to production, especially since the initial matrix permeability was assumed to be 0.010 md.

Consider the case where matrix permeability might be closer to the low end of the core measured values, for example 0.002 md. Equation 2 can be used to solve for the natural fracture conductivity component:

$$k_f * w_f = \overline{k_{sys}} * S - k_m * (S - w_f) \quad \text{Equation 4}$$

or,

$$k_f * w_f = 0.011 * 10 - 0.002(10 - 0.001/12) = 0.090 \text{ md} \cdot \text{ft}$$

This result suggests that although fracture conductivity represents about 90 percent of the mixed fracture and matrix components, it is, nevertheless, significantly reduced from the original estimate of 3.3 md-ft by about a factor of 40. For this case, Equation 1 yields a natural fracture width of about 10 μm which is at the low end of the core-measured apertures (Dunn and others, this volume). Note that fracture conductivity is width-cubed dependent; thus, production is extremely sensitive to any reduction in effective fracture width, whether natural or induced.

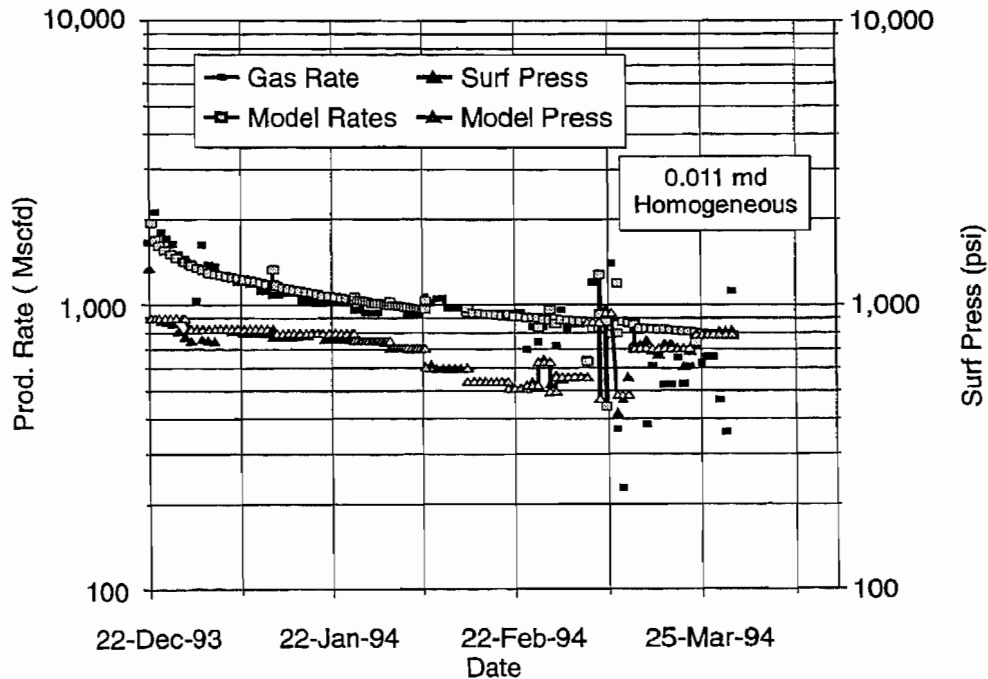


Figure 50 History Match Data from a Homogeneous Reservoir Model Overlying the Field Measured Data from the Champlin 254 Amoco B 2-H

The ZETA I NF naturally fractured reservoir model was re-initialized with a modified set of natural fracture properties to mimic the homogenous case described above. Table 10 is a list of the reservoir parameters with the revised fracture properties that were used for this simulation.

Table 10 Final Parameters for the Naturally-Fractured Reservoir Model

Parameter	Value
Matrix Permeability	0.0005 md
Fracture Spacing	10 ft
Fracture Permeability	1,250 md
Fracture Width	0.001 in. (25 μ m)
Matrix Porosity	10 %
Net Height	30 ft
Horiz Well Length	1,500 ft
Well Bore Diameter	8.5 in.
Depth	10,500 ft

Figure 51 shows the simulated rates and pressures overlying the measured production data. Notice that matrix permeability was reduced to 0.0005 md (Table 10) so that natural fractures could dominate the flow process. Furthermore, fracture width was equated to the average core-measured value of 25 μ m. However, to maintain an average reservoir permeability of 0.011 md, the natural fracture permeability needed to be reduced to 1,250 md (refer to Equation 4). Figure 51 shows the history match is excellent and in good agreement with the previously described homogeneous model results.

Further alterations to the natural fracture permeability were made to assess the possible effects of directionally dependent permeability. Fracture set permeabilities were varied up to a ratio of 50:1 where the high permeability fractures were normal to the borehole axis and the reduced permeability fractures were parallel to the borehole axis. There were no obvious differences in the history match of the field data for this highly anisotropic permeability case.

This result is reasonably consistent with the geometry and properties of this situation where the 1,500-ft borehole is draining an average 0.011 md reservoir over a relatively small lateral distance from the wellbore.

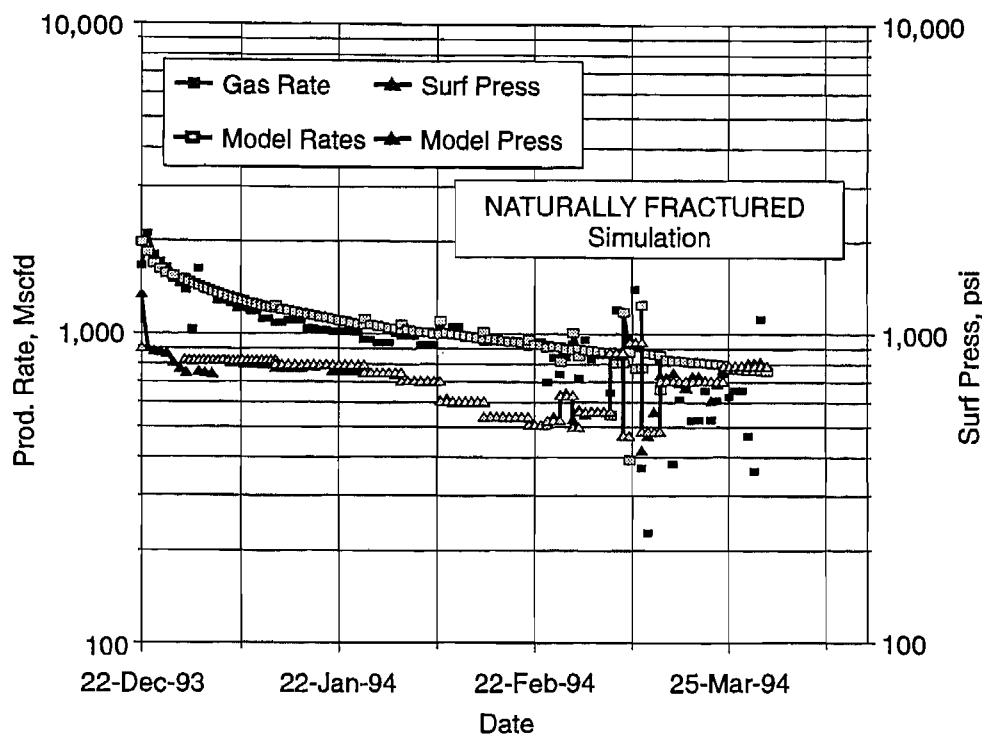


Figure 51 History Match Data from the Naturally Fractured Reservoir Model Overlaying the Field Measured Data

Original Well Model Summary

Reservoir simulation results suggest two possible scenarios for the average production processes occurring along this 1,500-ft horizontal wellbore. One scenario is that natural fractures contribute little, if any, to production; and the matrix, with an average permeability of 0.011 md, controls fluid flow. The alternative scenario is that matrix permeability is virtually insignificant and the natural fractures, although much reduced from their lab-derived values, are the primary conduit for production.

In either scenario, production is significantly lower than its anticipated value. This lower production is apparently caused by reduced conductivity in the natural fractures, either because they are significantly narrower than measured, or intervening completion practices have induced a damage mechanism that, in effect, reduced fracture conductivity. This could be simply the result of water lying stagnant in the horizontal wellbore creating a water block within the fracture system.

Field Testing Recommendations

Additional information regarding a planned bottomhole pressure buildup test was derived from these initial reservoir simulations. The tests were scheduled and intended to determine average system permeability and assess the various flow regimes. Figures 52 and 53 show the results of *simulated* pressure buildup tests displaying delta pressure and linear and radial derivative group curves (Branagan and others, 1993). To generate the

data for Figure 52, the model assumed the full vertical wellbore storage volume in addition to the horizontal wellbore volume; whereas, for Figure 53, the model assumed no wellbore storage in the vertical portion of the well. These simulations were run to evaluate the effects of the large, vertical wellbore storage volume on observing the early-time, radial flow regime that can be used to infer average system permeability. The effects of wellbore storage are seen in Figure 52 where the log-log delta pressure curve exhibits a unit slope for several hours after shut-in, indicating that storage dominates the early-time flow regime. In comparison, Figure 53 shows the storage period lasts less than an hour when the vertical storage volume is made very small. However, storage effects last considerably longer than the end of the unit slope, generally for almost a full log cycle. Notice in Figure 53 that the radial derivative indicates that radial flow dominates the flow process from the end of the storage effects (8 to 10 hrs) until the vertical boundaries exert their influence on flow streamlines (~100 hrs). It is during this radial flow period that average system permeability may be assessed. After the period of radial flow, it takes several hundred hours (10 to 15 days) for the flow regime to transition into linear flow.

However, for the case with full wellbore storage (Figure 52), the radial flow period is masked by the wellbore storage effects which last for almost 100 hours. Thus, unless the storage volume is reduced, k_{avg} cannot be ascertained. However, k_{avg} might be derived from the linear flow period which becomes dominant after 400 to 500 hours. Unfortunately, that shut-in time is too long, and the rate of pressure increase approaches the resolution of the pressure tool.

These two examples exhibit the classic flow regimes that are expected from a long horizontal well (i.e., early radial flow followed by an extended linear flow). However the 10,500-ft vertical wellbore volume seriously limits the ability to determine reservoir properties, especially K_{ave} . Thus, the use of a bottomhole shut-in device is recommended for conducting any future buildup test.

CHAMPLIN 254 AMOCO B 2-H REDRILL

In March 1994, the open, horizontal portion of the wellbore was collapsing. Amoco then decided to redrill the lateral by kicking out of the original vertical well, and drilling a sidetrack well about 200 ft west of the original wellbore (Reinert and Billingsley, this volume). This new well will be referred to as the "redrill."

Effects of Prior Production

To assess the effect of the previous production on reservoir pressure in the redrilled wellbore, the model used to history match the original production was extended to include a shut-in period from March to June, 1994. Figure 54 is a pressure contour plot of the reservoir at the end of production in late March, and Figure 55 is a comparable plot showing the reservoir pressure at the end of the redrill/shut-in period in late June.

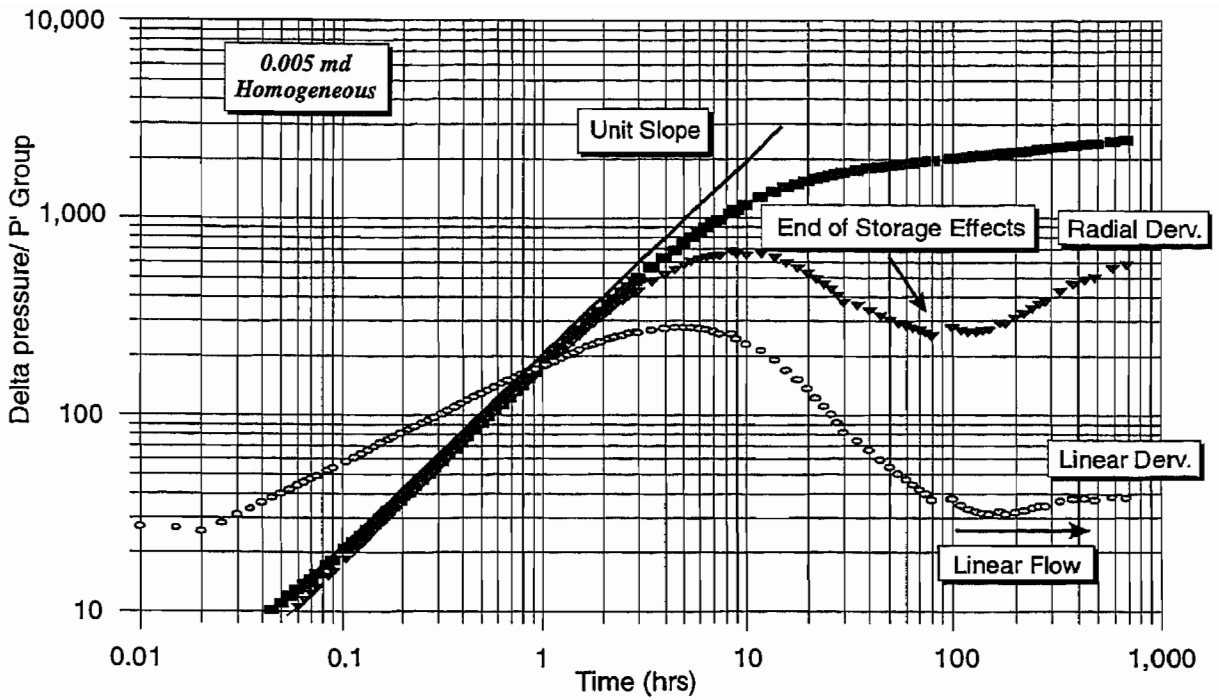


Figure 52 Simulated Pressure Buildup Data with the Full Horizontal and Vertical Wellbore Volumes

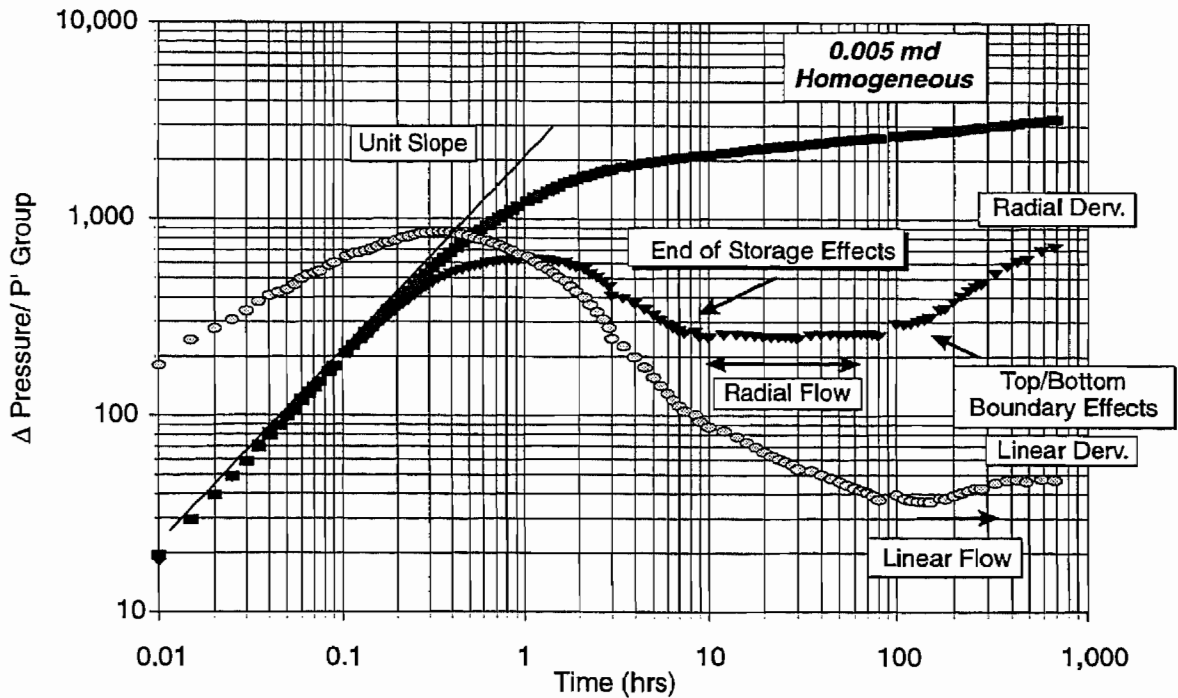


Figure 53 Simulated Pressure Buildup Data with the Horizontal Wellbore Volume Only

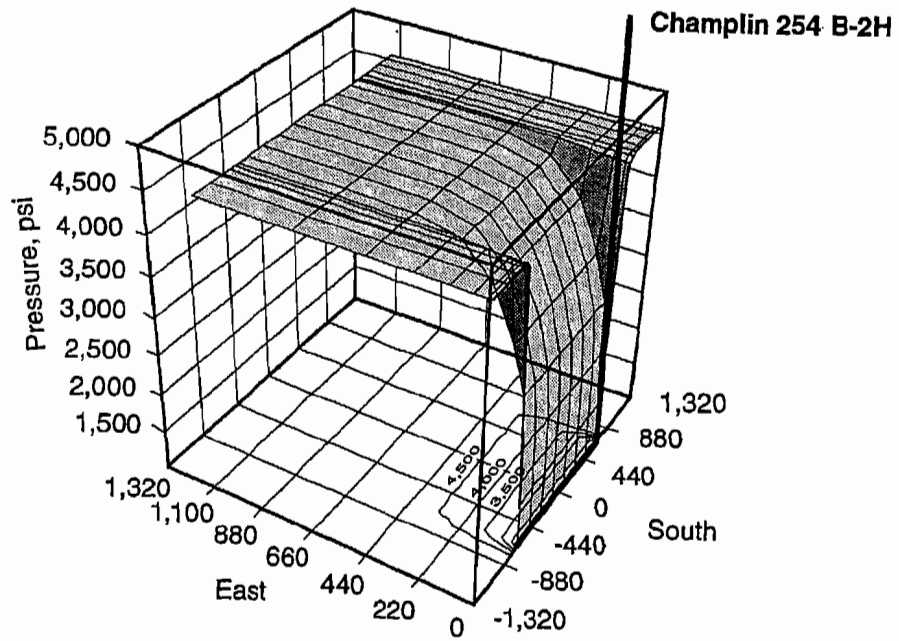


Figure 54 3-D Pressure Contour Map Surrounding the Champlin 254 Amoco B 2-H at the End of Initial Production Period, March 1994

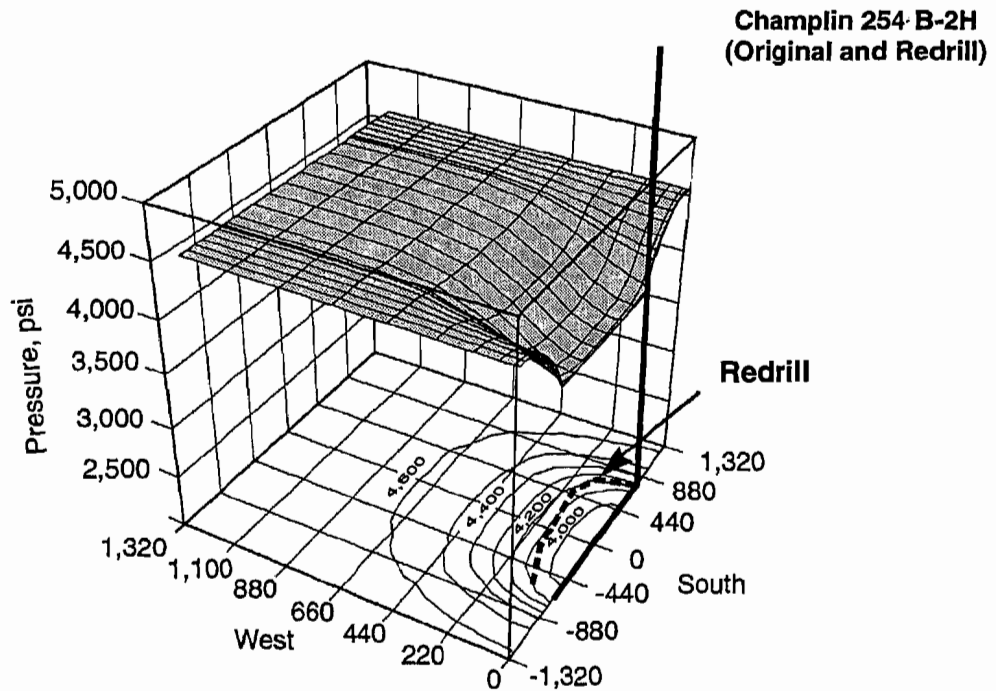


Figure 55 3-D Pressure Contour Map Surrounding the Champlin 254 Amoco B 2-H Just Prior to Production from the Redrill (dashed line), June 1994

Notice the steep drop in reservoir pressure during production (Figure 54) that is significantly diminished by late June (Figure 55). Figure 55 has been annotated to show the location of the redrill well. Reservoir pressure at the location of the redrill well is 4,200 psi, which is slightly reduced from the virgin reservoir pressure of 4,600 psi. This small pressure depletion should not seriously affect the drilling process or production.

Simulation Results (Redrill)

By mid June, 1994, the redrill well was completed and put on production. Figure 56 shows the field-measured production rate and surface pressure for the redrill from June 22 to November 8, 1994. These gas production rates are comparable to those from the original well, averaging just under 1,000 MSCFD.

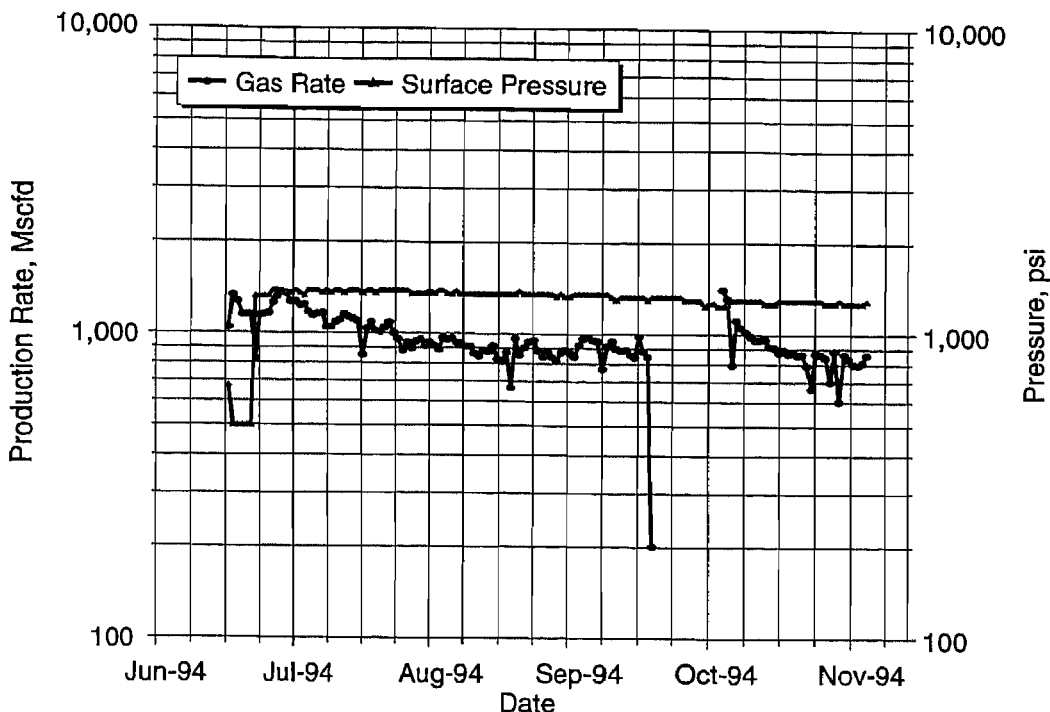


Figure 56 Daily Production Rates and Surface Pressures from the Redrill, Champlin 254 Amoco B 2-H

The naturally fractured reservoir model employed in this history match of the Champlin 254 Amoco B 2-H production was initialized with the same properties used in the original simulations (Table 10). Surface pressures were several hundred psi higher than during the original well production (~ 1,300 psi); therefore, initial model runs required a permeability of 0.020 md. This is nearly double the permeability used to match the original well data. Although this improved permeability could indicate that redrilling the well did less damage to the fracture system than drilling the original well, there were some discrepancies in the pressure data. For this reason, a pressure buildup test was performed on the redrill well

from September 23 to October 7, 1994, using bottomhole pressure bombs. These bottomhole pressure data and time equivalent surface pressure data are shown in Figure 57. This plot shows that surface pressures are insensitive to bottomhole pressure changes during both early-time (24 hrs) production and later buildup periods. Thus, bottomhole pressure data were used in the history match and reservoir evaluation rather than the errant surface data.

Figure 58 shows the actual bottomhole pressure buildup data, as delta pressure, and the linear, bilinear, and radial derivative curves (Branagan, 1993). This plot shows wellbore storage effects dominate the pressure buildup for the first 10 to 12 hours. Following the storage period, it appears the reservoir redistribution process is bilinear. This is a bit peculiar since radial flow should continue until the vertical, no-flow boundaries force the streamlines to become more linear. The fact that the pressure buildup is dominated by bilinear flow suggests there is limited wellbore conductivity. This is analogous to the bilinear flow regime in a vertical well such as occurs where a low-conductivity hydraulic fracture drains a low-permeability reservoir.

As previously described, prior production should have little affect on early production from the redrill well; however, the affect on pressure buildup tests is a different matter. Therefore, the reservoir simulation, by necessity, included the entire production history. The simulator was run with model parameters that matched the original well production (Table 10). The time interval from the collapse of the original well (March 1994) to the beginning of production from the redrill (June 1994) was simulated as a shut-in. A reduction in effective wellbore conductivity was made to the model at the beginning of the redrill production to simulate the apparent low conductivity suggested by the buildup data. Figure 59 shows the production data for the entire history of the Champlin 254 Amoco B 2-H including both the original and redrill well's data. Model results are in excellent agreement with the original well, and there is a good match with the redrill data. The bottomhole pressure data are plotted to provide matching parameters for the simulated buildup. There is also good agreement with the simulated pressure data until shut-in, and the pressure discrepancy after shut-in is interpreted to be caused by the erroneous surface pressure measurements previously described.

Redrill Well Model Summary

The reservoir model provides an excellent history match of all the available field data and affords a very acceptable description of the reservoir for both the original and redrill wells. Natural fractures, characterized by core and image logs, are interpreted to be abundant (Hill, this volume) and to have some remnant apertures at in situ conditions (Dunn, this volume). However, the reservoir modeling results indicate that the natural fractures are a minor component of reservoir permeability. This conflicting interpretation may be the direct result of the completion process.

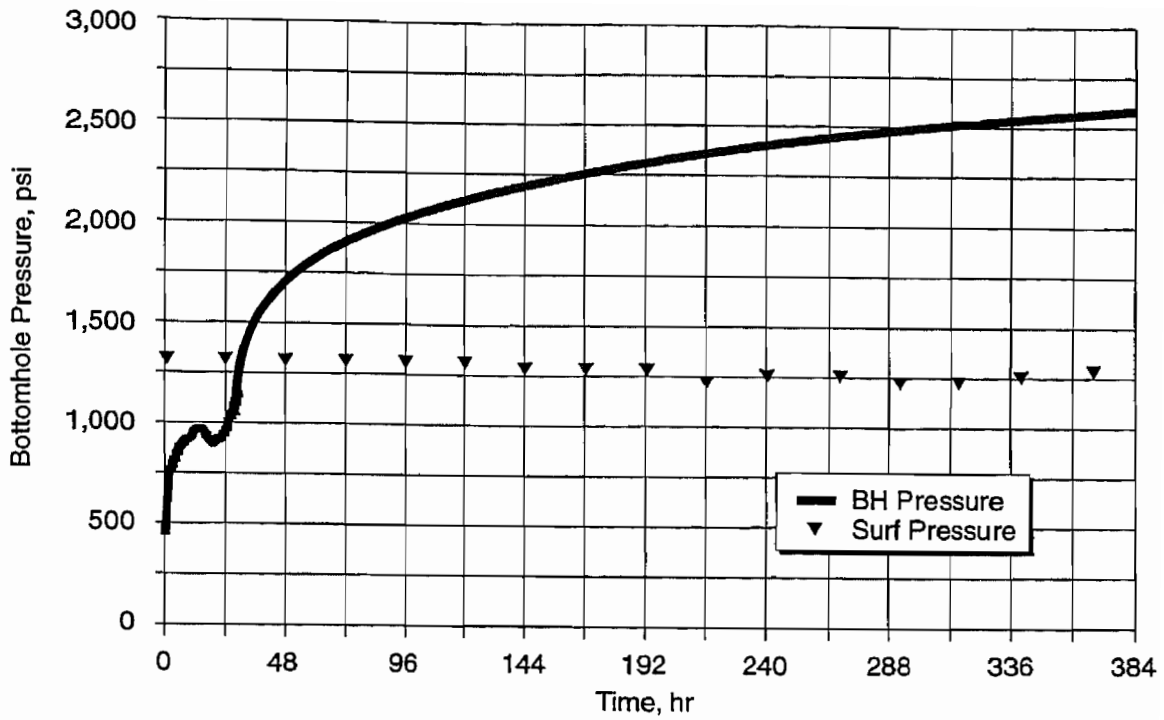


Figure 57 Bottomhole and Surface Pressure Data During a Pressure Buildup Test on the Redrill, Champlin 254 Amoco B 2-H

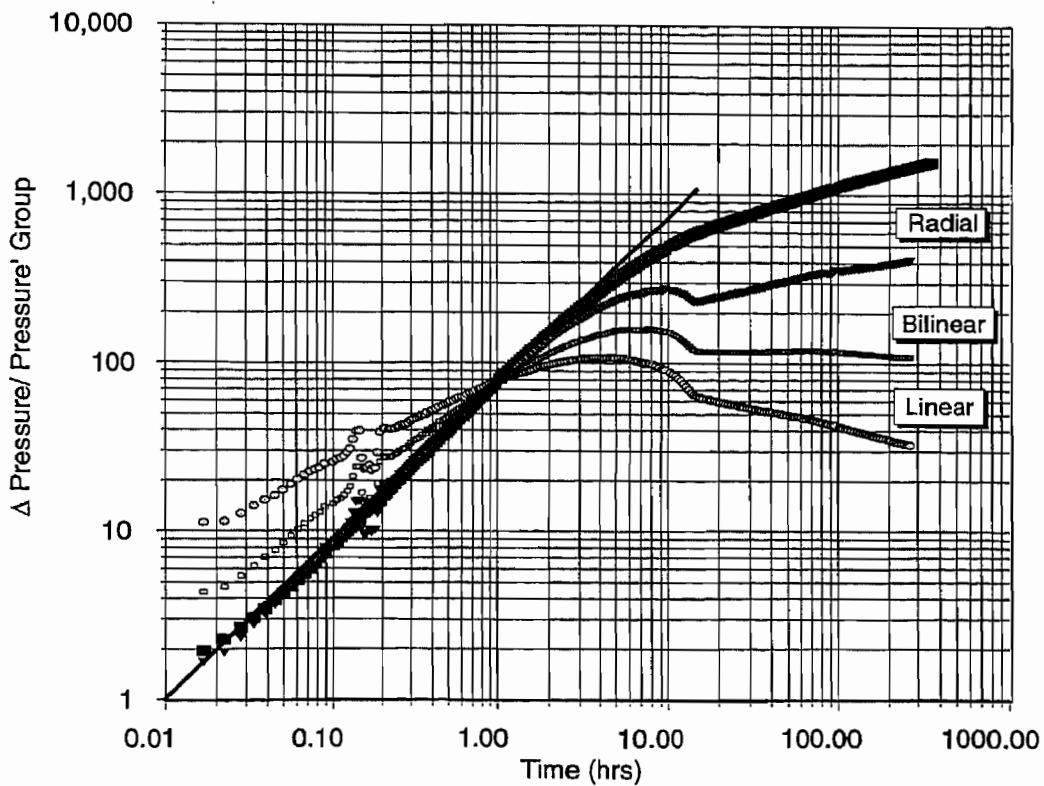


Figure 58 Derivative Plot for the Redrill Bottomhole Pressure Buildup Test, Showing Radial, Bilinear and Linear Flow Derivatives

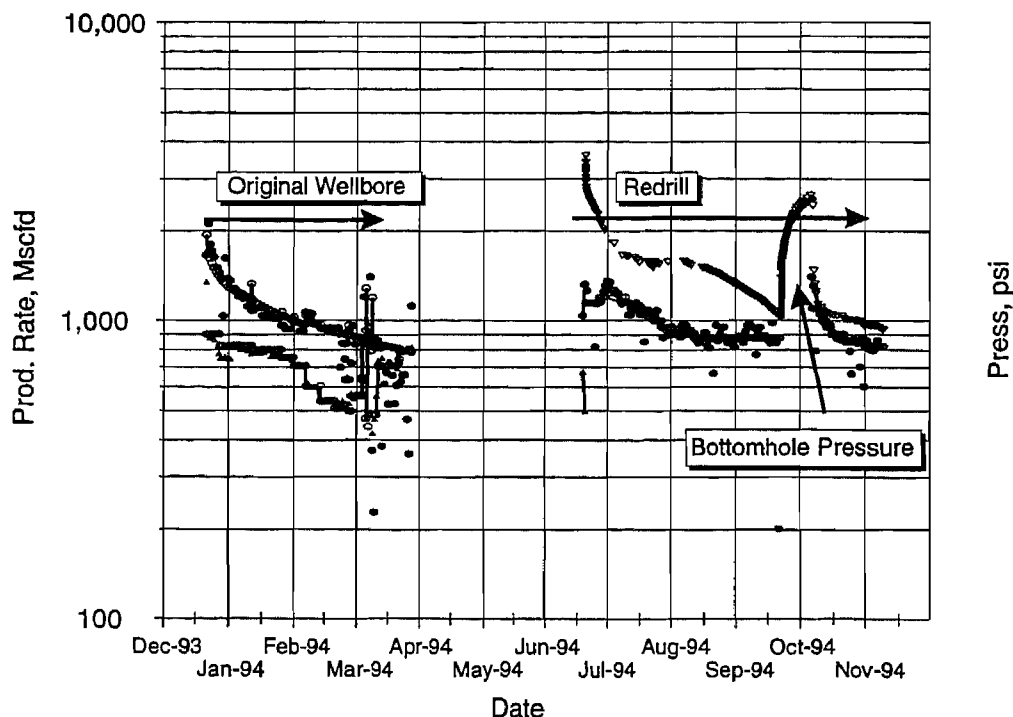


Figure 59 Final Simulated Production History Match with Bottomhole Pressure Buildup Data

The long, bilinear flow period in the pressure buildup data suggests a limited-conductivity horizontal well and further supports the hypothesis that the wellbore and natural fractures both exhibit reduced conductivities because of an intervening fluid (e.g., water) that substantially impedes the flow of gas. If water is the problem, then either continuous swabbing or long-term production may eventually dewater the wellbore and nearby fractures, thus increasing gas production.

REFERENCES

Amyx, J., D. Bass and R. Whiting, 1960: Petroleum Reservoir Engineering-Physical Properties, pg 85, McGraw-Hill.

Lorenz, J.C. and S.E. Laubach, 1994: "Description and Interpretation of Natural Fracture Patterns in Sandstones of the Frontier Formation Along the Hogsback, Southwestern Wyoming," Gas Research Institute Topical Report, GRI-94/0020, 89 p.

Lorenz, J.C., 1994: "Regional Assessment of Natural Fractures and State of Stress in the Green River Basin," GRI/DOE/IPAMS Consortium for Emerging Gas Resources in the Greater Green River Basin Meeting, Denver, Colorado, Nov. 4, 1994.

EVALUATION AND COMPARISON OF HYDRAULICALLY FRACTURED VERTICAL WELLS WITH THE CHAMPLIN 254 AMOCO B 2-H HORIZONTAL WELL

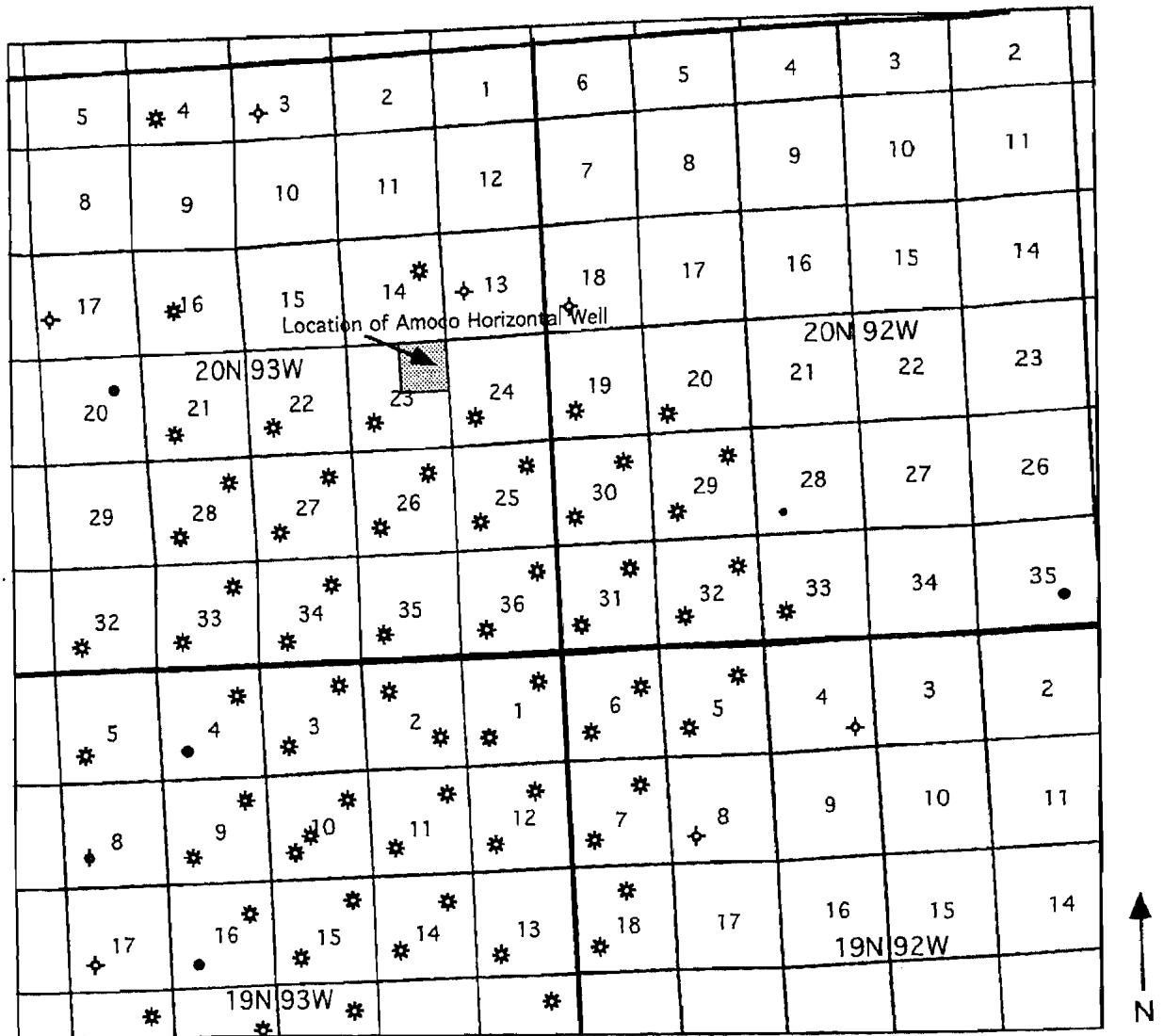
*Bradley M. Robinson, P.E.
S.A. Holditch & Associates, Inc.*

INTRODUCTION

Most of the wells in the Echo Springs Field were drilled during the late 1970s or early 1980s on 640-acre spacing. Within the past few years, infill development drilling on 320-acre spacing has occurred as shown in Figure 60. All of the wellbores were drilled vertically and completed with hydraulic fracture treatments. This "conventional" completion procedure has been successful for most of the Echo Springs Field. However, some of the wells along the perimeter of the field have been marginal producers because reservoir quality degrades towards the edge. One of the main reasons why Amoco drilled the Champlin 254 Amoco B 2-H was to determine if a horizontal wellbore would result in economic production in these marginal areas of the field.

The principal producing horizon in the Echo Springs Field is the upper Mesaverde, or Almond sandstone. The formation is generally considered to be low permeability even though a few wells have good gas flow rates (greater than 1 MMSCFD) without fracture stimulation. Based on pre-fracture flow tests, reported permeabilities are normally less than 0.1 md; therefore, hydraulic fracturing is required to stimulate production. The presence of natural fractures has also been documented in the upper Mesaverde; however, the importance of natural fractures in the overall well productivity has not been quantified. Characterization of the natural fractures was also a goal in drilling the horizontal well.

The purpose of this study is to evaluate the economic benefits of drilling horizontal gas wells in the Upper Almond. To evaluate the benefits, it is necessary to determine what a vertical well would produce if it were drilled into the same type of reservoir that the horizontal well was drilled. One of the first tasks was to analyze production and pressure data from a large number of the vertical wells that had been completed in the field. The analysis provided the average permeability-thickness product, the degree of stimulation that had been achieved by the conventional hydraulic fracture treatments, and an estimate for the reserves. With these results, the distribution of reservoir quality and gas reserves for the area of interest, and specifically for a well drilled at the same location as the horizontal well, was determined. It was then possible to calculate the net present value of production from both types of wells.



- * Gas Well
- Oil Well
- ◇ D & A

1 Mile

Figure 60 Base Map of Echo Springs Field

ANALYSIS OF VERTICAL WELLS

To determine the reservoir properties and gas productivity of the vertical wells, the following types of data were analyzed on as many wells as possible:

- pre-fracture flow tests,
- pre-fracture pressure buildup tests,
- post-fracture pressure buildup tests, and
- long-term production history.

Conventional test analysis methods [Horner plot (Horner, 1951); type-curve plots (Gringarten and others, 1979); and one-point flow calculations (Lee, 1982)] were used to analyze the pre-fracture and post-fracture test data. Long-term production from each well was history matched using a model called *PROMAT* (Murtha and others, 1994) which was developed in the GRI Devonian Shales research program. The model uses analytical solutions to the various flow equations to calculate the expected gas flow rate and continues to iterate on selected reservoir parameters until a match is obtained with the actual gas production. An example of one history match is shown in Figure 61. For the example shown, the best match of the actual production data was achieved with the following properties:

Permeability	0.18 md
Net Pay	18 ft
Drainage Area	161 acres
Fracture Length	218 ft
Fracture Conductivity	209 md-ft
Reservoir Pressure	5,100 psi

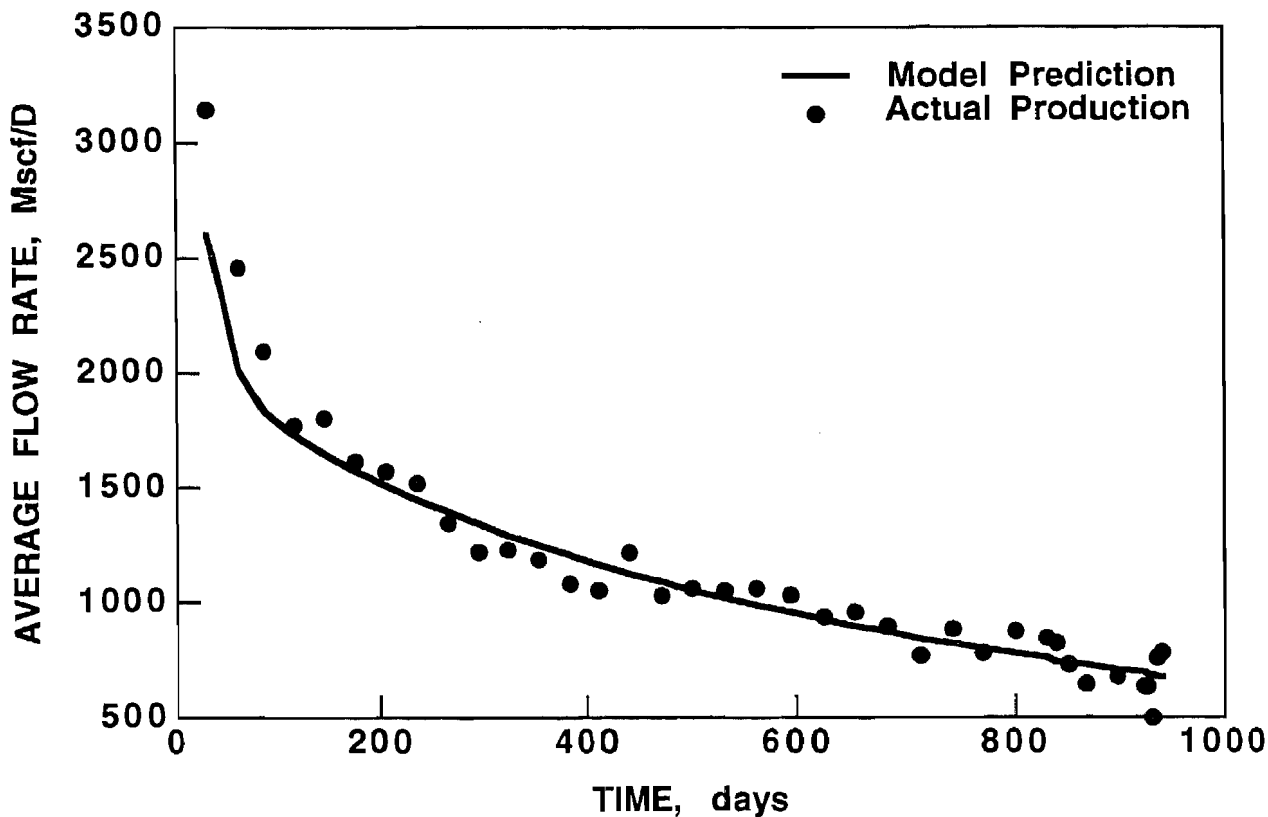


Figure 61 Example "PROMAT" History Match of Production

Tables 11, 12 and 13 present the results from the pre-fracture production and pressure analysis, post-fracture pressure buildup analysis, and post-fracture production matching, respectively. Unfortunately, production from many wells in the Echo Springs Field is commingled between the Almond and other deeper zones in the Mesaverde. This study is based on the wells that were completed only in the Almond or where production could be accurately allocated to the Almond.

In analyzing the production and pressure data on these wells, it was observed that the permeability-thickness (kh) product, which basically defines the flow properties of the reservoir, is almost always considerably larger after the hydraulic fracture treatment. While it is not unusual for the post-fracture kh to be different than the kh determined from pre-fracture data, it is not expected to always be higher, especially by a factor of 2 to 3 and, in some cases, 50 times greater. Table 14 compares the kh determined from pre-fracture data with the kh determined from post-fracture data. These results indicate that in almost every case, the hydraulic fractures intersect a reservoir that is more productive than what was tested before the fracture treatment was performed. It is interpreted that the hydraulic fractures have intersected natural fractures and, therefore, increased the effective productivity of the reservoir. This interpretation is supported by the stress orientation data that indicated hydraulic fractures azimuths may be 45° to 90° different than the natural fracture strike (see Hill, this volume).

To fairly compare the production from the Amoco horizontal well to that of a vertical well drilled in the same location, it is necessary to first evaluate the trends in reservoir quality and productivity. These trends are determined by analyzing production data on the wells of interest, then mapping the parameters that best determine the well's productivity and ultimate recovery.

Using in-house production data analysis software, a "production indicator" was determined for each well that best correlates to long-term well performance. The best production indicator can vary from field to field, but is usually related to an extended production test period of six to twelve months. The software automatically evaluates different indicators to determine the most accurate correlation to long-term well performance. Figure 62 presents the correlation between the production indicator and ten-year cumulative production for the Echo Springs Field. A linear regression through the data resulted in an R² value of 0.93, indicating an excellent correlation was obtained.

Table 11 Results of Pre-Fracture Analyses

Well Location	Type Test	Net Pay, ft	Permeability, md	Skin Factor	p*, psia
Sec 19 (SW), T20N R92W	PBU	22	0.007	+4.4	5,215
Sec 31 (SW), T20N R92W	PBU	24	0.09	+17	5,022
Sec 25 (SW), T20N R93W	PBU	30	0.001	-1.0	5,290
Sec 24 (SW), T20N R93W	Single Rate	29	0.004	-1.5	N.A.
Sec 27 (SW), T20N R93W	PBU	18	0.12	+7.7	5,100
Sec 35 (SW), T20N R932	PBU	25	0.01	+5.0	5,700
Sec 3 (SW), T19N R93W	PBU	35	0.15	+2.0	5,000
Sec 23 (SW), T20N R93W	Single Rate	21	0.014	-1.5	N.A.
Sec 11 (SW), T19N R93W	PBU	36	0.23	+10.8	4,950

Table 12 Results of Post-Fracture PBU Analyses

Well Location	Net Pay, ft	Permeability, md	Fracture Length, ft	Fracture, Conductivity, md-ft
Sec 35 (SW). T20N R93W	25	0.23	521	380

Table 13 Results of Post-Fracture Production Matching

Well Location	Net Pay, ft	Permeability, md	Fracture Length, ft	Fracture Conductivity, md-ft	Drainage Area, acres
Sec 25 (SW), T20N R93W	36	0.034	250	500	184
Sec 24 (SW), T20N R93W	29	0.023	125	100	56
Sec 27 (SW), T20N R93W	18	0.18	218	209	161
Sec 35 (SW), T20N R93W	25	0.18	400	120	180
Sec 14 (NE), T20N R93W	26	0.002	400	200	18
Sec 3 (SW), T19N R93W	35	0.18	10	200	140
Sec 11 (SW), T19N R93W	36	0.45	40	170	600

Table 14 Comparison of Pre- and Post-Fracture Analyses

Well	Pre-Frac Permeability-Thickness, md-ft	Post-Frac Permeability-Thickness, md-ft
Sec 25, T20N R93W	0.032	1.22
Sec 24, R20N R93W	0.11	0.66
Sec 27, T20N R93W	2.23	5.25
Sec 35, T20N R93W	0.25	5.85
Sec 3, T19N R93W	5.13	6.12
Sec 11, T19N R93W	8.2	16.2

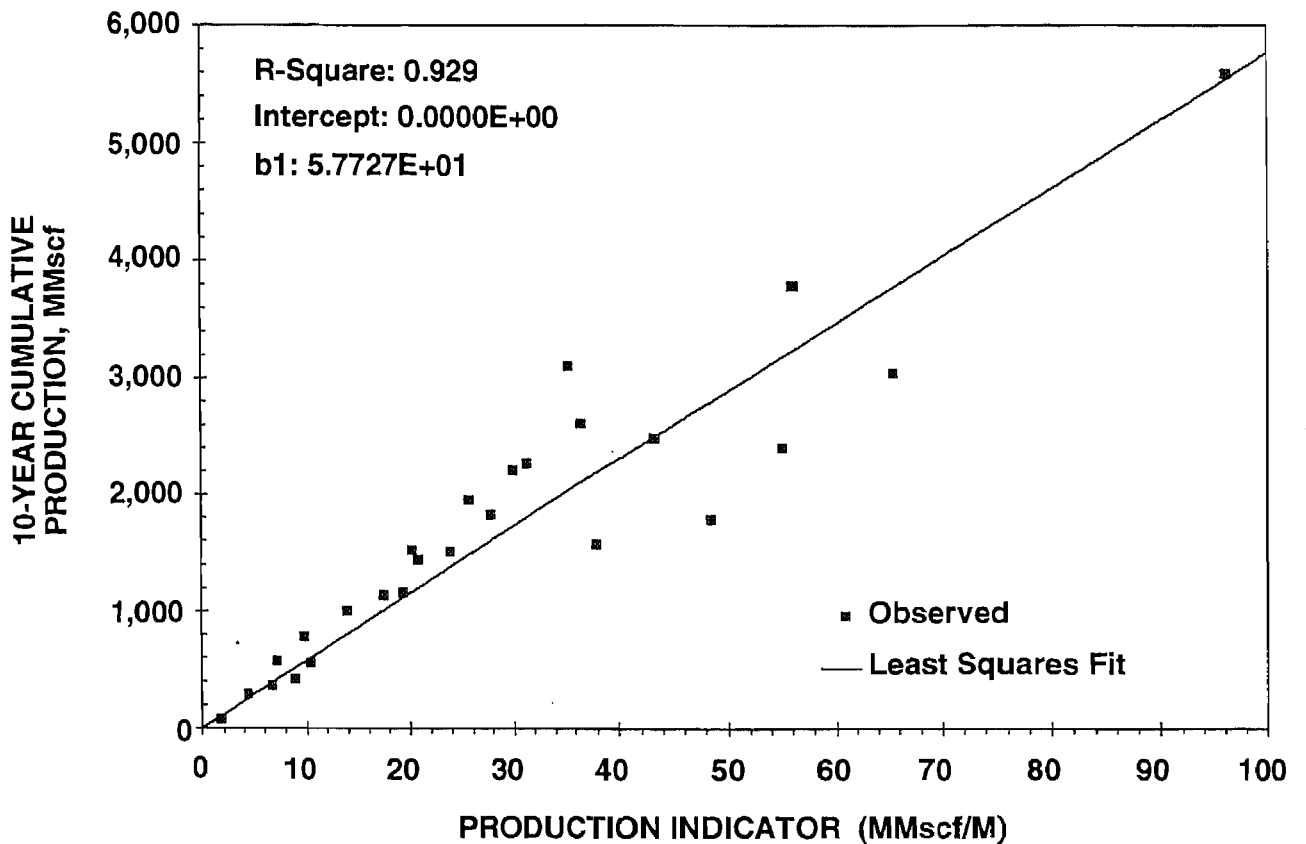


Figure 62 Production Indicator Correlated to 10-Year Cumulative Production, Echo Springs Field

Figure 63 is a contour map of the production indicator, and Figure 64 is a map of the ten-year cumulative production. These contour maps indicate that a vertical well drilled at the same location as the horizontal well would be expected to recover between 0.5 and 1.0 BCF of gas during the first ten years of production. The production analysis can also be used to develop an average production rate curve for a well in a particular area of interest.

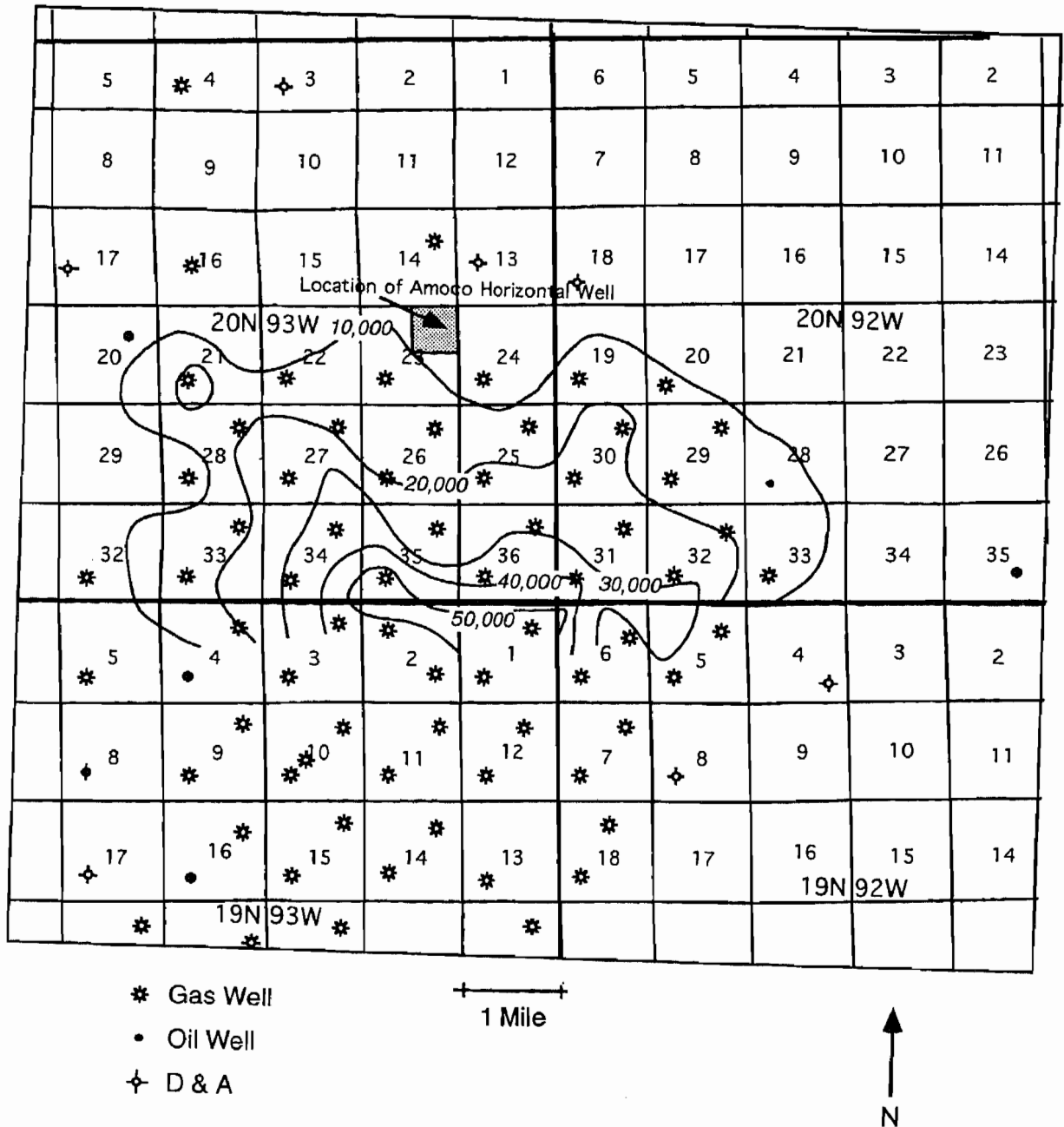
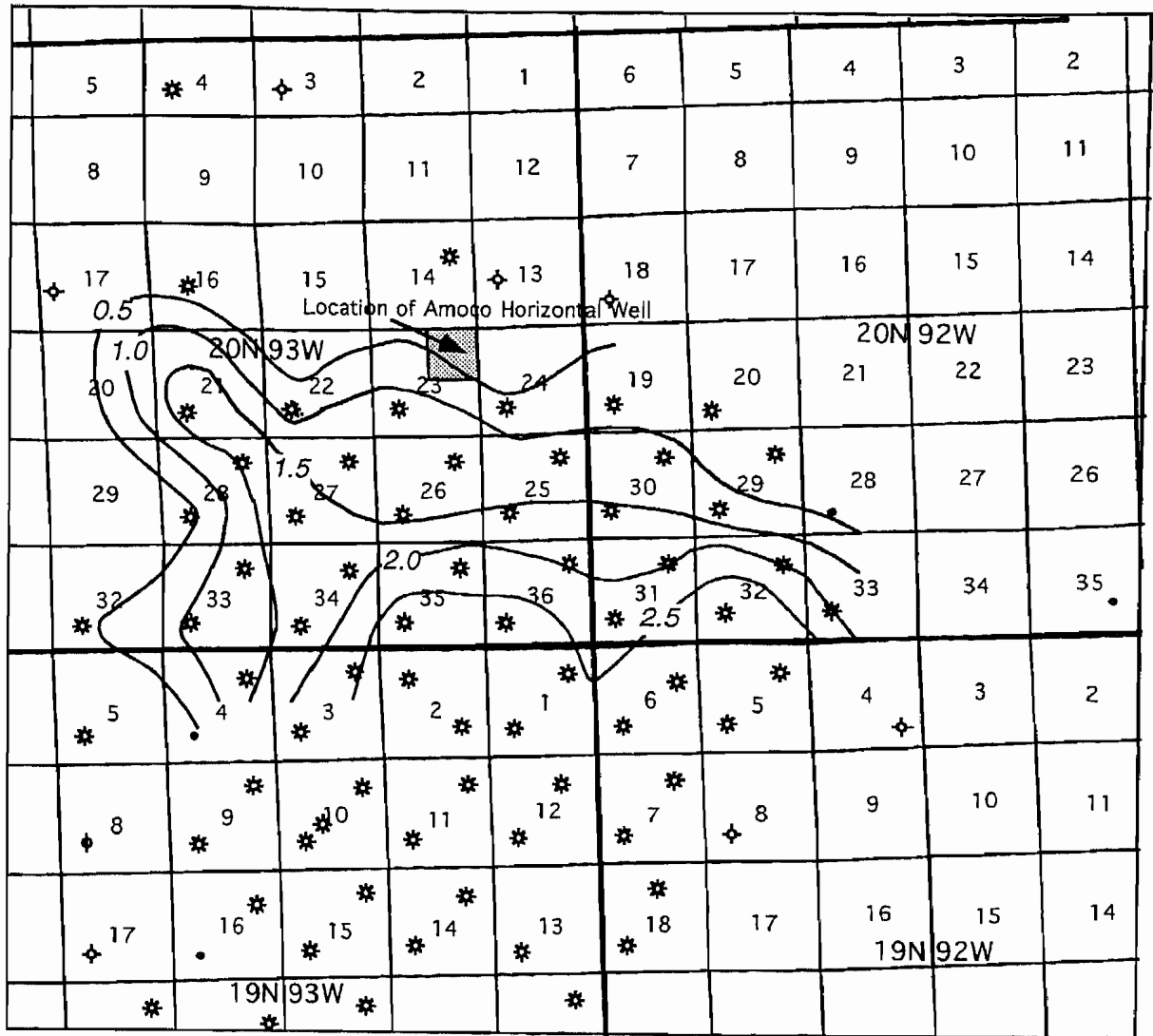


Figure 63 Contour Map of Production Indicator, C.I. = 10 MSCFM



- * Gas Well
- Oil Well
- ⊕ D & A

1 Mile



Figure 64 Contour Map of 10-Year Cumulative Production, C.I.= 0.5 BCF

Figure 65 shows the average production curve generated for a well that has a production indicator and 10-year cumulative gas production equal to the northeast corner of Section 23, T20N, R93W. Using a 3-D reservoir simulator, it is possible to history match the average production curve (Figure. 64) to estimate the reservoir properties and gas in place for a vertical well drilled at this location. Based on the reservoir model, the ultimate recovery can be projected for the vertical well and compared to the model predictions of ultimate recovery for the horizontal well.

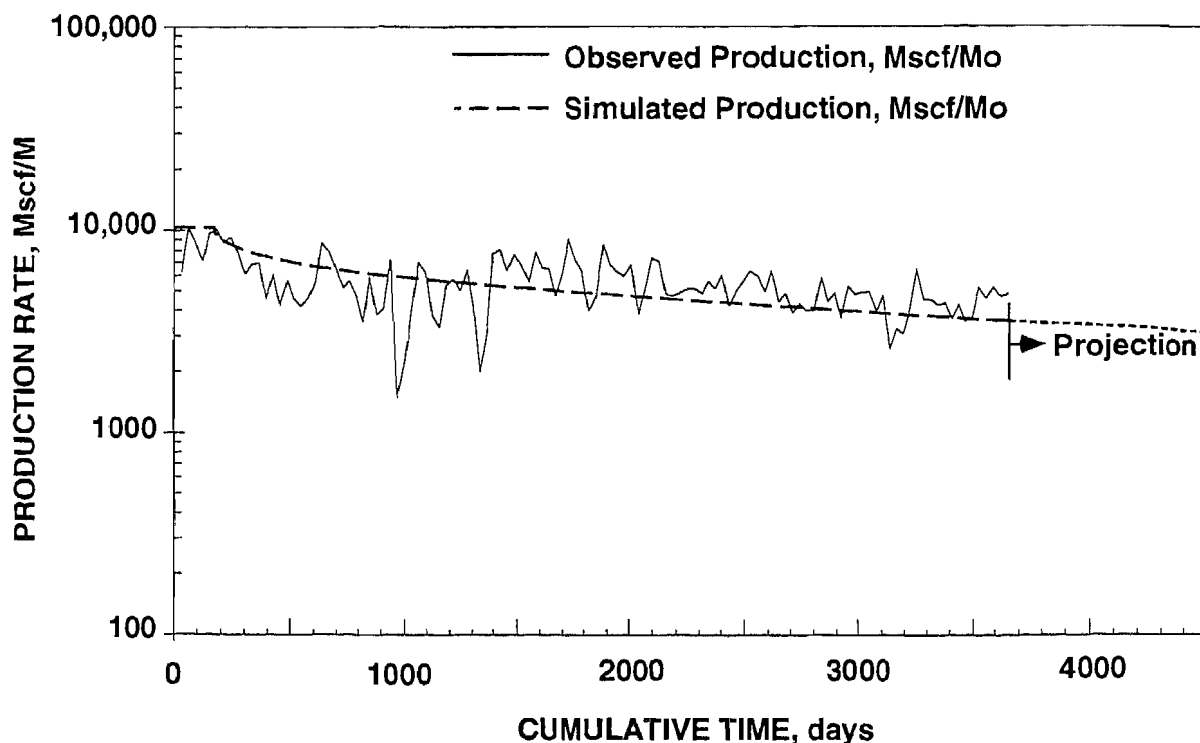


Figure 65 Average Production Rate for Wells Comparable to NE 4 Sec. 23, T20N, R93W

COMPARISON OF VERTICAL WELL PERFORMANCE TO HORIZONTAL WELL PERFORMANCE

The actual production data from the Champlin 254 Amoco B 2-H horizontal well has been provided and discussed by previous authors in this report. Based upon these production data, the horizontal well is estimated to have a production indicator of about 22 MMSCF/month. A plot of the distribution of production indicators that were calculated for vertical wells in the Echo Springs Field can be used to evaluate how the horizontal well compares to the rest of the field. Figure 66 is a plot of the distribution of production indicators for the Echo Springs Field. As can be seen in terms of productivity, the horizontal well appears to be about average (50 percentile) over the entire field. The production indicators for vertical wells drilled into comparable reservoir quality (shown by the gray shaded area) range from 7 to 10 MMSCF/month. These results indicate that productivity of the horizontal well is on the order of two to three times greater than would be expected for a vertical well drilled in the same location.

Table 15 compares the long-term production performance that has been forecast for the horizontal well (see Branagan, this volume) with two vertical well cases (i.e., 80-acre and 160-acre spacings). The first year's production, 10-year cumulative production, and the estimated ultimate production for each case is shown. It is evident from Table 15 that the horizontal well will produce at a higher gas flow rate during the first 10 years of production and will ultimately recover more gas than the vertical well cases. However, because the

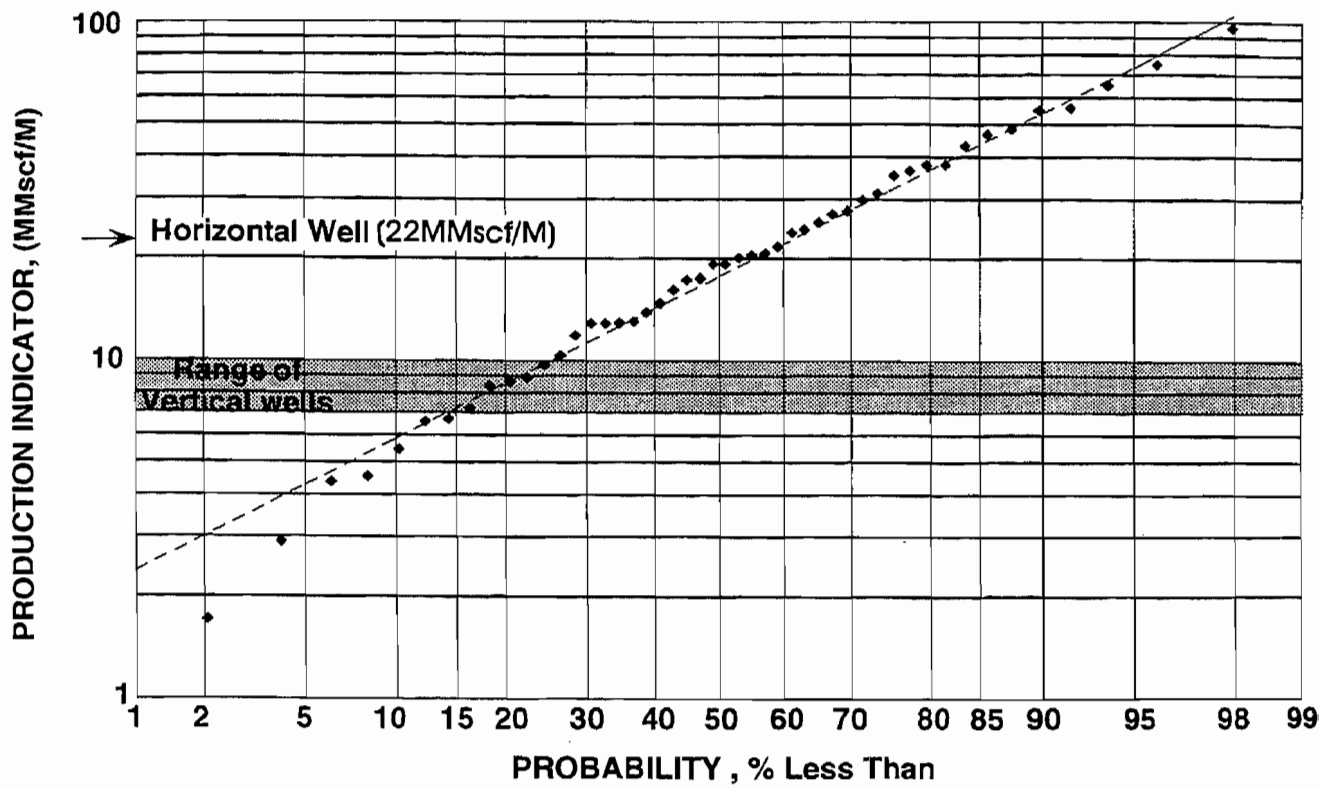


Figure 66 Distribution of Productivity Indicators in Echo Springs Field

Table 15 Comparison of Long-Term Production Performance

	Horizontal Well	Vertical Wells	
		80 Acres	160 Acres
First Year Production, MMSCF	270	157	157
10-Year Cumulative, MMSCF	1363	709	719
Est. Ultimate Recovery, MMSCF	2636	1353	1,529

horizontal well also costs more than the vertical wells, a detailed economic evaluation is necessary. Table 16 details the cost information used to compare an economic evaluation of a horizontal well with a vertical well. Obviously, costs may vary from one operator to another, but every effort was made to determine realistic costs for drilling these types of wells. Table 17 summarizes the results of the economic evaluation. The forecast was allowed to run until the economic limit was reached; however, the producing time was limited to only 30 years. It is clear that the horizontal well will generate more net cash flow and undiscounted profit than the vertical well cases because of the greater ultimate gas production. However, when one discounts future revenue at 10 percent, it appears that both horizontal and vertical wells will essentially break even.

Table 16 Basic Cost Information for Economic Evaluation

	Vertical Well, \$	Horizontal Well, \$
Pre-Drilling	47,000	47,000
Drilling	272,000	1,200,000
Completion	137,000	152,000
Stimulation	147,000	-
Production Facilities	47,000	50,000
Totals	650,000	1,449,000
Net Revenue Interest		87.5%
Initial Gas Price		\$1.50 (\$3.00 max)
Operating Costs		\$24,000/yr
Cost and Price Escalation		3%/year
Production Taxes		13.25%
Discount Factor		10%

Table 17 Economic Evaluations - Wells in NE Sec 23, T20N, R93W

	Horizontal Well	Vertical Wells	
		80 Acres	160 Acres
Well Life, years	30	30	30
Total Net Cash Flow, \$1000's	5,563	2,775	3,229
Total Well Costs*, \$1000's	3,319	2,131	2,189
Net Profit - Undisc., \$1000's	2,244	644	1,040
Net Profit - Disc. @ 10%, \$1000's	14	-29	24
Payout - Undisc., years	8.6	8.5	8.4
Payout - Disc. @ 10%, years	27	>30	22
Rate of Return, %	10.2	9.4	10.8

*Drilling, completion, and operating costs including taxes.

These results indicate that horizontal wells will significantly improve gas reserves in more marginal areas of the field. If drilling and operating costs can be controlled and minimized, then horizontal wells may also be attractive economically even though it appears the benefits may not be much greater than conventionally drilled vertical wells.

The reservoir model used to forecast future production for these cases included matrix and natural fracture properties as previously described (see Branagan, this volume). Even though the permeability of the fractures is fairly high (greater than 1 darcy) in the model, the flow of gas through the fractures appears to be restricted. There are three plausible explanations for the flow restriction: 1) the fracture permeability is less than assumed (in the reservoir model) due to increased water saturation in the fractures; 2) fracture widths are much more narrow than measured in the cores; and/or 3) damage exists to the natural fractures. All of these factors would affect the fracture flow capacity (or conductivity) which is the product of permeability time fracture width. The "flow capacity" of the fractures is one of the most important factors controlling well productivity.

It is generally believed that the flow capacity of the natural fractures (and possibly matrix permeability) is considerably higher in the better portion of the field. Therefore, to evaluate the benefits of a horizontal well drilled in an area where the reservoir and natural fracture system is much better, forecasts were generated that assume the flow capacity of the natural fractures is 50 times higher than along the edge of the field. In analyzing production

data in some of the better areas, it was observed that the wells were capable of draining from 320 to 640 acres. Along the edge of the field, calculated drainage areas were more on the order of 80 to 160 acres (thus, the reason for choosing 80- and 160-acre spacings for the previous cases). Therefore, it was necessary to increase the size of the drainage area in the model for these new projections. Table 18 summarizes an economic evaluation that compares a horizontal well to a vertical well that is drilled in an area where better fracture flow capacity exists.

Table 18 Economic Evaluation With Higher Fracture Flow Capacity

	Horizontal Well	Vertical Well
Ultimate Recovery, BSCF	10.790	9.326
Well Life, years	19	30
Total Net Cash Flow, \$1000's	17,180	17,847
Total Well Costs *, \$1000's	4,240	4,062
Net Profit - Undisc., \$1000's	12,940	13,785
Net Profit - Disc. @ 10%, \$1000's	9,703	6,106
Payout - Undisc., years	0.4	0.81
Payout - Disc. @ 10%, years	0.4	0.86
Rate of Return, %	100	100

* Drilling, completion and operating costs including taxes.

The ultimate gas recovery for the horizontal well is about 1.5 BCF higher than the vertical well case, but more significant is the fact that the gas reserves are produced over a much shorter period of time. Instead of taking over 30 years to produce the gas, a horizontal well will accelerate production to a more realistic time frame of less than 20 years. Even though the total net cash flow for each case is about the same, the discounted net profit for the horizontal well is about 50 percent higher (\$9.7 million vs. \$6.1 million) because of the accelerated production. These results clearly show that in a better part of the field where there are more natural fractures and/or fractures with more flow capacity, horizontal wells are more economic than vertical wells.

REFERENCES

Horner, D. R., 1951: "Pressure Buildup in Wells," Proceedings, Third World Pet. Congl. The Hague, Sec. II, 503-523.

Gringarten, A.C., D.P. Bourdet, P.A. Landel, and V.J. Kniazeff, 1979: "A Comparison Between Different Skin and Wellbore Storage Type-Curves for Early-Time Transient Analysis," SPE 8205, presented at the 54th Annual SPE Fall Technical Conference and Exhibition, Las Vegas, September 23-26.

Lee, W. J., 1982: "Well Testing," Society of Petroleum Engineers of AIME, New York, 1.

Murtha, J. A., J.M. Gatens, III, D.E. Lancaster, H.S. Lance, W.J. Lee, J.S. Olarewaju and A.T. Watson, 1987: "Practical Methods for Analyzing Well Test and Production Data from Devonian Shale Reservoirs," Topical Report GRI-88/0017, GRI Contract No. 5084-213-0980, Oct. 6.

Appendix 1

CHAMPLIN 254 AMOCO B 2-H AND CHAMPLIN 320 C-1A-H DATA INVENTORY

**Champlin 254 Amoco B 2-H
Data Inventory
March 28, 1995**

PILOT HOLE DATA

Item No. P-1

Data Type: Core description, fracture descriptions (includes horizontal core descriptions)
Organization/Service Company: Amoco
Data Format: Hard copy

Item No. P-2

Data Type: Core fracture photographs
Organization/Service Company: Amoco
Data Format: 5"x7" color glossy

Item No. P-3

Data Type: Photographs of whole core (wet and dry)
Organization/Service Company: Amoco
Data Format: 8"X10" color glossy

Item No. P-4

Data Type: ASR Report
Organization/Service Company: Sandia National Laboratories
Data Format: Hard copy

Item No. P-5

Data Type: ASR Report
Organization/Service Company: Amoco Production Research
Data Format: Hard copy

Item No. P-6

Data Type: Core analysis (porosity & permeability tabular data)
Organization/Service Company: K & A
Data Format: Hard copy

Item No. P-7

Data Type: Vertical Seismic Profile Monitor Record with CSI
Organization/Service Company: Schlumberger Well Services
Data Format: Folded hardcopy blueline log

Item No. P-8

Data Type: Vertical Seismic Profile Observers Notes
Organization/Service Company: Unknown
Data Format: Hardcopy & 3.5" disk tabular data

**Champlin 254 Amoco B 2-H
Data Inventory
March 28, 1995**

Item No. P-9

Data Type: Shear Wave Vertical Seismic Profile Survey Report
Organization/Service Company: Schlumberger Well Services
Data Format: Hardcopy report with Observer's Notes, Input Data, Results

Item No. P-10

Data Type: Near Offset Vertical Seismic Profile
Organization/Service Company: Schlumberger Well Services
Data Format: 9-track tape, 6250 BPI, SEG-Y format

Item No. P-11

Data Type: Far Offset Vertical Seismic Profile
Organization/Service Company: Schlumberger Well Services
Data Format: 9-track tape, 6250 BPI, SEG-Y format

Item No. P-12

Data Type: Far Offset Vertical Seismic Profile Tape Dump
Organization/Service Company: Schlumberger Well Services
Data Format: Hardcopy tabular data

Item No. P-13

Data Type: Incident Vertical Seismic Profile Tape Dump
Organization/Service Company: Schlumberger Well Services
Data Format: Hardcopy tabular data

Item No. P-14

Data Type: Wellbore Directional Survey Report
Organization/Service Company: Gyrodata
Data Format: Hardcopy tabular data

Item No. P-15

Data Type: Rock Properties Measurement Report (Velocities, P&P, Mineralogy)
Organization/Service Company: Geophysical Rock Properties Group
Amoco Production Research Center
Data Format: Hardcopy tabular data

Item No. P-16

Data Type: Wireline Log Data (Dual Laterolog, LithoDensity, Compensated Neutron)
10,465 ft to 2,520 ft
Organization/Service Company: Schlumberger Well Services
Data Format: 1600 bpi 9-track tape

**Champlin 254 Amoco B 2-H
Data Inventory
March 28, 1995**

Item No. P-17

Data Type: Wireline Log Data:
Dipole Sonic Imager (6,900 - 10,456 ft)
Formation MicroImager Acquisition Record (7,000 - 10,456 ft)
Compensated Neutron/LithoDensity/GR (6,900 - 10,456 ft)
Dual Laterolog/MicroSFL/GR (2,538 - 10,456 ft)
Organization/Service Company: Schlumberger Well Services
Data Format: Hardcopy folded paper logs

HORIZONTAL HOLE DATA

Item No. H-1

Data Type: Fractured core analysis (strike/dip, classification)
Organization/Service Company: Amoco
Data Format: Hard copy

Item No. H-2

Data Type: Core photos of whole core
Organization/Service Company: Core Laboratories
Data Format: Color Xerox copies

Item No. H-3

Data Type: Core Gamma
Organization/Service Company: Core Laboratories
Data Format: Hard copy

Item No. H-4

Data Type: Core fracture analysis including strike/dip of fractures & bedding,
distribution plots (includes pilot hole data)
Organization/Service Company: Core Laboratories
Data Format: Hard copy

Item No. H-5

Data Type: FMS well advisor plot (wellbore profile)
Organization/Service Company: Schlumberger Well Services
Data Format: Hard copy

Item No. H-6

Data Type: ASR Report
Organization/Service Company: Amoco Production Research
Data Format: Hard copy

Champlin 254 Amoco B 2-H
Data Inventory
March 28, 1995

Item No. H-7

Data Type: Core analysis (full-diameter porosity & permeability)

Organization/Service Company: Core Laboratories

Data Format: Hard copy

Item No. H-8

Data Type: Mudlog

Organization/Service Company: Cate Logging

Data Format: Hard copy

Item No. H-9

Data Type: Well Report (drilling info, geology, surveys)

Organization/Service Company: Cate Logging

Data Format: Hard copy

H-10

Data Type: Well Operations Report (includes Cost Estimate Report, Casing Report, Cementing Report, Cost Estimate Report, Daily Drilling Report, Daily Cost Summary, Final Pipe Tally, Daily Completion Workover Report)

Organization/Service Company: Amoco Production Company

Data Format: Hard copy

H-11

Data Type: Directional Survey Log

Organization/Service Company: Schlumberger Well Services

Data Format: Hard copy

H-12

Data Type: Directional Gamma While Drilling Log and Survey Tabular Data (Pilot and Horizontal Holes)

Organization/Service Company: Sperry-Sun Drilling Services

Data Format: Hard copy

H-13

Data Type: Completed Wellbore Sketch

Organization/Service Company: Amoco Production Company

Data Format: Hard copy

H-14

Data Type: Production Data (12/22/93 to 2/28/94); includes water, tbg press, choke, csg press

Organization/Service Company: Amoco Production Company

Data Format: Hard Copy

**Champlin 254 Amoco B 2-H
Data Inventory
March 28, 1995**

H-15

Data Type: Wireline Log Data (Formation MicroScanner, LithoDensity, Compensated Neutron)
12,309 ft to 9,168 ft

Organization/Service Company: Schlumberger Well Services
Data Format: 6,250 bpi 9-track tape

H-16

Data Type: FMS Horizontal Well Workstation Analysis; includes fracture orientation graphics (strike histograms, Wulff stereonet), FMS color borehole images with fracture-fit sinewave curves, Fracview Log with fracture strike and dip, FMS workstation logs (Section Advisor Plot and False Aspect Ration Plot)
12,300 ft to 9,170 ft

Organization/Service Company: Schlumberger Well Services
Data Format: Hard copy (3-ring notebook)

H-17

Data Type: Compensated Neutron/LithoDensity/Gamma Ray
12,310 ft to 10,272 ft

Organization/Service Company: Schlumberger Well Services
Data Format: Hard copy

H-18

Data Type: Final Results of Acid Injection Tests
Organization/Service Company: K&A Laboratories
Data Format: Hard Copy

**Champlin 320 C-1A-H
Data Inventory
March 28, 1995**

320 V1

Data Type: Wireline Log Data (FormationDensity, Compensated Neutron, Dual Induction-SFL, Cyberlook)
10,795 ft to 2,487 ft

Organization/Service Company: Schlumberger Well Services

Data Format: Hard copy

320 V2

Data Type: Cased Hole Wireline Log Data (Cement Bond with Nuclear Log, Differential Temperature Log)
10,640 ft to 8,300 ft

Organization/Service Company: Gearhart-Owen Wireline Services

Data Format: Hard copy

320 V3

Data Type: Cased Hole Wireline Log Data (Temperature Survey Log)
9,911 ft 9,600 ft

Organization/Service Company: Petro-Log

Data Format: Hard copy

320 P1

Data Type: Wireline Log Data (LithoDensity, Compensated Neutron, Dual Laterolog-MSFL, Dipole Shear Sonic Imager, Oriented Caliper Data)
10,500 ft to 7,000 ft

Organization/Service Company: Schlumberger Well Services

Data Format: Hard copy

320 P2

Data Type: MWD Log Data (Hole Direction, Gamma ray, ROP)
10,290 ft to 9,600 ft

Organization/Service Company: Sperry Sun

Data Format: Hard copy

320 P3

Data Type: FMI Workstation Analysis; includes fracture orientation graphics (strike histograms, Wulff stereonet), FMS color borehole images with fracture-fit sinewave curves, Fracview Log with fracture strike and dip, FMS workstation logs (Section Advisor Plot and False Aspect Ration Plot)
10,530 ft to 9,500 ft

Organization/Service Company: Schlumberger Well Services

Data Format: Hard copy (3-ring notebook)

**Champlin 320 C-1A-H
Data Inventory
March 28, 1995**

320 H1

Data Type: Mud Log
13,021 ft to 7,000 ft
Organization/Service Company: Cate Logging
Data Format: Hard copy

320 H2

Data Type: MWD Log Data (Hole Direction, Gamma ray, ROP)
12,970 ft to 9,312 ft
Organization/Service Company: Sperry Sun
Data Format: Hard copy

320 H3

Data Type: Wireline Log Data (LithoDensity, Compensated Neutron, FMS Hilite
Enhanced Images
13,010 ft to 11,780 ft
Organization/Service Company: Schlumberger Well Services
Data Format: Hard copy

320 H4

Data Type: Core Analysis Results (k, phi, RHOGD, fracture description, and bedding
orientation data)
Core No. 1 : 10,345 to 10,406 ft
Core No. 2 : 10,474 to 10,505 ft
Core No. 3 : 12,220 to 12,250 ft
Core No. 4 : 12,250 to 12,281 ft
Organization/Service Company: Core Laboratories
Data Format: Hard copy

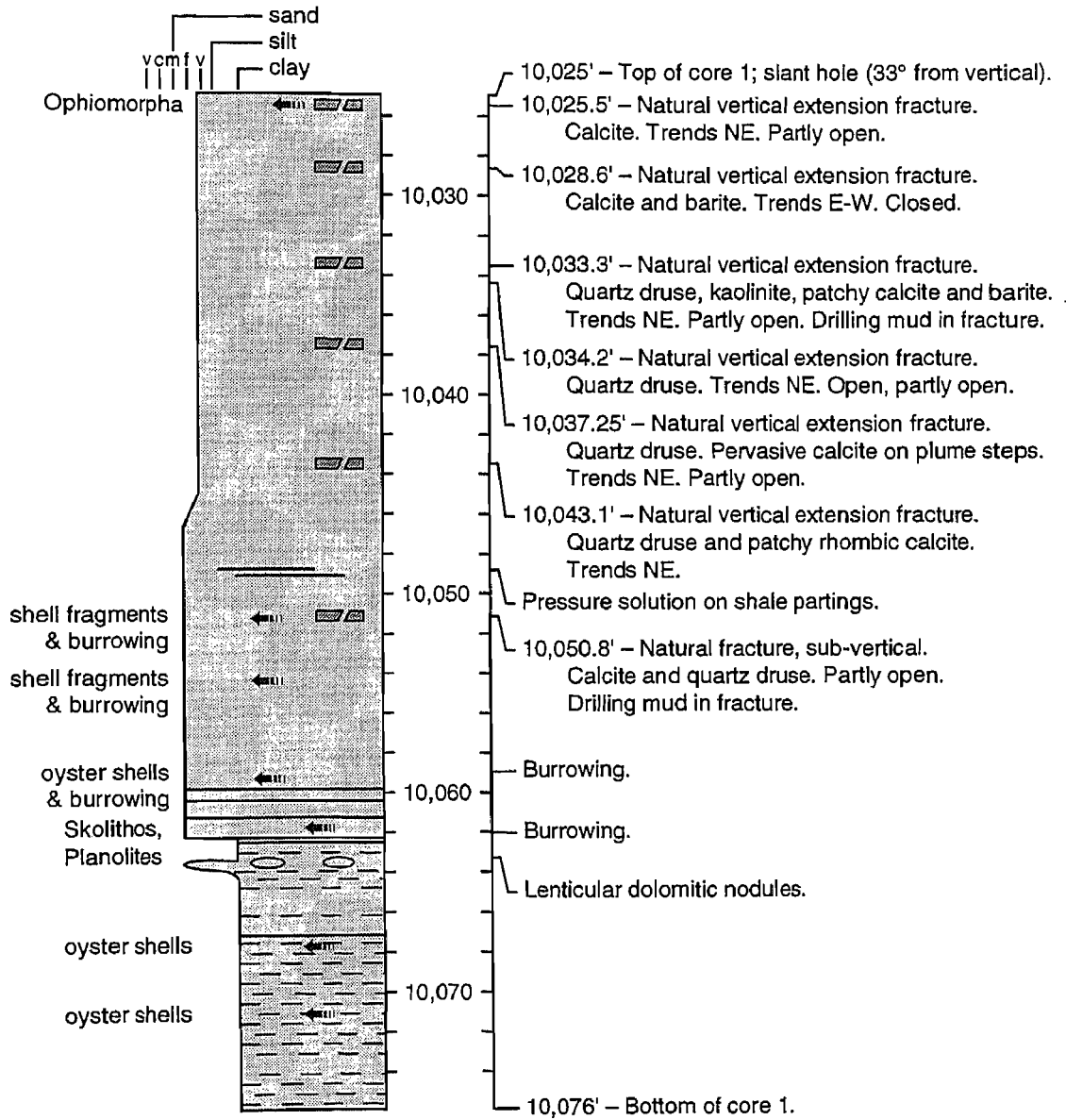
320 H5

Data Type: Fax of Additional Requested Data (FMI Rose Diagram of fracture orientation
(Pilot Hole/Lewis Shale), Hole Survey Orientation, ASR Orientation Results
Memo)
Organization/Service Company: Amoco
Data Format: Hard copy

Appendix 2

CHAMPLIN 254 AMOCO B 2-H CORE DESCRIPTION

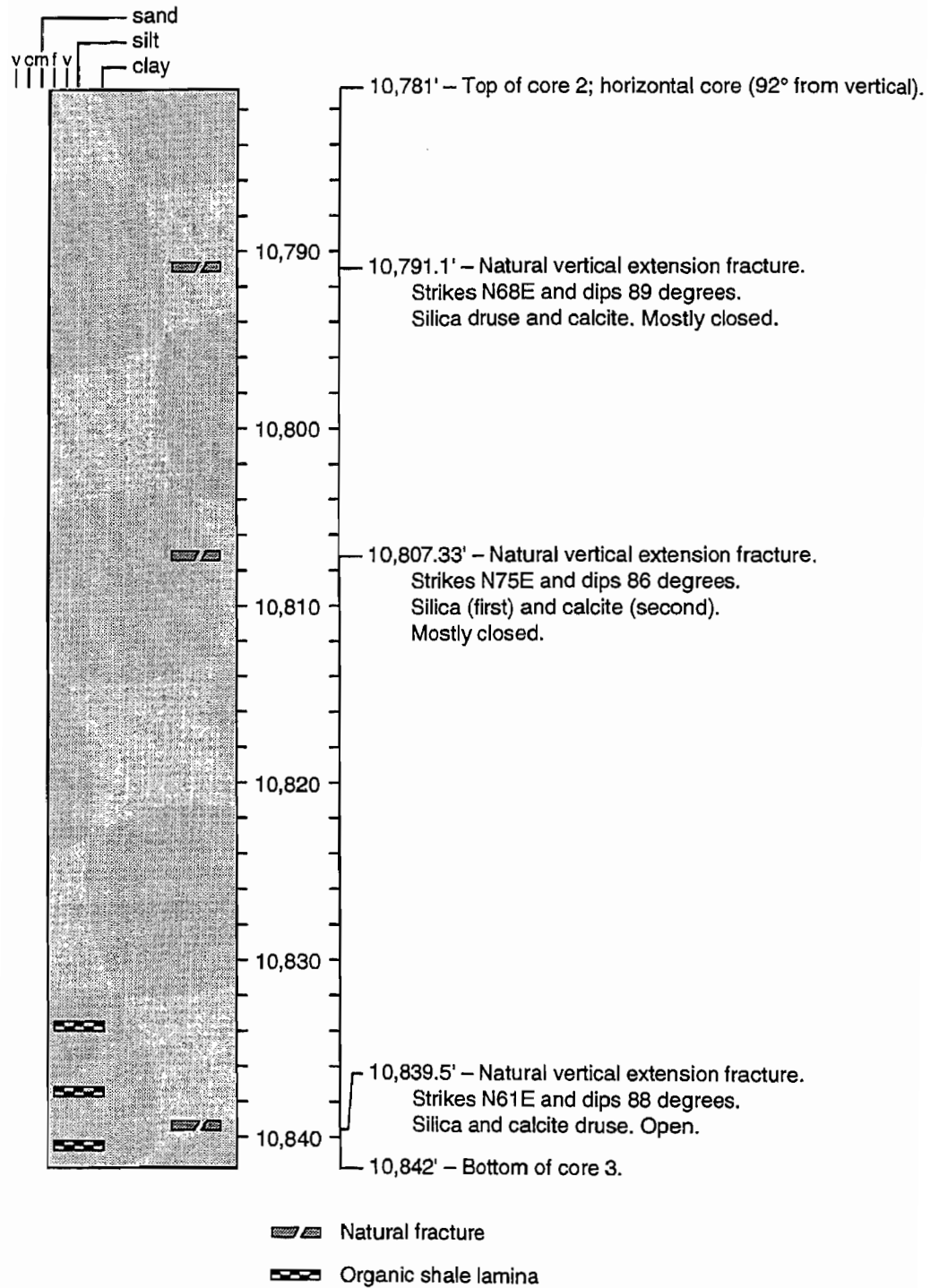
Core 1, CH 254B-2H



-  Natural fracture
-  Fossils and trace fossils

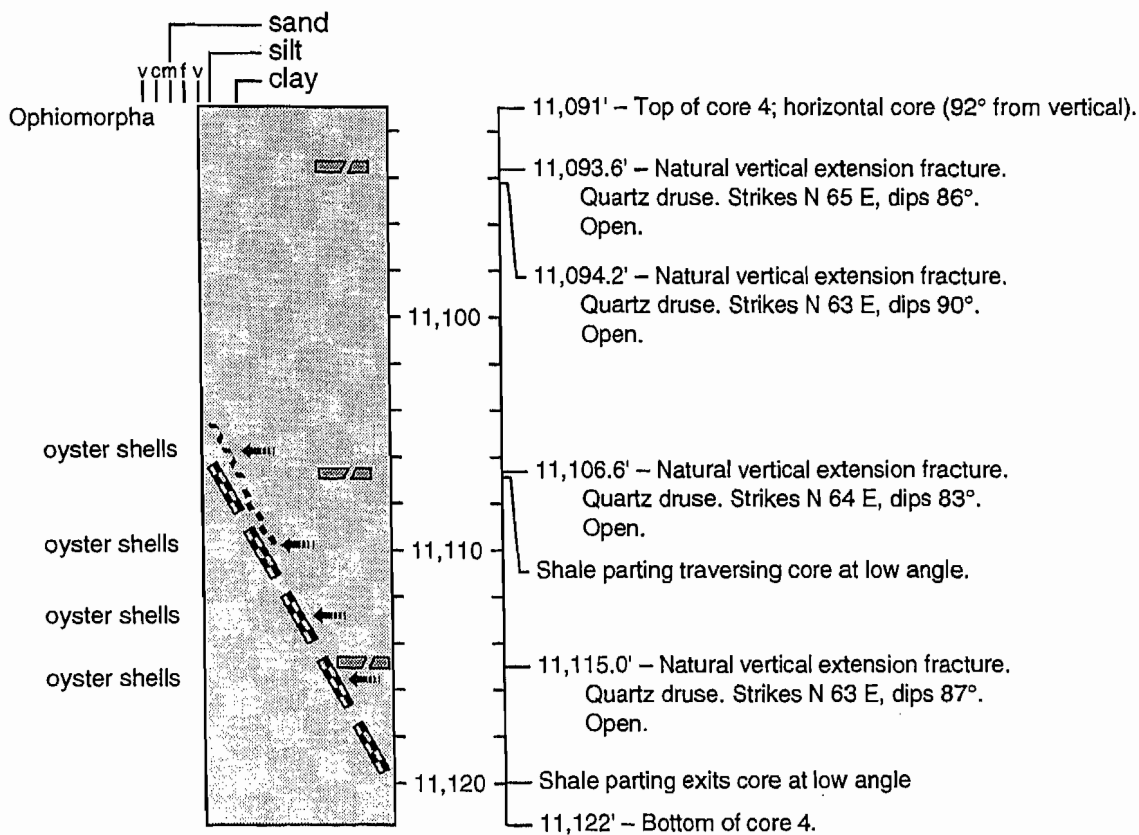
— modified from unpublished notes of Reinert and Dunn

Cores 2 and 3, CH 254B-2H



— modified from unpublished notes of Reinert and Dunn

Core 4, CH 254B-2H



— modified from unpublished notes of Reinert and Dunn